Universitetet i Stavanger

FACULTY OF SCIENCE AND TECHNOLOGY

MASTER'S THESIS

Study program / Specialization: MSc Petroleum Engineering / Reservoir Engineering	Spring semester, 2018 Open
Author: Anibal Jose Ceballos Hurtado	…… (signature of author)
Supervisor(s): Pål Østebø Andersen (UiS / IOR Centre) Co-Supervisor: Dag C. Standnes (UiS / Equinor) Co-Supervisor: Arild Lohne (IRIS)	
Title of master's thesis: **Simulation of Oil Recovery Process – Co-current Spontaneous Imbibition in Fractured Reservoirs**	
Credits: 30 ECTS	
Keywords: Naturally Fractured Reservoir Spontaneous Imbibition Co-Current Imbibition Viscosity Ratio Capillary Pressure Simulation History Matching Oil Recovery	Number of pages: Stavanger, 15 June 2018

Simulation of Oil Recovery Process – Co-current Spontaneous Imbibition in Fractured Reservoirs

---

Master Thesis by Anibal Jose Ceballos Hurtado

University of Stavanger

Spring 2018

Acknowledgements

My deepest appreciation and gratitude go to my supervisors, Dr. Pål Østebø Andersen and Dag Standness and co-supervisor, Arild Lohne at IRIS who helped me to get into IORCoreSIM to build the model for this thesis, for their excellent guidance, advice.

It was a wonderful and a great experience writing my thesis since I gained lots of knowledge and insight specifically knowledge in simulation and model-build. Owing to that, I have developed my technical skills..

Furthermore, I would like to say ¨Thank you¨ to my family for their prayers, loves, and continuous support during my study abroad, and especially Juan Felipe who always motivated, encouraged, and supported me during my thesis. Last but not least, thanks go out for my fellow students and friends from around the world who helped and supported me during my study.

Abstract

A large fraction of the world petroleum reserves is made up by Naturally Fractured Reservoirs (NFR) which are usually produced by waterflooding. The injected water flows primarily through the fracture network and cover the blocks; one of the main production mechanisms is “Spontaneous Imbibition” which is driven by Capillary Forces and can be either countercurrent or co-current displacement.

Several studies of spontaneous imbibition have been carried out to model the process of oil displacement from the matrix to the fracture. For co-current spontaneous imbibition case, there are some experiments that have been carried out by Meng et al. from China University of Petroleum. This type of experimental setup represent two ends open free spontaneous imbibition (TOEFSI) boundary condition where the inlet of the glass column is in contact with water, while the outlet is in contact with oil.

This thesis project will address the spontaneous imbibition phenomenon focused on simulation of co-current imbibition in fractured reservoirs. One-dimensional (1D) horizontal homogeneous model of spontaneous imbibition is proposed with initial and boundary conditions of the experimental setup by considering the domination of co-current flow takes place during displacement. For simplicity, the oil displacement in the model is only governed by capillary forces. By modelling this type of phenomenon from a core scale approach, it can be obtained an analytical model which clearly describes the flow processes that occurs in the oil recovery.

Furthermore, sensitivities analyses were made to have a better understanding of the dynamics of the imbibition process and the coherence of production profile between experimental and simulated results during History Matching. The main findings obtained were the imbibition rate and oil production varies according to the mobilities ratio; the co-current production was always more dominating than counter-current production along the imbibition process. The imbibition rate is proportional to the co-current oil production and inversely proportional to the counter-current oil production; as the oil viscosity increases, the front saturation decreases which leads to a lower saturation at breakthrough. The counter-current production obtained was higher compared to the experimental results and this lead to a reduction on the imbibition rate as well as the co-current oil production. For the Air and Kerosene experiments, the imbibition rates showed a decreasing trend and the mismatch between the curves was smaller compared to the WHOIL15 and WHOIL32 experiments which showed an increasing trend and a bigger mismatch among the simulated and the experimental results.

Table Of Contents

List of figures

List of Tables

Abbreviation

1D	- One Dimensional
HM	- History Matching
kr	- Relative Permeability
NFRs	- Naturally Fractured Reservoir
P_c	- Capillary Pressure
TEOFSI	- Two-ends Open Face Spontaneous Imbibition
COCSI	- Co-current spontaneous imbibition
TEO	- Two ends Open

1. INTRODUCTION

1.1.Background

Most hydrocarbon reservoirs are affected in some way by natural fractures, however the effects of fractures are not quite understood and mostly underrated. The naturally fractured reservoirs present a production contradiction; they include reservoirs with low hydrocarbon recovery that initially may appear highly productive (Bratton et al., 2006).

On the other hand, fractured reservoirs represent an important proportion of the world's hydrocarbon reserves and most productive reservoirs on Earth. These types of reservoirs mainly consists of two different systems: fracture system and matrix system. The matrix system, which has low permeability, is normally surrounded by fracture system, which has high conductivity; the oil in the fracture system is specially recovered by water injection or aquifer drive owing to the high conductivity. Regarding the matrix system, the recovery mechanism is the spontaneous imbibition (SI), which is driven by capillary pressure (Meng, Q. et al, 2017). In naturally fractured reservoirs, defined as those systems where the fractures are assumed to have a significant impact on oil recovery, the fractures properties must be evaluated because they control the efficiency of oil production (Fernø, M., 2012).

The term imbibition refers to an increase in the saturation of the wetting phase, whether this is a spontaneous imbibition process or a forced imbibition process such a waterflood in a water-wet material (Abdallah et al., 2007). The Spontaneous imbibition process is the reduction of interfacial energy which occurs by the action of capillary pressure; for this to happen, the water-rock interfacial energy must be lower than the oil-rock interfacial energy (Meng, Q. et al, 2017). The process is complex and depends on several parameters such as wettability of the porous medium, shape, size, boundary conditions and permeability of the rock material in addition to fluid properties, for instance, viscosities and oil-water interfacial tension (IFT) (Standnes, 2004).

The Spontaneous Imbibition can occur in two different modes: Co-current when the wetting phase and the non-wetting phase flow in the same direction, while counter-current takes place when the wetting phase and the non-wetting phase flow in opposite directions from the same inlet.

The process of spontaneous imbibition is complex by nature and it is affected by several parameters. Therefore, understand the behaviour and interrelation of these parameters is mandatory to obtain the best oil recovery in NFRs. For co-current spontaneous imbibition case, some experiments were carried out by (Meng et al., 2015) from China University of Petroleum whose glass-beads experiments will be simulated and matched against the experimental results.

1.2. Objectives

The main objective of this thesis is to develop an analytical model describing One-Dimensional (1D) co-current spontaneous imbibition (COCSI) and compared its behaviour against full numerical solutions and to interpret experimental data by (Meng et al., 2015). Furthermore, to analyse and understand the behaviour of adjusted parameters that affect co-current oil production during imbibition by making sensitivity analyses and how the production profile in the simulation results will be matched with the experimental data by making a History Matching.

1.3. Outlines

In the introduction, the theoretical background of this thesis project is decribed; some introduction about the theoretical aspects, forward plan to accomplish the main goals during the thesis project. For the Theory section, fundamental aspects related to the main topic for this thesis are summarized and reviewed, the analytical solution is outlined and the software used for building the model in the end of this chapter. In the chapter 3, the mathematical model of co-current imbibition is explained and the description of flow modelling that occur in the numerical model. In the chapter 4, the experimental setup used by Meng et al. is explained, the experimental data to be matched is shown, finally the input data and the assumptions to run the model. This chapter will be followed by a sensitivity analysis for relative permeability, capillary pressure, mobility ratio, viscosity ratio and the length of the glass column followed by a History Matching in the section of result and analysis. Finally, the thesis is concluded by making conclusions from all the findings from previous chapters.

2. THEORY

2.1. Capillary Pressure

The capillary pressure is defined as the pressure difference between two fluids forming an interface (Glover, 2010) where one fluid pressure lies on the non-wetting phase and the other fluid pressure is in the wetting phase. The concept is expressed by the following relation:

$$P\_c = Po - Pw \quad (2.1)$$

Where P_c is the capillary pressure, P_o is pressure of the oil as the non-wetting phase, P_w is the pressure of water as the wetting phase. The size of the capillary pressure is related to the saturation of each phase, the nature of the continuous phase, the distribution, shape, and size of the pores and pore throats. For instance, the fluid rise in a capillary tube Figure 2-1, where the fluid above the water is oil since the glass prefers water, the effect of capillary pressure can be observed easily on the following expression:

$$P\_c = \frac{2\sigma}{r} \quad (2.2)$$

In the equation (2.2), the σ is the interfacial tension between the two fluids and r is the radius of the capillary tube. Owing to the complexity of the porous media, the bundle of capillary tube model is often used as an ideal representation of the capillary phenomenon in oil bearing rocks and can be related to fluid contacts and saturation distribution in a reservoir.

Note that the pressure is proportional to the surface tension, but inversely proportional to the radius of the tube. The difference in pressure (the capillary pressure) causes the interface to go up through the capillary tube until the weight of the suspended column of fluid balances the capillary force associated with the capillary pressure as seen on Figure 2-1 below.

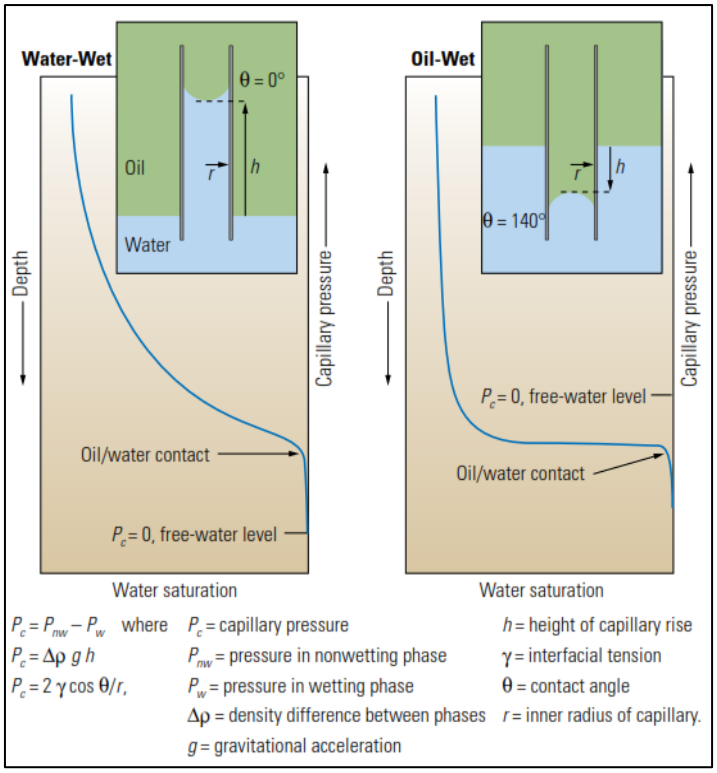

Figure 2-1 Illustration of the capillary tube experiment for a water-wet and oil-wet system in a reservoir system (Abdallah et al., 2007)

The imbibition is defined as the displacement of nonwetting phase (oil) by wetting phase (generally water) where the water saturation increases along the system and the driving force is the capillary pressure (Yadav et al., 2014). The spontaneous imbibition takes place when oil pressure is reduced gradually which yields in a decrease of the high positive capillary pressure to zero, the water will imbibe spontaneously from the reservoir and displaces the oil until the capillary pressure reaches the value of zero. On the other hand, the forced imbibition occurs when water displaces oil continuously as the water saturation increases, generated by a negative capillary pressure owing to a surge of water pressure over the oil pressure. The displacement ceases when Capillary Pressure goes to infinity which it is the point where the residual oil saturation (S_{or}) is reached.

Three sections can be observed in the capillary pressure curve Figure 2-2, a drainage capillary pressure curve (dotted) where the capillary pressure is increased from zero to a large positive value and reduces the saturation of the wetting phase (water). A spontaneous imbibition curve (dashed) determined after the drainage capillary pressure is measured where the capillary pressure, initially at a large positive value, is generally decreased to zero allowing the wetting phase to imbibe. Finally, the forced imbibition curve (solid), where the capillary pressure is

lowered from zero to a large negative value; this phenomenon takes place when the pressure in the wetting phase (water) is higher than the pressure in the non-wetting phase oil, forcing water into the core. Also, it can be seen the capillary pressure behaviour for both water-wet and mixed-wet reservoirs; the capillary pressure stays positive over most of the saturation range for the strongly water-wet case owing to all surface imbibes water. Respect to the mixed-wet case its sign has both positive and negative sections, which means parts of the surface imbibe water and others imbibe oil.

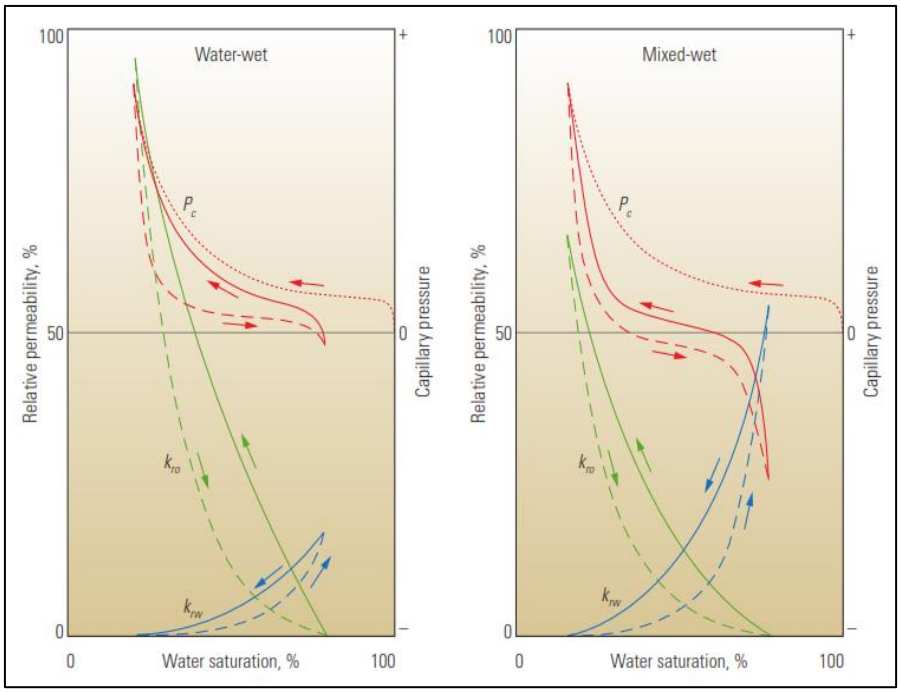

Figure 2-2 Illustration of the capillary pressure and relative permeability for water-wet and mixed-wet conditions (Abdallah et al., 2007)

2.1.1. Capillary Pressure Leverett J-function

For correlation objective and modelling purposes, the capillary pressure can be expressed by a dimensionless capillary pressure, Leverett-J function that is function of water saturation. Since core properties such as porosity and permeability influence the capillary pressure, it was defined the following empirical J-function to correct this impact as follows (Leverett, M.C., 1940)

$$J(S_w) = \frac{P_c}{\sigma}\sqrt{\frac{k}{\varphi}} \qquad 2\text{-}3$$

Where P_c is the capillary pressure, σ is the interfacial tension, k is the permeability and ϕ is the porosity. The physical interpretation of the Leverett J-function is for reservoirs whose lithology is similar and have fixed saturations. Furthermore, the differences caused by different media or fluids can also be removed by the J-function (Hongjung et al., 2013).

2.2. Relative Permeability

The relative permeability defined as the relationship between effective and absolute permeability in a porous system, it is a strong function of the respective phase saturations and it is expressed as follows

$$k_{ri} = \frac{k_i}{k} \qquad 2\text{-}4$$

Where i denotes the fluid type (oil and water), k_i is the fluid effective permeability, and k is absolute permeability. On Figure 2-2, the relative-permeabilities curves for water, k_{rw} (blue) and oil, k_{ro} (green) for water-wet (left) and mixed-wet (right) reservoirs; the k_{ro} values are low at low water saturation in the mixed-wet case, because the oil is competing with water in the larger pores. Conversely, the k_{rw} at high water saturation is low in the water-wet case because the oil has a preference of occupying the larger pores (Abdallah et al., 2007).

The role of the wettability on the relative permeability curve governs the imbibition process in the core that lead to a controlled oil production. Therefore, to generate the relative permeability curve, the constrained end-point values must be determined. These values are unique for every core, a classification system based on the limitation of end-point relative permeability curves and their respective wettability shown in the Figure 2-3 was created by Craig et al. in 1971. Also, he suggested several rules of thumb shown on the Table 2-1 to characterize the effect of wettability in the relative permeability.

Table 2-1 Rule of Thumb for Oil-Water Relative Permeability Characterization (Craig, 1971)

	Strongly Water-Wet	Strongly Oil-Wet
Connate water saturation.	Usually greater than 20% to 25% PV.	Generally less than 15% PV, frequently less than 10%.
Saturation at which oil and water relative permeabilities are equal.	Greater than 50% water saturation.	Less than 50% water saturation.
Relative permeability to water at maximum water saturation; i.e., floodout.	Generally less than 30%.	Greater than 50% and approaching 100%.

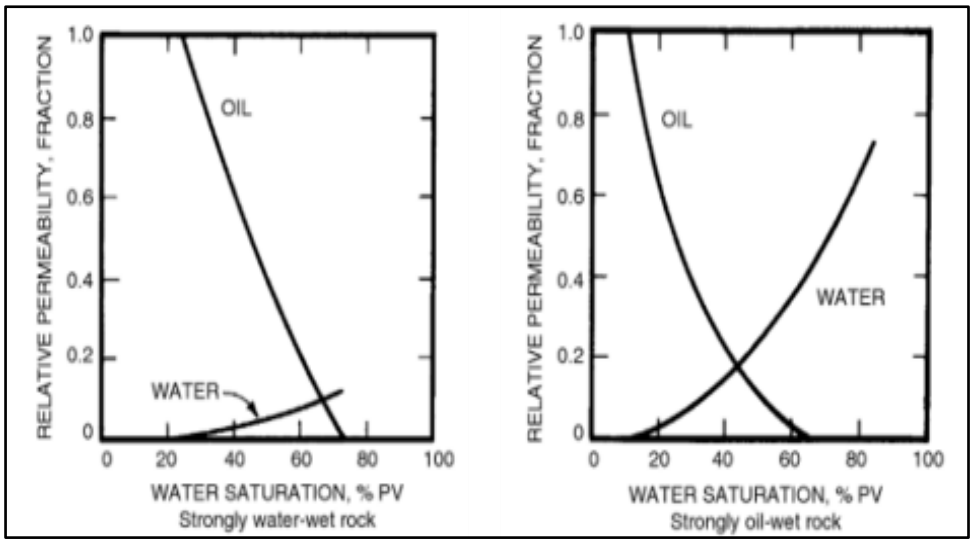

Figure 2-3 Relative Permeability Curves for Strongly Wetting (Craig, 1971)

The effect of wettability in the relative permeability influences the fluid distribution and flow in porous medium. As shown on Figure 2-3, the oil relative permeability is more concave than the strongly water-wet. In strongly wetting, the oil relative permeability decreases while the water relative permeability increases as the wettability alters to more oil-wet. In partially wetting (mixed wet system), the continuous oil-wet path alters the relative permeability.

2.3. Relative Permeability Correlation

The relative permeability of reservoir rock to each of the fluids flowing through is important in the prediction of reservoir behaviour. Several experimental measurements to determine the conductivity of porous rock to fluids and the factors affecting it have long been registered in the literature (Corey, 1954).

2.3.1. Corey-type Relative Permeability

Simplified relative permeability models can be created from experimental data by simulating a series of water saturation within constrained end-point values (S_{wirr} and S_{or}) as it is a simple power law function with only one empirical parameter, the power itself (Lomeland et al., 2005). Corey et al. created a simplified imbibition relative permeability correlation which it is generally valid for unconsolidated sands applying various empirical exponents which are power-law function of water saturation. Corey proposed a set of correlations for relative permeability in oil-water saturation; this model assumes the water and oil phase relative permeabilities to be independent of the saturation of the other phase and relative permeability

equations for water and oil phases (Torabi et al., 2015). However, the Corey model and similar models frequently show limitations to exhibit the flexibility that it is required to represent relative permeability for the entire saturation range; Corey's equation for water and oil relative permeability are expressed as follows (Corey, 1954):

$$k_{rw} = k_{rew} \, (S_{wn})^{n_w} \qquad 2\text{-}5$$

$$k_{ro} = k_{reo} \, (1 - S_{wn})^{n_o} \qquad 2\text{-}6$$

Where k_{rew} and k_{reo} are the end-points for water and oil relative permeability, respectively, n_w and n_o are respectively water and oil Corey exponent. The oil and water Corey exponent correspond to the rock wettability which determines the value of end-point of relative permeability and the curvature for a certain wet system. The consistency of these Corey exponent with the wettability is mandatory. (McPhee et al., 2015) generally correlated those Corey exponents with the wettability shown in the Table 2-2 below.

Table 2-2 Oil Water Corey Exponent with Wettability (McPhee et al., 2015)

Wettability	No (kro)	Nw (krw)
Water-wet	2–4	5–8
Intermediate-wet	4–6	3–5
Oil-wet	6–8	2–3

2.4. Mobility Ratio

The basic mechanics of the oil displacement by water can be understood by considering the mobilities of the separate fluids (Kantzas, Apostolos et al., 2016). The mobility of a fluid is defined as follows:

$$\lambda = \frac{K k_r}{\mu} \qquad 2\text{-}7$$

Where K is the absolute permeability and k_r is the relative permeability. The Mobility Ratio (M) is defined as the mobility of the displacing fluid behind the front (λ_w), divided by the mobility of the displaced fluid ahead of the front (λ_o):

$$M = {}^{\lambda_w}/_{\lambda_o} = \frac{k_{rw*}\mu_o}{k_{ro*}\mu_w} \qquad 2\text{-}8$$

Here the subscripts o and w refer to oil (displaced fluid) and water (displacing fluid). Below it is shown the phenomenon of oil displacement by water

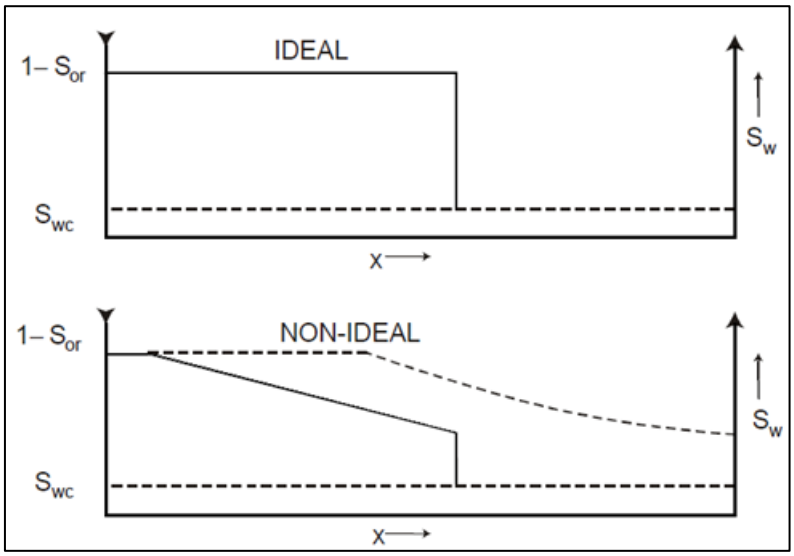

Figure 2-4. Water Saturation Distribution as a function of distance between injection and production wells for Ideal or Piston-like displacement (Above) and Non-ideal displacement (Below). (Kantzas, Apostolos et al., 2016)

For the ideal case, there is a sharp interface between the oil and water. Ahead of this, the oil is flowing in the presence of connate water, while behind the interface water alone is flowing in the presence of residual oil. This type of displacement will only take place if the ratio M' is known as the end point mobility ratio, since both k'_{ro} and k'_{rw} are the end point relative permeabilities, is a constant. If M ≤1 it means that, under an imposed pressure differential, the oil travels with a velocity equal to, or greater than of the water. As the water is pushing the oil, there is no tendency for the oil to be by-passed which yields in the sharp interface between the fluids.

The displacement shown in Figure 2-4 (a) is called "piston-like displacement". The most remarkable feature of this case is that the total amount of oil that can be recovered from a linear reservoir block will be obtained by the injection of the same volume of water which is also called the movable oil volume.

For the non-ideal displacement shown in Figure 2-4 (b) which is more common in nature, takes place when M>1. In this case, the water can travel faster than oil and, the non-wetting phase (oil) will be by-passed which leads to an early breakthrough of the displacing fluid and reduced

E_v because of the increased gravity segregation, unstable displacement and uneven flow through the layers owing to permeability variations. Also, water tongues or fingers create an unfavorable water saturation profile.

2.5. Wettability

Wettability is described as the preference of a solid to be in contact with one specific fluid rather than another (Abdallah et al., 2007). For reservoir rocks, the solid surface is composed of mineral grains, and the fluids in the pore are typically an immiscible combination of water, oil and gas; the wettability is mostly controlled by the balance of forces between the solid surface and the fluids and the interfacial tension between the fluids.

The wettability as such does not describe the saturation state of the rock; it does describe the preference of a solid surface to be contacted by a fluid. For instance, an oil-saturated water-wet rock when contacted by water will naturally imbibe water and eject oil. The saturation history of the material may influence the surface wetting; pore-wall surfaces previously contacted by oil may be oil-wet, but those never contacted by oil may be water-wet as shown in Figure 2-5.

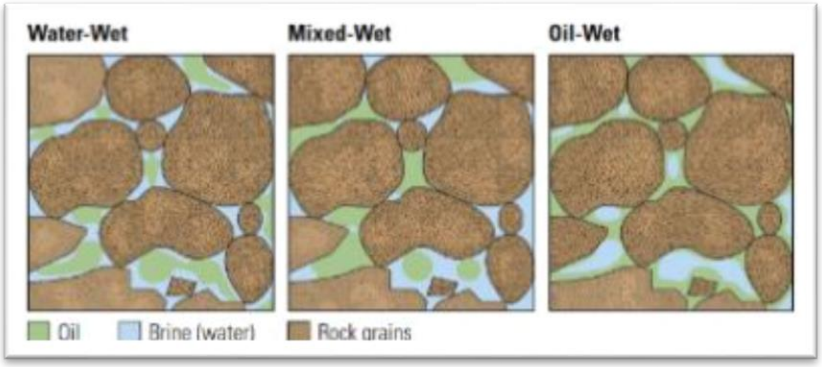

Figure 2-5 Wetting in pores (Nolen-Hoeksema, Richard, 2016)

The measurements of wettability on core samples included spontaneous imbibition and forced imbibition and centrifuge capillary pressure measurements. For example, if a core sample imbibes water spontaneously but not oil, it can be said it is water-wet; if a sample imbibes oil, it is oil-wet. In the case it imbibes significant amounts of both fluids, it is mixed-wet.

2.6. Characterization and Recovery Mechanism of NFRs

Most reservoir rocks are to some level fractured; however, the fractures have in many cases irrelevant effect on fluid flow performance and may be overlooked. Naturally fractured reservoirs, defined as reservoirs assumed to have fractures where they have an important impact on performance and oil recovery, fracture properties should be assessed because they control the efficiency of oil production (Fernø, M., 2012). These types of reservoirs are geological formations characterized by a heterogeneous distribution of porosity and permeability; the fractures are mostly caused by brittle failure induced by geological features such as folding, faulting, weathering and release of lithostatic pressure. For the most part, matrix blocks with low porosity and low permeability are surrounded by a tortuous, highly permeable fracture network. For this case, the fluid flow in the reservoir system strongly depends on the flow properties of the fracture network, with the isolated matrix blocks acting as the hydrocarbon storage.

The different properties of fracture and matrix determines the oil recovery mechanism. The flow-path-fracture affect advection flow and plays a dominating role on oil displacement and bypasses the oil-storage. On the other hand, the capillary action and gravity forces are the main parameters which determine the oil sweeping from the matrix to fracture. Figure 2-6 shows the imbibition process.

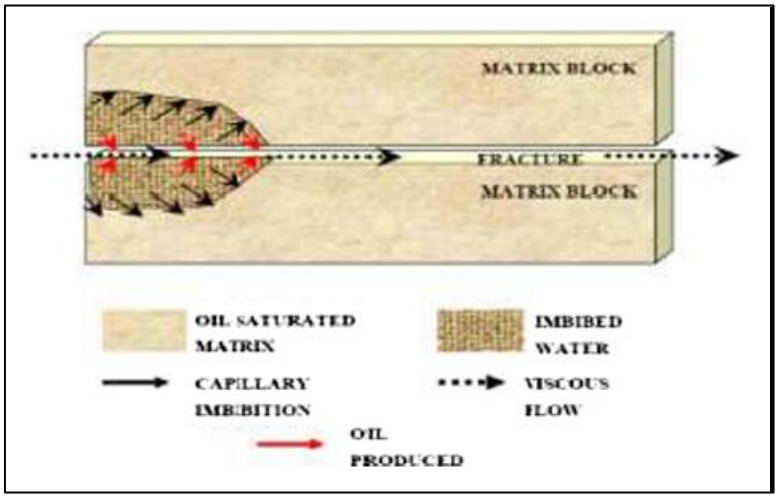

Figure 2-6 Schematic representation of the imbibition displacement process in fractured media (Meher, 2011)

The presence of fractures influences the flow of fluids in a reservoir because of the large contrast in transmissibility between the fracture and the matrix. The fractures with high permeability carry most of the flow, and therefore limit the build-up of huge differential

pressures across the reservoir (Fernø, M., 2012). In this scenario, the recovery mechanism is capillary imbibition rather than viscous displacement; the oil recovery by imbibition mechanism in fractured reservoirs is a significant research area in multiphase flow in porous media specially for water-flooding process in fractured oil reservoir (El-Amin, M.F.; Sun, Shuyu, 2011). The waterflooding works well with the water-wet condition, and imbibition can lead to significant recoveries, while poor recoveries and early water breakthrough occur with oil-wet condition. When other external drives like gravity or viscous forces are negligible, the boundary conditions control the type of displacement to be either counter-current spontaneous imbibition (COUCSI) or co-current spontaneous imbibition (COCSI) (Mirzaei-Paiaman et al., 2017).

2.6.1. Counter Current Imbibition

Counter current spontaneous imbibition is believed to be one of the principal mechanism of oil recovery from naturally fractured reservoirs. Basically, when brine is pumped into the porous rock, it flows primarily through the fractures and surrounds the matrix, avoiding the oil displacement (Unsal et al., 2009). In this fluid process, the oil and water flow in opposite directions and oil escapes by flowing back along the same direction along which water has imbibed (Behbahani et al., 2005). However, if the rock is wetted by the brine, then brine is drawn from the fractures into the pore space of the rock and to maintain the local volume balance, oil droplets are expelled back into fluid flowing in the fracture.

Counter-current occurs mainly because the core plugs are small and gravity forces are negligible compared to capillary forces. The matrix boundaries are usually either sealed or fully submerged in water (Haugen et al., 2014). Furthermore, it is often the only possible displacement mechanism for cases where a region of the matrix is surrounded by water in the fractures; experimentally this process can be studied by surrounding a core sample with water and measuring the oil recovery as a function of time. The imbibition rate is controlled by the permeability of the matrix, porosity, the oil/water interfacial tension and the flow geometry.

During the counter-current spontaneous imbibition, for instance, the flow has lower oil and water mobilities, lower mobile saturations (lower relative permeabilities) and higher viscous interactions (Fernø et al., 2015) which leads to an oil displacement less efficient compared to co-current. For counter-current laboratory measurements on small cores may underestimate both production rate and ultimate recovery when scaled to field conditions. Consequently, the low production of oil to produce counter currently is mostly induced by the role played by capillary back pressure explained further in the next sub-section.

2.6.2. The Capillary Back Pressure in the Counter-Current Production

The capillary back pressure is defined as the pressure difference between the non-wetting phase and the wetting phase at the brine face of the porous media (Fernø et al., 2015). For the case of spontaneous imbibition to progress, the imbibition pressure must be higher than the capillary back pressure to allow the non-wetting phase (oil) to escape from the largest pores. This is visually evident in experiments, where the non-wetting phase appears at the face of the core in the form of the small bubbles or droplets. In some cases, the non-wetting fluid may be produced as droplets that take some time to form and detach, making the capillary backpressure a function of time. The existence of oil snap off which lead to the formation of oil droplets at the inlet boundary depends on the water saturation at this point. This means the occurrence of the capillary back pressure is based on the applied water saturation in the inlet boundary (Foley et al., 2017).

2.6.3. Co-Current Imbibition

The co-current imbibition phenomenon, the water and oil flow in the same direction, and water pushes oil out of the matrix (Foley et al., 2017). Core plugs used in laboratory are generally much smaller than matrix blocks in oil producing fractured reservoirs where the block heights will promote co-current flow by gravity forces. Co-current imbibition occurs generally if the matrix blocks are partially exposed to water, for instance in gravity segregated fractures, where oil will flow favourably towards the boundary in contact with oil. The co-current imbibition is faster and can be more efficient than counter-current imbibition as the displacement efficiency is higher.

For core plugs, the co-current imbibition takes place when the boundary condition of the core is TEO (two-ends-open) where one end of the core (inlet) is in contact with the water (wetting phase), whereas the other end is in contact with the non-wetting phase (oil). With the TEO free spontaneous imbibition boundary condition, brine can enter one end of the core, but the oil can be produced from both ends. The production of oil occurs counter-currently from the end face in contact with brine if the oil pressure at the front exceeds the capillary back pressure at the open face. The counter-current production of oil ceases when oil cannot be produced against the back pressure. The pure co-current flow behaviour can be compared to an interface moving along a single capillary tube containing liquids at different viscosities (Haugen et al.,

2014). The schematic representation of the co-current imbibition is according to (Yadav et al., 2014) is shown in the Figure 2-7.

Figure 2-7 Schematic of Co-Current and Counter-current Imbibition for a piston-like TEO free spontaneous imbibition.

In the process of co-current imbibition, the capillary pressure developed by the interface pushes non-wetting phase out and draws wetting phase in. Depending on the viscosity ratio of the two phases the interface can speed up or slow down as imbibition advances (Haugen et al., 2014). For instance, if the tube is originally filled with an oil whose viscosity is the same as water, the displacement varies linearly with time. On the other side, if the tube is initially filled with viscous oil, then velocity will increase as the viscous oil is displaced from the tube.

2.7.Scaling Group of Spontaneous Imbibition

The spontaneous imbibition is a complex process, which depends on numerous variables such as the boundary condition, the fluid viscosity, the length of the core, the relative permeability, and the capillary pressure. The main goal is to predict the rate of recovery from fractured reservoirs from laboratory imbibition tests on rock samples. Hence, it is needed to study these parameters to understand their effects on the oil recovery and predict the effect on the production rate (Morrow & Mason, 2001). Due to significant differences on the recovery performances between counter-current and co-current imbibition processes, the corresponding scaling equations cannot interchangeably be used (Mirzaei-Paiaman et al., 2014). Several studies showed that the scaling equations developed for the COUCSI (Counter-current spontaneous imbibition) process fail to scale up the COCSI (Co-current spontaneous imbibition) data. The purpose of these equations was to extract a simple scaling equation free of capillary pressure and relative permeability functions; according to the authors, these scaling equations were then validated using a limited number of one-dimensional COCSI experiments obtained from literature with satisfactory results.

2.7.1. Boundary Condition Effect

In continuum modelling of imbibition experiments, the choice of boundary conditions plays an important role because the solution of the continuum equations depends upon them. The boundary conditions are the fixed points of the differential equations and are one of the few things that the experimentalist can control (Mason & Morrow, 2013). There are four types of boundary conditions that were taken by (Morrow & Mason, 2001) from several experiments (Figure 2-8), such as All Faces Open (AFO), One End Open (OEO), Two-Ends-Open (TEO), and Two Ends Closed system (TEC). Each boundary condition creates a different two-immiscible phase flow that contribute to the oil recovery. In this thesis, only TEO is specified for modelling co-current spontaneous imbibition.

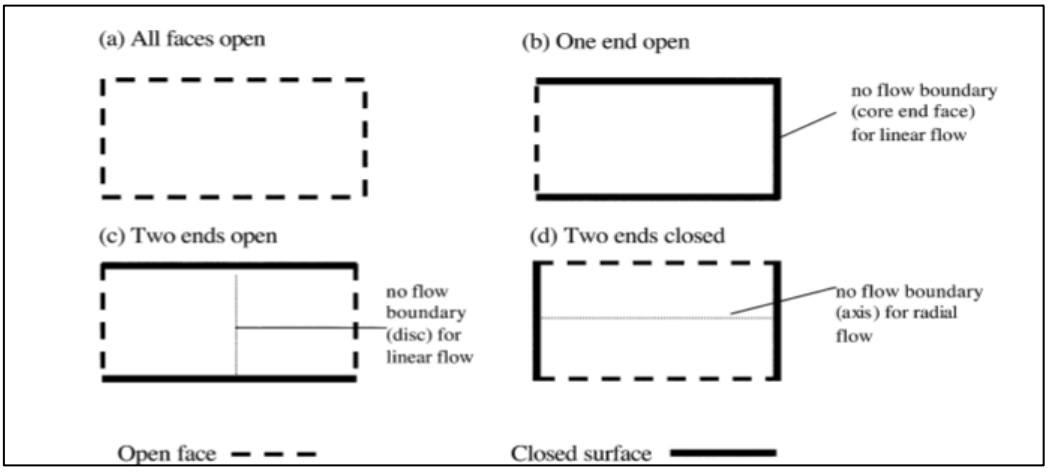

Figure 2-8 Type of Boundary Condition (Morrow & Mason, 2001)

2.7.2. Two-Ends-Open (TEO)

In this boundary condition, one-end of the core is in contact with the wetting phase while the other end-face is in contact with the non-wetting phase at the same pressure for both sides. When this boundary condition is used in horizontally positioned core plugs, the oil produced from each open end face was usually unpredictably asymmetrical, in despite of the amount of water imbibed from each end face was equal and symmetric with respect to the core centre (Fernø, M.A. et al., 2015) which implied that oil may flow across the so-called no-flow boundary at the middle of the core. The observed asymmetric oil production means that there must be simultaneous co- and co-counter-imbibition; the explanation lies in the need to overcome the capillary back pressure (CBP) at the outlet faces of the matrix. This pressure exists because the production mechanism at the open-end faces is like a drainage process and is determined by the largest pores at the surfaces (Haugen et al., 2014).

In a pure one-dimensional COCSI process, the WP enters the porous medium at a surface completely covered by the WP while the NWP leaves the porous medium at a surface completely covered by the NWP (Mirzaei-Paiaman et al., 2017). However, such a pure COCSI process does not exist and there is a minor backflow production of the NWP at the face covered by the WP.

2.8. Analytical Solution

The TEOFSI phenomenon corresponds to a sharp saturation front moving from the inlet to the outlet (Andersen et al., 2018). The total flux is uniform and equals the water flux behind the front u_w^L and the oil flux ahead the front u_o^R

$$u_w = -\frac{Kk_{rw}^{max}}{\mu_w} * \frac{P_w^{fr} - P_w^{inl}}{x_f} \quad (2\text{-}9) \qquad u_{nw} = -\frac{Kk_{rnw}^{max}}{\mu_{nw}} * \frac{P_{nw}^{out} - P_{nw}^{fr}}{L - x_f} \quad (2\text{-}10)$$

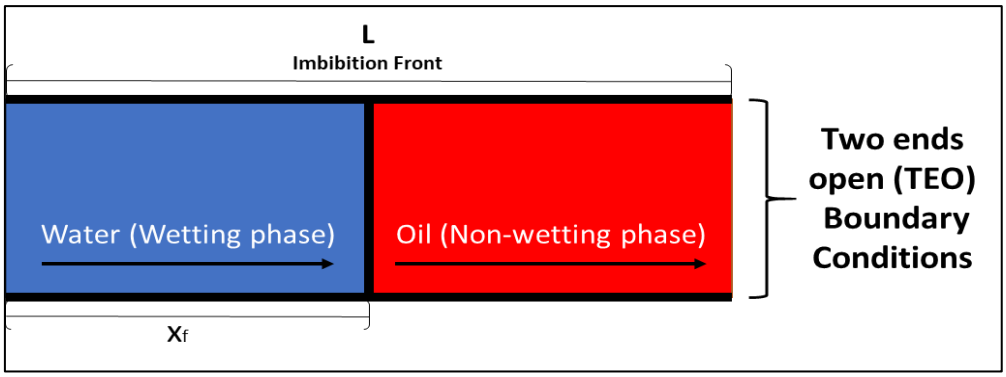

Figure 2-9 Picture of the spontaneous imbibtion phenomenon.

Where $u_w^L = u_o^R, p_w^{fr}, p_{nw}^{fr}$ denote the phase pressures at the front, p_w^{inl}, p_{nw}^{out} the external pressures which are equal to zero. p_{nw}^{fr} denotes the NW pressure at the core (x=L) and x_f the position of the front, measured from the inlet. $k_{rw}^{max} and\ k_{rnw}^{max}$ represents the end-points of the wetting phase and non-wetting phase permeabilities.

$$-\frac{Kk_{rw}^{max}}{\mu_w} * \frac{P_w^{fr} - P_w^{inl}}{x_f} = -\frac{Kk_{rnw}^{max}}{\mu_{nw}} * \frac{P_w^{fr} - P_w^{inl}}{L - x_f} \quad 2\text{-}11$$

The front pressures are related by the front capillary pressure:

$$p_c^{fr} = p_{nw}^{fr} - p_w^{fr} \quad 2\text{-}12$$

From the above relations, p_w^{fr} is obtained as follows

$$p_w^{fr} = \frac{\frac{Kk_{rnw}^{max}}{\mu_{nw}} * \frac{P_c^{fr}}{L-x_f}}{\frac{Kk_{rnw}^{max}}{\mu_{nw}} * \frac{1}{L-x_f} + \frac{Kk_{rw}^{max}}{\mu_w} * \frac{1}{x_f}} \qquad 2\text{-}13$$

Now, considering $u_T = u_W$ yields

$$u_T = -\frac{Kk_{rw}^{max}}{\mu_w} * \frac{P_w^{fr}}{x_f} \qquad 2\text{-}14$$

By replacing p_w^{fr} and making some mathematical procedures on the equation above yields the final expression for the flux shown below:

$$u_T = \frac{P_c^{fr}}{\frac{x_f}{\frac{Kk_{rw}^{max}}{\mu_w}} + \frac{L-x_f}{\frac{Kk_{rnw}^{max}}{\mu_{nw}}}} \qquad 2\text{-}15$$

From the expression above, the flux depends on the position of the front and the length of the column, the capillary pressure of the front, the viscosities of the wetting and non-wetting phases, the end-points relative permeabilities of the phases and the absolute permeability of the glass beads. As shown, the fluid mobility plays an important role on the imbibition rate because it determines the efficiency, the velocity and stability of the recovery process.

2.9.IORCoreSim Software (BugSim Version 1.2)

In this thesis, IORCoreSim simulator software is used for creating one-dimensional model based on experimental data to investigate spontaneous imbibition process in numerical simulation. This type of software is a second version of simulator *Bugsim* that has been developed by Arild Lohne to investigate oil recovery mechanism (MEOR) at laboratory and in small-field-scale model (Lohne, 2013).

The purpose of simulating experiments was to extract properties which could be used to further simulate and predict the processes at other conditions (Andersen et al., 2017). In a reservoir simulator, the flow of two phases inside a formation is a function of absolute properties (Absolute permeability and porosity) and saturations functions (Relative permeability and capillary pressure)

3. Mathematical and Numerical Model Description

3.1. Mathematical Model of Co-Current Imbibition

A mathematical model for co-current imbibition has been described by (Andersen et al., 2017). Consider the transport equation for water and oil in 1D homogeneous incompressible reservoir rock with incompressible fluid as follows:

$$\varphi \frac{\partial S_w}{\partial t} + \frac{\partial U_w}{\partial x} = 0 \qquad 3\text{-}1$$

$$\varphi \frac{\partial S_o}{\partial t} + \frac{\partial U_o}{\partial x} = 0 \qquad 3\text{-}2$$

Where S_w and S_o is water and oil saturation respectively, φ is porosity and it has been assumed that there are no external source terms. The two phases flow is dominated by Darcy's velocity where the water enters the open face with its velocity (U_w) and the oil flows out from the core with its velocity (U_o) co-currently to the other open face. The Darcy's velocity for each phase (i = o, w) are expressed by absolute permeability (K) and pressure gradient as follows

$$U_i = -\lambda_i \frac{\partial P_i}{\partial x} \qquad 3\text{-}3$$

where the gravity is neglected and the fluid mobility (λ_i) is defined as,

$$\lambda_i = \frac{K k_{ri}}{\mu_i} \qquad 3\text{-}4$$

where kr_i is fluid relative permeability and μ_i is fluid viscosity.

The saturations and pressures are constrained by the following equations

$$S_w + S_o = 1 \qquad 3\text{-}5$$

$$P_c\,(S_w) = P_o - P_w \qquad 3\text{-}6$$

The co-current flow is described by Andersen et al. (2017 & 2018) which expresses the total velocity (U_T) as:

$$U_T = U_o + U_w \qquad 3\text{-}7$$

Summing the equations for oil and water 3-1 and 3-2 yields

$$\partial_t\big(\varphi(S_o + S_w)\big) = -\partial_x\big((U_o + U_w)\big) = -\partial_x(U_T) = 0 \quad \text{3-8}$$

Shows that the total Darcy velocity $U_T = (U_o + U_w)$ has zero divergence.

From 3-6 P_c is the capillary pressure, which is a known function. Summing both oil and water mass conservation results in water pressure change per unit length of reservoir, $(Pw)_x$

$$\frac{\partial P_w}{\partial x} = -\frac{\lambda o}{\lambda_T}\frac{\partial P_c}{\partial x} \qquad \text{3-9}$$

Furthermore, the fractional flow function is introduced which it is defined below

$$f_w = \frac{\lambda_w}{\lambda_w + \lambda_o} = (1 + \frac{\mu_w}{\mu_o}\frac{k_{ro}}{k_{rw}})^{-1} \quad \text{3-10}$$

Using equations 3-5, 3-6, 3-8, 3-9 and 3-10, the variables P_w, P_o, S_o are replaced by $P_c(S_w), U_T, f_w(S_w)$. The equation 3-1 can then be written into 3-11 which produces the water transport equation which include fractional water flow parameter. For this expression, the change in storage is affected by an advective term and a capillary diffusion term.

$$\varphi\frac{\partial Sw}{\partial T} + \frac{\partial}{\partial x}\Big(U_T\, f_w + K\,\lambda_o\, f_w\,\frac{\partial P_c(Sw)}{\partial x}\Big) = 0 \qquad \text{3-11}$$

3.1.1 Initial and Boundary Condition of Co-Current Imbibition

a) Initial condition is specified as follows:

$$S_w(x,0) = S_{w,i}(x) \quad \text{3-12}$$

$$P_w(x,0) = P_{w,o}(x) \quad \text{3-13}$$

b) Boundary condition at the inlet (x = 0) is in contact with water and the flow water is governed by water pressure (P_w) such as

$$S_w(0,t) = 1 \quad \text{3-14}$$

At the outlet (x=L), only oil is in contact with and produces at the outlet and the controlled oil pressure (P_o) influence the oil displacement,

$$S(L,t) = 0 \quad \text{3-15}$$

$$P_w(L,t) = P_o\,(t) - P_c(S_w(L,t)) \quad \text{3-16}$$

$$f_w(L,t) = 0 \quad \text{3-17}$$

3.2. Numerical Model

3.2.1. Grid Model

In this thesis, the model is built in the cartesian coordinates that divides the length of model which approximately 40 cm in x direction with 100 grid blocks. For simplicity, one-dimensional model is built, the cartesian coordinates will be 100 x 1 x 1 in x, y, and z-direction respectively. To imitate the experimental setup by Meng et al., initially the model is assumed to be saturated with 100% oil and using the TEOFSI boundary condition, let the water to be in contact at the open-inlet and the oil is in contact with the open-outlet. Since experimental setup used the cylindrical tube, the cross-sectional area in the tube must be the same as in 1D cartesian grid model is required. The correction of radius tube for constant cross-sectional area is described in the sub-section 4.5 in the chapter 4. The residual oil saturation for all experiment is approximately in the range of 0.10. The average fractional porosity and the residual oil saturation for all experiment is mentioned in the Table 3-1. The built model is shown in the Figure 3-1.

Table 3-1 The Grid Properties Model

Purpose	Grid Properties of Model								
	Sandpack Length [cm]	Corrected Width of Tube [cm]	x	y	z	Fractional Porosity (φ)	k [mD]	S_{wi}	S_{or}
For Sensitivity Analysis	40	0.8720	1-100	1	1	0.362	3540	0	0.1
History Matching	40	0.8720	1-100	1	1	0.362	3540	0	0.08

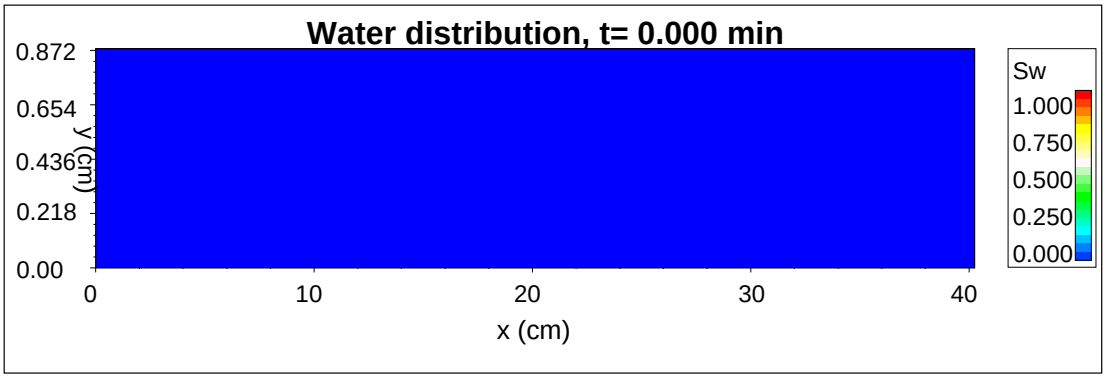

Figure 3-1 The Cartesian Grid Model that Used for Simulation with Initial Condition

3.2.2. Flow Modelling

One-dimensional model is built using IORCoreSim software that generated by Lohne, A. (2013). Referred to the manual of this software, “wimb” and “wprod” keywords are the main controller to generate the boundary condition in the model to be two-ends open free spontaneous imbibition TEOFSI (Lohne, 2013). “wimb” keyword defines the imbibing fluid and “wprod” keyword defines the fluid that want to be produced. Since the model allows for both counter-current and co-current flow to occur, those keywords are thus specified in the input data. Regarding this software, the flow equation in the model, which is described by Lohne, A. (2013) is expressed as follows:

There are two flow occurs at the inlet mode, such as counter-current and co-current flow. Counter-current flow push the oil to produce through the inlet, while co-current flow force water to imbibe the model. These flow equations expressed by,

$$Q_{k,o,prod} = -T_{w,k}\,\lambda_{k,o}(P_{w,k} + P_{cb,o} - P_{i,o} + d_{hz}\gamma_o) \quad 3\text{-}20$$

$$Q_{k,w,inj} = T_{w,k}\,\lambda_{k,t}(P_{w,k} - P_{i,w} + d_{hz}\gamma_w) \quad 3\text{-}21$$

where $Q_{k,o,prod}$ and $Q_{k,w,inj}$ is volumetric flow rate of displaced phase (oil) and the imbibing phase (water) for interval k connected to cell *i*, respectively. λ_l is fluid mobility, and $\gamma_l = \rho_l g.\, d_{hz}$ defines the height difference between the boundary connection k and the center of cell *i*. $P_{cb,o}$is additional boundary capillary pressure. $P_{w,k}$is water pressure in the connection k. $P_{i,l}$ is fluid pressure in the center of *i*. $T_{w,k}$ is the transmissibility or connection factors with flow in x-direction for open face condition that is given by

$$T_{w,k} = \frac{2k_x \Delta y_i \Delta z_i}{\Delta x_i} \quad 3\text{-}22$$

By referring the concept of capillary back pressure in the sub-section 2.5.2 (chapter 2), the counter-current production occurs as the oil pressure in the center of cell *i* is lower than oil pressure in the interval k and oil boundary pressure,

$$P_{i,o} < (P_{w,k} + P_{cb,o}) \quad 3\text{-}23$$

This type of production starts to cease if the oil is snap off in the inlet and hard to form the droplet. Once the counter-current production is stopped, hence, the additional oil boundary pressure is equal to the oil pressure in the center of cell *i*,

$$P_{cb,o} = P_{i,o} \quad 3\text{-}24$$

Note that the imbibition process uses downstream total mobility, λ_t, while the production uses upstream fluid mobility, λ_l. At the production boundary, only flow out of the model is allowed. Since only oil is produced, then the oil flow equation will be,

$$Q_{k,o,prod} = -T_{w,k}\,\lambda_{k,o}(P_{w,k} + P_{cb,o} - P_{i,o} + d_{hz}\gamma_o) \qquad 3\text{-}25$$

4. INTERPRETATION DATA

Input data to run simulations for this thesis are taken from experimental results by (Meng et al., 2015) from China University of Petroleum. There are 4 types of experiments conducted with two different experimental setups, one for the air-brine experiment and the others for the Oil-Brine experiments. In the following section, the information about the glass column tube, fluids properties, glass beads properties, and fluid preparation of the experiment with the selected experimental results are outlined.

4.1. Experimental Results

The experimental setup by (Meng et al., 2015) for spontaneous imbibition experiments on a glass columns filled with glass-beads was selected for this thesis. For these experiments, the piston-like displacement was used for all the cases where the non-wetting phase was displaced by the wetting phase, the oil recovery results for the four experiments are outlined below in the Table 4-1 and are plotted against time shown in the Figure 4-1. As seen on the figure, as the viscosity of the non-wetting phase increases, the breakthrough time takes more time to occur and the oil recovery decreases. Also, for the first two cases (Air and kerosene) the oil recovery showed a decreasing trend and for the other two cases (WHO No. 15 and WHO No. 32) the oil recovery showed an increasing trend.

Table 4-1 Summary of Experimental Setup for glassbeads.

Experiment	Porosity	Oil Recovery at Breakthrough [fraction]				Oil Recovery at residual oil saturation [fraction]		
		Breakthrough time (min)	Counter-Current	Co- Current	Total	Counter-Current	Co- Current	Total
Air	0.362	42		0.900	0.900		0.908	0.908
Kerosene		210	0.015	0.880	0.896	0.015	0.881	0.897
White oil-15		780	0.019	0.862	0.881	0.019	0.868	0.887
White oil-32		2720	0.020	0.851	0.871	0.020	0.853	0.873

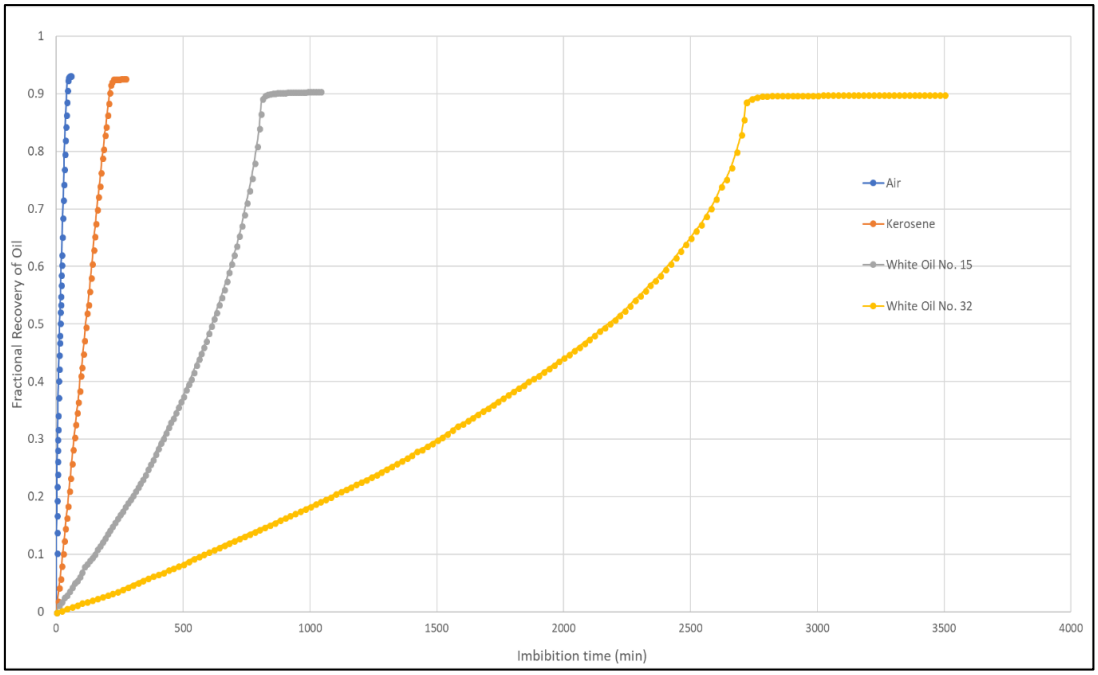

Figure 4-1 Oil/gas recovery vs. Imbibition time for glass-beads packs (Meng et al., 2015).

4.2. Glass Column Properties

A glass column was filled with glass beads; the column had an inner diameter of 0.984 cm and a length of 41 cm. For the experiments, the plexiglass column was chosen because of the material resistance whose properties are given in the Table 4-2. A ruler was placed above of the glass column to measure the advancing distance of the imbibition front. For this experiment, the end piece was used to ensure that the entire cross-section of the packed column was open to brine. The air vent, which could be used to remove the air in the end piece and inlet tube, was punched at the top of the end piece. A wire mesh was used to hold the glass beads at the left side of the glass column and the right side was sealed using a rubber stopper. The glass column is shown in the Figure 4-2.

Table 4-2 Imbibition Glass Column Properties

Glass Tube Properties		
Column Length [cm]	Inner Diameter of the Column [cm]	Glass column material
41	0.984	Plexiglass

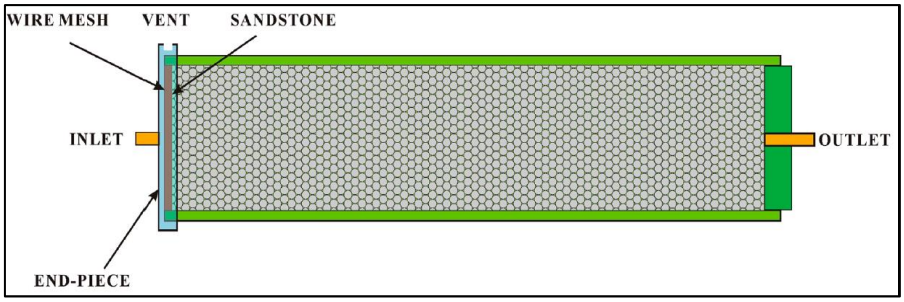

Figure 4-2 Schematic of the glass column used to contain glass beads (Meng et al., 2015)

4.3.Fluid Preparation

4.3.1. Fluids Properties

There are five types of fluids used in the experiments. A synthetic reservoir brine used as the wetting phase; air, kerosene, white oil-15, and white oil-32 used as the non-wetting phase. The fluids properties are listed in Table 4-3.

Table 4-3 Properties of fluids used in the Experiments (Meng et al., 2015)

Fluids	**Density, ρ (g/cm3)**	**Viscosity, μ (cP)**	**Interfacial tension (mN/m)**
Brine	1.02	1.00	
Air	0.0013	0.0018	72.1
Kerosene	0.80	2.8	30.1
White Oil-15	0.83	25.6	38.4
White Oil-32	0.84	103.4	42.3

4.3.2. Permeabilities of the packed column for the glass beads experiment

The properties of the permeability of the packed column for the glass beads experiment are shown in the Table 4-4.

Table 4-4 Permeability of the packed column for the glass beads (Meng et al., 2015)

Fluid	**Glass beads packed column (mD)**
Air	3528
Kerosene	3563
White Oil-15	3523
White Oil -32	3540

4.4. Experimental Setup

A schematic of the experimental apparatus is shown in Figure 4-3. A ruler was placed above the glass column to measure the advancing distance of the imbibition front. The glass-measuring cylinder was used as a fluid collector. Because air could not be collected by a fluid collector, it was collected in a sealed bottle such that the equivalent volume of water was expelled into the fluid collector. The water level in the water container, the packed glass column, the water level in the sealed bottle, and the open end of the outlet tube were all the same level during the imbibition experiments, so that the effect of gravity could be neglected.

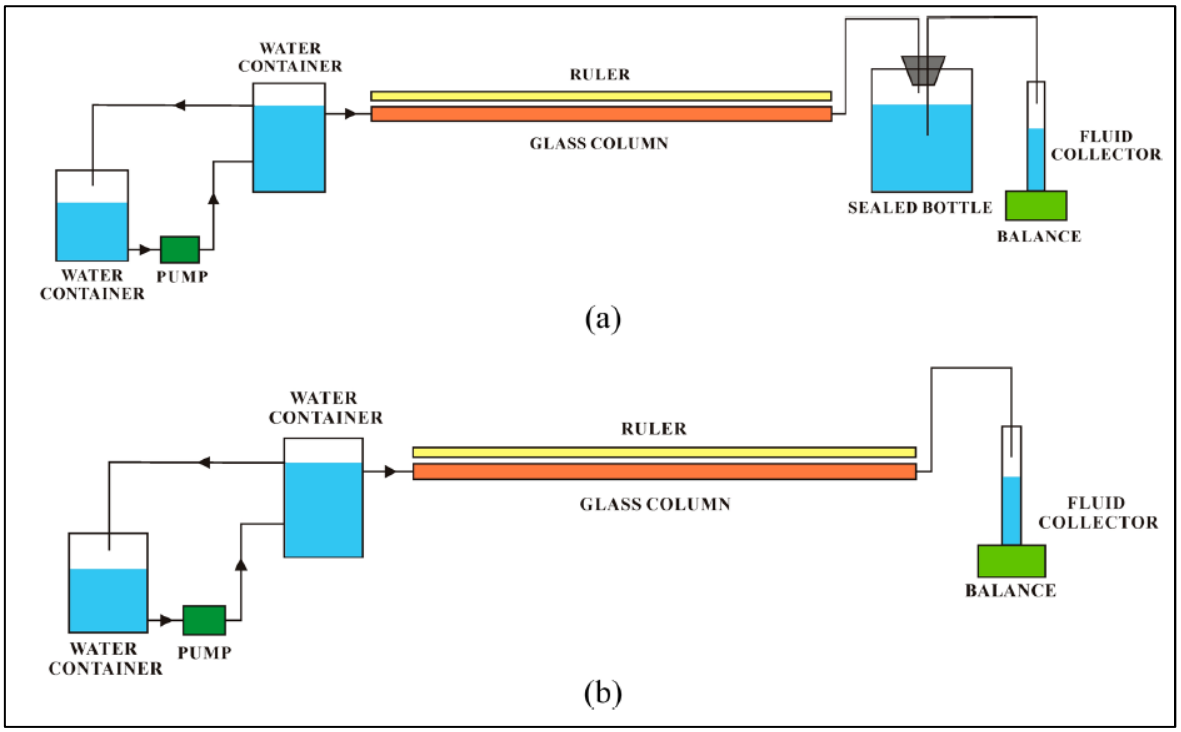

Figure 4-3 Schematic of the apparatus for spontaneous imbibition experiments: (a) Apparatus for air-brine experiments and (b) apparatus for oil-brine experiments (Meng et al., 2015).

4.5. Interpretation Data for Input Model

As one of the main objectives of this project is to simulate spontaneous imbibition for an oil recovery process for four different fluids (non-wetting phase) with the same displacing fluid, some information are needed to run the simulations based on the experimental setup. For the chosen experiments, the imbibition properties are identical except for fractional porosity and absolute permeability that vary for each experiment. For building the numerical model, an average porosity and absolute permeability are required, the glass column length and petrophysical properties of the porous medium are outlined in the Table 4-5. For simplicity, the cartesian grid is used for the model geometry. Thus, the correction of cross section area for 2 phases flow is required. The area of the cylinder glass column is obtained as follows

$$Area_{circle} = \frac{\pi}{4} D^2 = \frac{3.14153}{4} (0.984\ cm)^2 = 0.7604\ cm^2$$

Assume a circle is inscribed in a square, the circle diameter is equal to the side length of the square. To obtain the cross section area, the square side length (s) should be:

$$s_{square} = \sqrt{Area_{circle}} = \sqrt{(0.7604\ cm^2)} = 0.8720\ cm$$

Hence, the corrected width and height for cartesian grid are shown in the Table 4-5:

Table 4-5 Corrected glass column dimensions for cartesian grid.

Properties of Glass Column				
Length [cm]	**Width [cm]**	**Height [cm]**	**k [mD]**	**φ**
40	0.8720	0.8720	3540	0.362

4.5.1. Reference J-Function Curve for Sensitivity Analysis and Curve Match.

Reference J-Function curve is built based on the equation outlined below. The following table contains the parameter values for the J-Function curve shown below in the Figure 4-4.

Table 4-6 Parameter Values Forming Reference Capillary Pressure Curve

Parameter Capillary Pressure Curve								
C_{L1}	C_{R1}	C_{01}	E_{L1}	E_{R1}	S_{L1}	S_{R1}	ϕ [fraction]	k,abs [mD]
0.000998	0.010	0.995	3.0	5.0	1	-0.37	0.362	3540

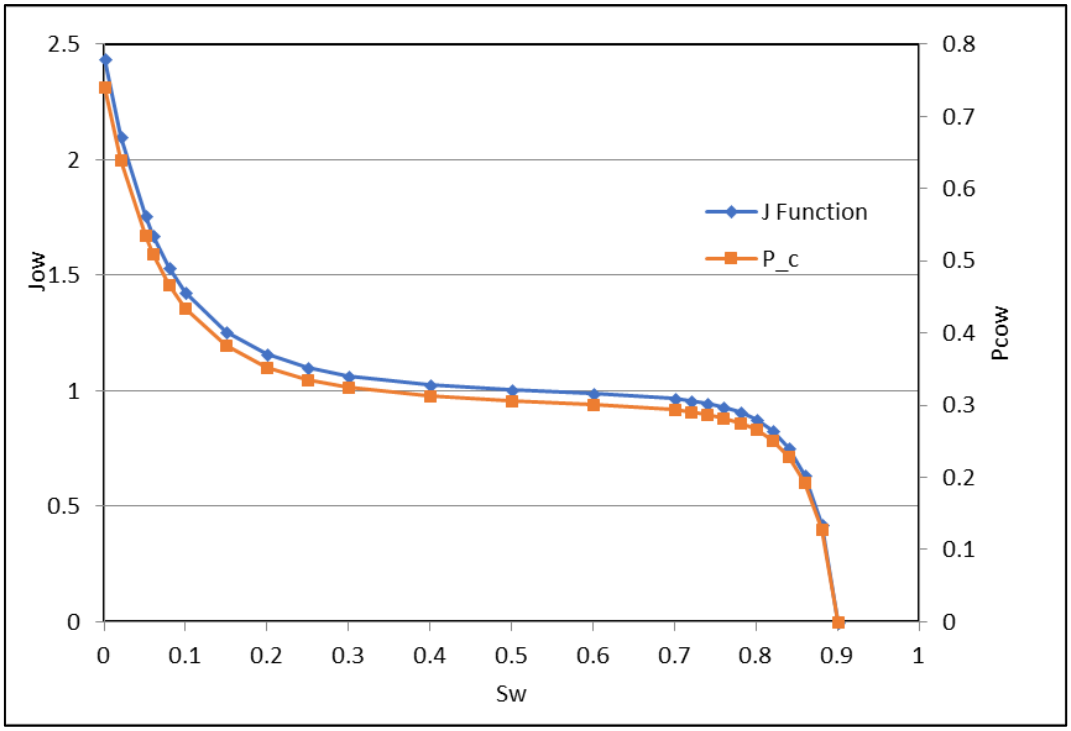

Figure 4-4 The Reference J-Function and Capillary Pressure Curves.

The Capillary Pressure input should be specified for the simulations, missing input will result in zero capillary pressure. The capillary pressure correlation used in this software as input data is J-function outlined below:

$$J_{ow} = C_{L1}\,(S_w - S_{L1})^{-E_{L1}} - C_{R1}\,(S_{R1} - S_w)^{-E_{R1}} + C_{01} \qquad 4\text{-}1$$

$$P_{cow} = P_o - P_w = J_{ow} IFTow \sqrt{\frac{\varphi}{K_{abs}}} \qquad 4\text{-}2$$

$$C_{01} = C_{L1}\,(1 - S_{or} - S_{L1})^{-E_{L1}} - C_{R1}\,(S_{R1} - 1 - S_{or})^{-E_{R1}} \qquad 4\text{-}3$$

Where J_{ow} is J-function for oil-water, S_w is water saturation, C_{L1} and C_{R1} are capillary pressure parameter, S_{L1} and S_{R1} are minimum and maximum saturation parameters, respectively, E_{L1} and E_{R1} are respectively first and second capillary pressure exponent, and lastly, C_{01} is capillary pressure constant (Lohne, 2013).

4.5.2. Reference Relative Permeability for Sensitivity Analysis and Curve Match.

Reference relative permeability curve is built based on Corey's equation outlined below. Since the model is assumed to be only strongly water-wet, only one saturation table will be generated.

Table 4-7 Parameter Value Forming Reference Relative Permeability Curve

Parameter Relative Permeability Curve			
k_{rew}	0.300	n_w	6
k_{reo}	1	n_o	2

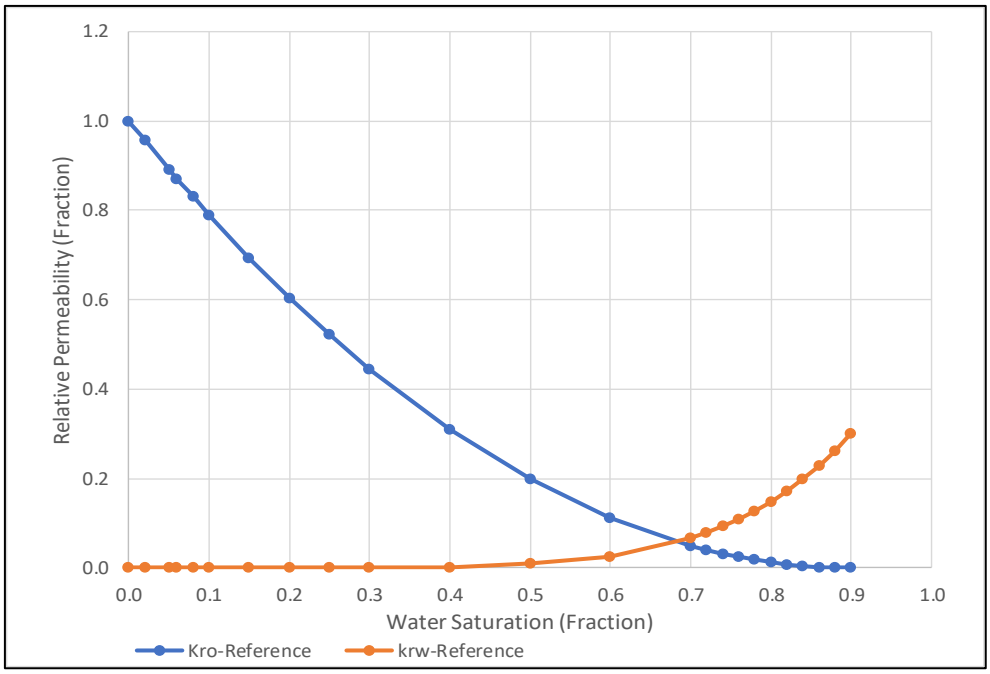

Figure 4-5 Reference Relative Permeability Curve

4.5.3. Capillary Pressure Correlation in IORCoreSim Software (BugSim Version 1.2)

For relative permeability correlation, the Corey-type relative permeability to generate flow in the model. The model Corey's equation expressed However, the notation of Corey's equation in the IORCoreSim is different (e.g. in the notation of Corey exponent) that is expressed as follows,

$$k_{rj} = k_{rej} \left(\frac{S_j - S_{rj}}{1 - S_{rj}}\right)^{E_j} \qquad 4\text{-}4$$

where j is for oil, water, and gas. k_{rj} is fluid relative permeability and k_{rej} is the end-point fluid relative permeability. $S_j$is fluid saturation and S_{rj} is residual fluid saturation. E_j is fluid Corey exponent (Lohne, 2013).

4.6. Model assumptions

To run the simulations, it is necessary some assumptions to make the model simple which are outlined below:

1) 1D horizontal incompressible porous medium.
2) Immiscible 2-phase flow of incompressible fluid where the wetting phase displaces the non-wetting phase under the piston-like displacement.
3) Porous medium is 100% oil saturated ($S_{wr} = 0$) and strongly water-wet.
4) $Pc > 0$ to initiate spontaneous imbibition.
5) Neglecting the play role of paper filter in the system to allow counter-current production.
6) Boundary condition is two ends open (TEO) by the inlet side is in contact with water (wetting phase) and the other side is in contact with oil (non-wetting phase)

5. RESULT AND ANALYSIS

5.1. Sensitivity Analysis

The technological advances on computer performance and more efficient numerical methods has made possible the solution of complex mathematical models (Langtangen, 1991). As explained in previous sections, this thesis project consists of solving out a mathematical model in terms of partial differential equations for one-dimensional multiphase porous media flow which contains physical assumptions and input data that are subject to large uncertainties. There are several uncertain physical input parameters to reservoir simulation models ranging from rock properties to rock-fluid mixtures properties to pure fluid parameters. The input parameters are ranked according to their computed impacts on the time to water breakthrough in the production well and the main goal is to gain a better understanding of the dynamics of the recovery process.

A parametric study was carried out to evaluate the influence of relative permeability, viscosity ratio, glass column length, capillary pressure, and mobility ratio on the production rate and the oil recovery. This investigation can also improve the coherence of production profile with experimental result during history matching. For the scope of this thesis project, the water breakthrough is defined when the water has reached the outlet or the producer owing to the capillary effect.

5.1.1. Parameter Study of Relative permeability

In co-current spontaneous imbibition which involves immiscible two-phase flow system, the relative permeability correlation of Corey Exponent is applied. To analyse the parameters, Corey exponent for water and oil are adjusted to investigate a change of water breakthrough time and the oil recovery. There are 2 cases which will be analysed in the model, such as:

5.1.1.1. Case A: Change of oil recovery with increasing n_w with constant n_o for mobility ratio M = 0.84

In this case, water Corey exponent (n_w) is adjusted from the reference relative permeability to investigate the change of oil recovery. The altered water Corey exponent causes a modification on the end-point of water relative permeability pictured in the Figure 5-1 and whose equation is outlined above in the section 4.5.3. Note that oil relative permeability is kept constant during the parameter study due to the model is 100% oil saturated at irreducible water saturation (S_{wr}=0).

Table 5-1 Parameter of Relative Permeability for Case A (an increase of water Corey exponent)

μ_o/μ_w = 2.8 (μ_o = 2.80 & μ_w = 1.00)			
	Case A1	Reference	Case A2
n_w	2	6	10
k_{rew}	0.7	0.3	0.105
n_o	2		
k_{reo}	1		

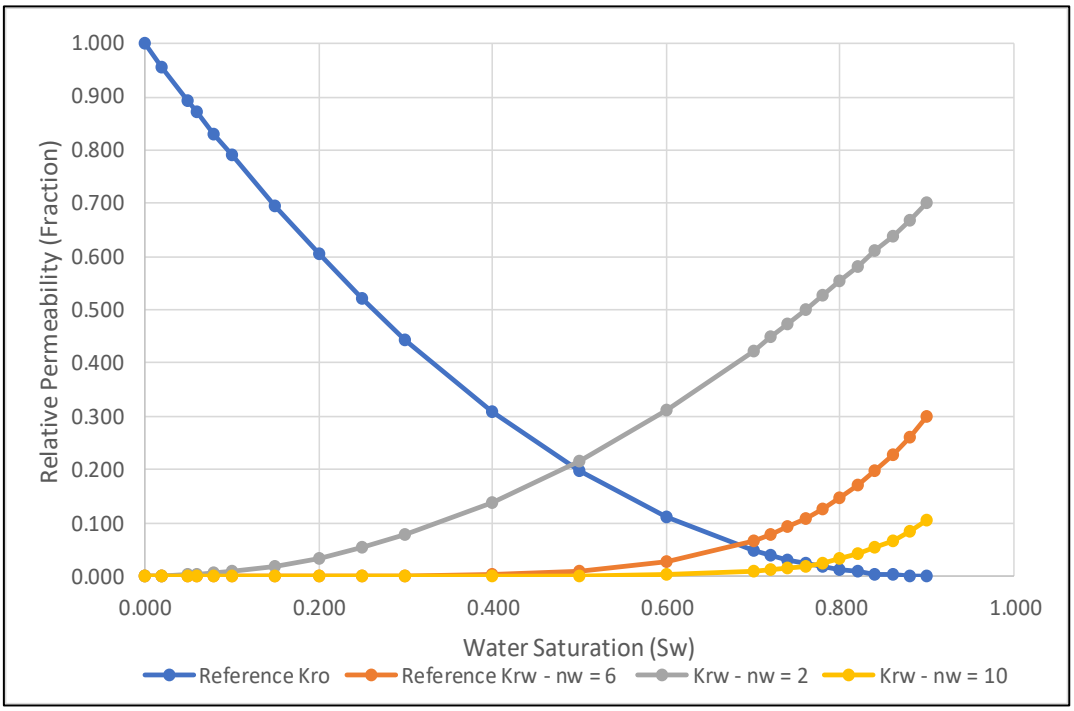

Figure 5-1 Relative Permeability Curves - Case A (An Increase of Water Corey Exponent).

The Figure 5-1 shows that the relative permeability curve moves to the right as the end-point of water relative permeability decreases and the water Corey exponent increases. As several relative permeability curves are plotted, the analised parameter is assessed by studying the impact of those different relative permeability curves on the oil recovery. The results and charts are outlined below:

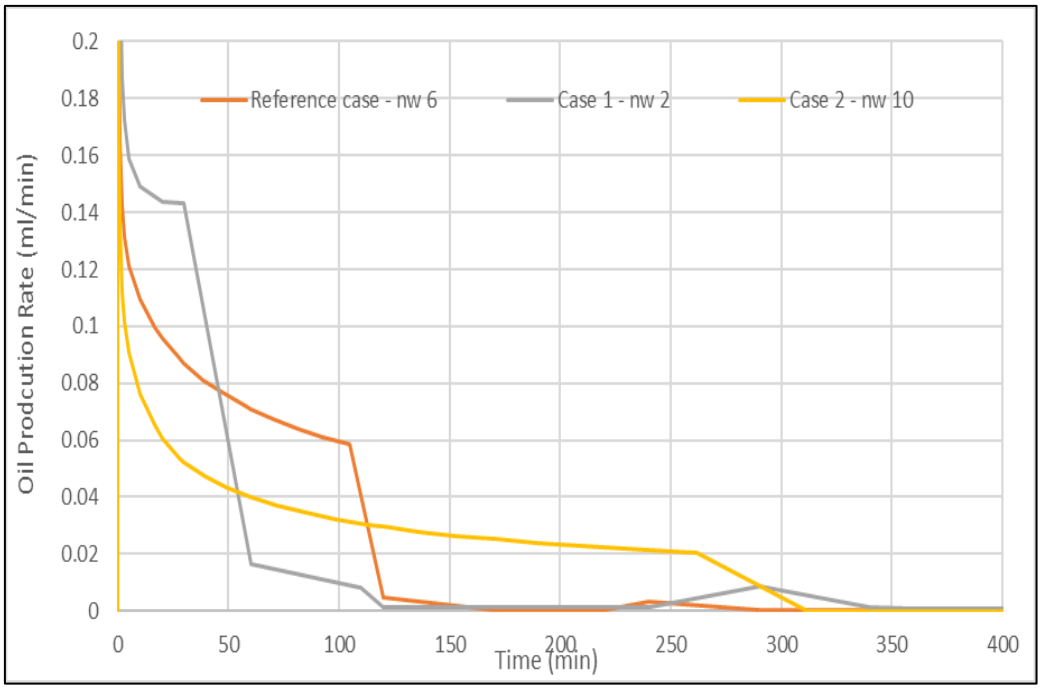

Figure 5-2 Total (Co-Current + Counter-Current) Oil Producation Rate - Case A (An increase of water Corey exponent)

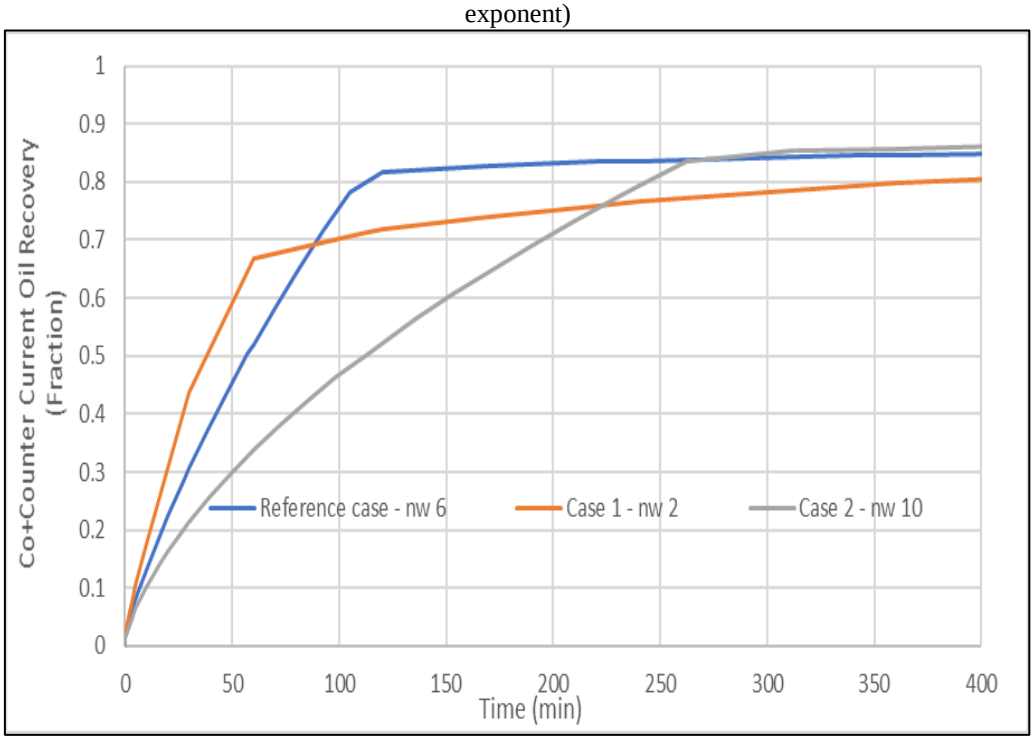

Figure 5-3 Total (Co-Current + Counter-Current) Oil Recovery - Case A (An increase of water Corey exponent)

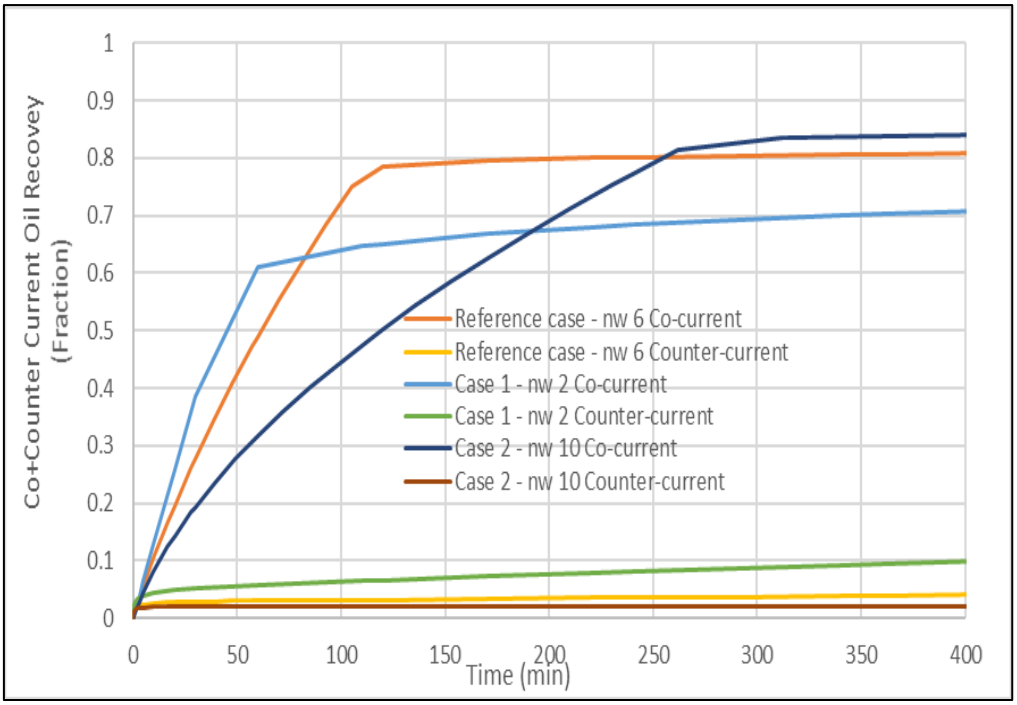

Figure 5-4 Co-Current + Counter-current Oil Recovery - Case A (an increase of water Corey exponent)

On Figure 5-2 a delay and decrease on oil production rate can be observed as water Corey exponent increases. By increasing the exponent, a drop on water relative permeability end-point takes place which makes the oil production rates declines gradually, so the oil production rate is influenced by the water relative permeability. By comparing Figure 5-2 and Figure 5-3, the water breakthrough and the drop of oil production rate are linearly proportional; the more time it takes water breakthrough to occur, the more oil is recovered.

Also, when n_w=2 and k_{rw}=0.7 the mobility ratio is above 1 where an early breakthrough is seen and a lower oil recovery is obtained as the velocity of water is higher than oil. On the other hand, when n_w=10 and k_{rw}=0.105 the mobility ratio is below 1 which means the oil travels faster than water, makes the process more efficient, more oil is recovered and water breakthrough takes place at a later time as shown on the Figure 5-2. In the Table 5-2, after the breakthrough, the total oil recovery continues increasing until it reaches the maximum oil recovery at the residual oil saturation which is 90% of the pore volume.

Table 5-2 The Change of Oil Recovery with Increasing water Corey Exponent

	Break-through Time [min]	**Oil Recovery at the Breakthrough**			**Oil Recovery after the Breakthrough**		
		Counter Current	**Co Current**	**Total**	**Counter Current**	**Co Current**	**Total**
Case A1 ($n_w = 2$)	30	0.057	0.385	0.438	0.130	0.749	0.88
Ref. ($n_w = 6$)	105	0.032	0.750	0.782	0.055	0.825	0.88
Case A2 ($n_w = 10$)	262	0.021	0.814	0.835	0.028	0.859	0.89

5.1.1.2. Case B: Change of oil recovery with increasing n_o with constant n_w for mobility ratio M = 0.84

For case B, the oil Corey exponent is adjusted from Reference Relative Permeability to investigate the Oil Recovery. Like case A above, the oil relative permeability end-point is kept constant due to the initial conditions of the model. The Table 5-3 contains the values of oil Corey exponent.

Table 5-3 Parameter of Relative Permeability for Case B (an increase of oil Corey exponent)

μ_o/μ_w = 2.8 (μ_o = 2.80 & μ_w = 1.00)			
	Reference	Case B1	Case B2
n_o	2	4	6
k_{reo}	1		
n_w	6		
k_{rew}	0.300		

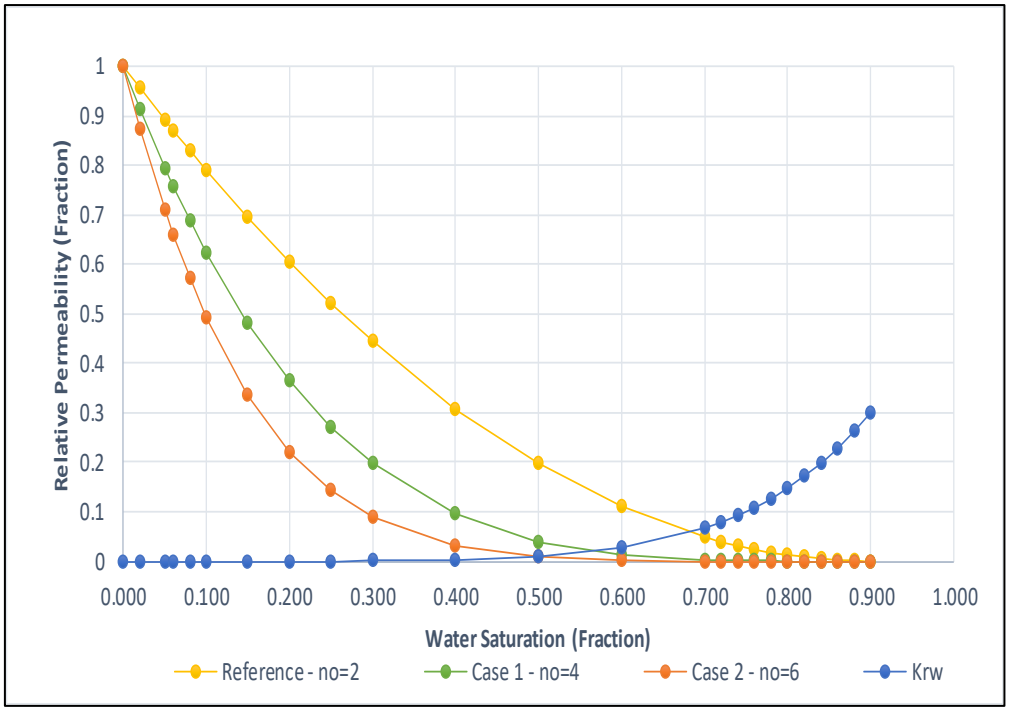

Figure 5-5 Relative Permeability Curves - Case B (an increase of oil Corey exponent)

The Figure 5-5 shows that the relative permeability curve shifts to the left as the oil Corey exponent increases which causes the shape of oil relative permeability be more concave up. The end point of water and oil relative permeability remained constant; as the various relative permeability curves are generated, the parameter study is assessed by exploring the impact of the different relative permeability curves on the oil recovery. The results and analysis are explained as follows:

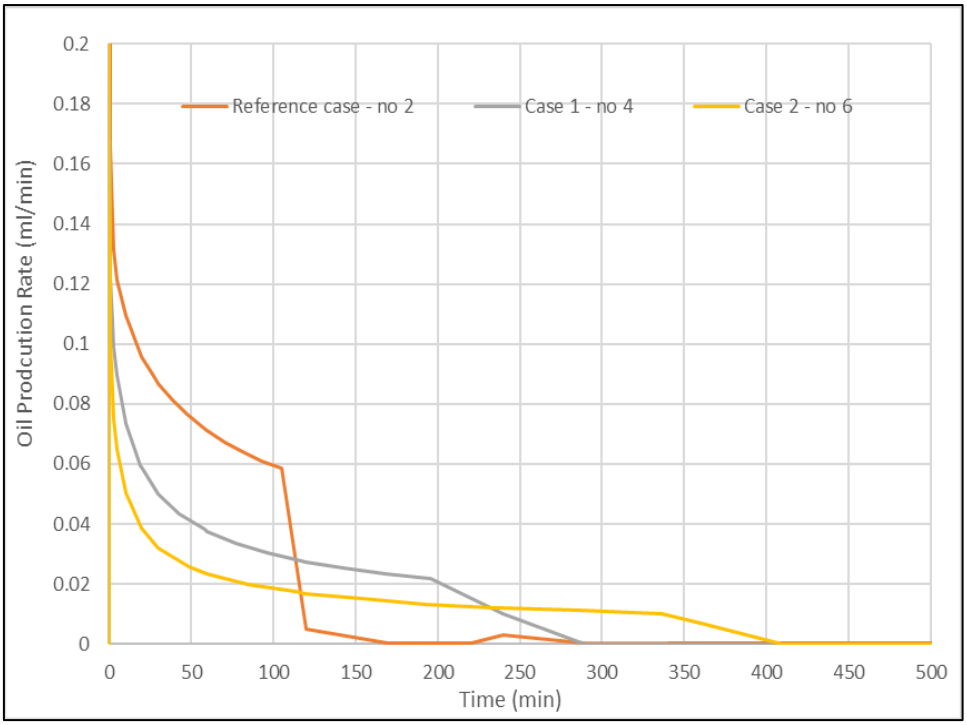

Figure 5-6 Total (Co-Current + Counter-Current) Oil Producation Rate - Case B (an increase of oil Corey exponent)

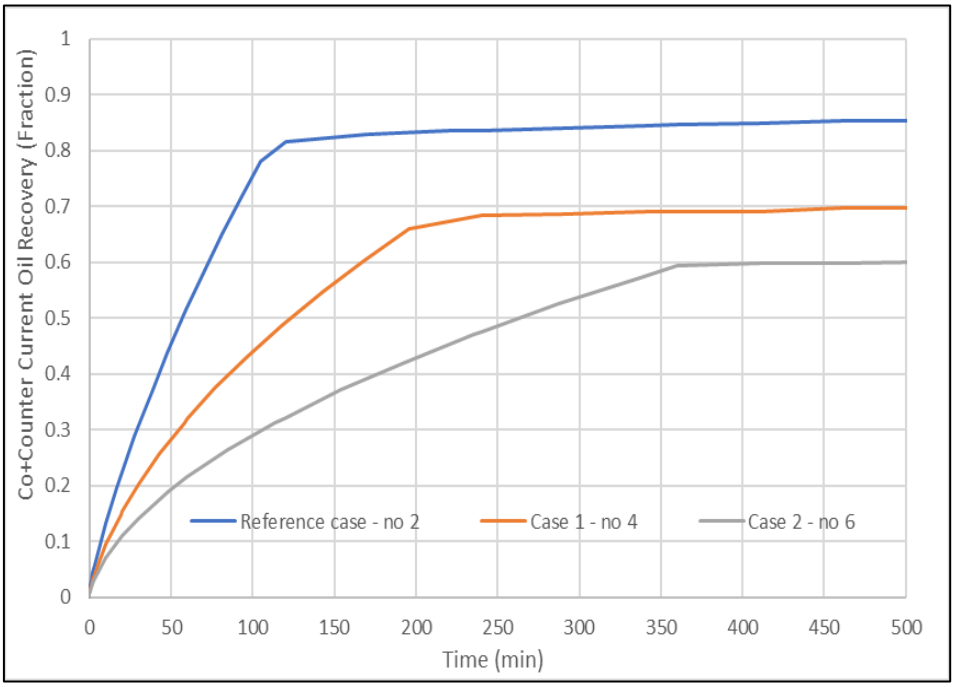

Figure 5-7 Total (Co-Current + Counter Current) Oil Production Rate - Case B (an increase of oil Corey exponent)

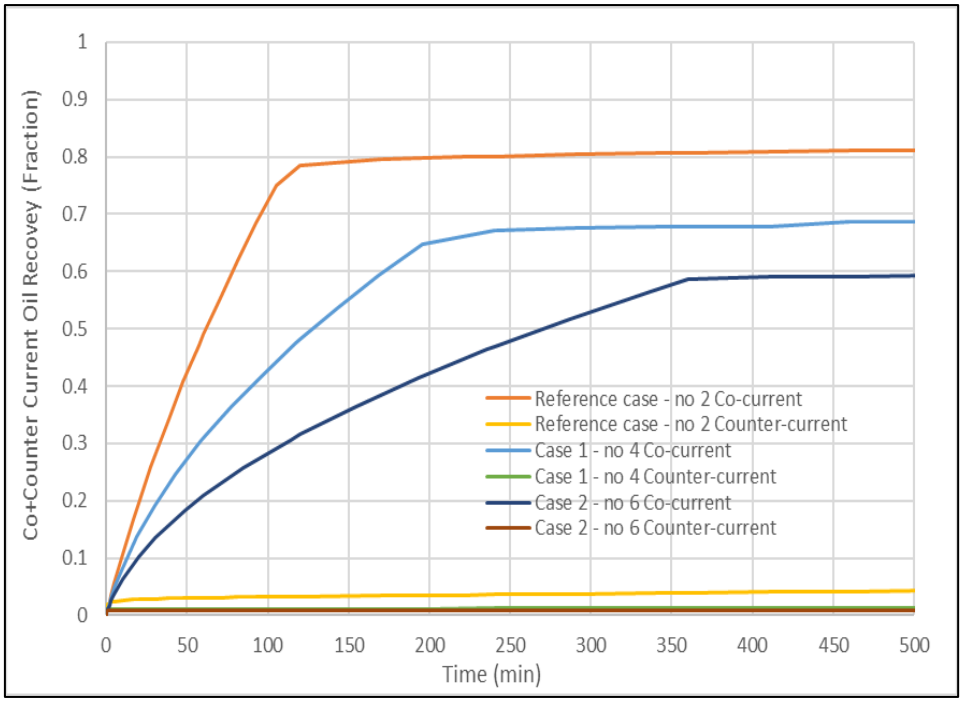

Figure 5-8 Co-Current + Counter-current Oil Recovery - Case B (an increase of oil Corey exponent)

As in the case A outlined above, in the Figure 5-6 a delay on oil production rate drop holds up the water to reach the outlet as the Oil Corey exponent is increased. However, in the case A, the co-current production increases as water Corey exponent increases; for the case B, the co-current production drops with increasing Oil Corey exponent, while the counter-current oil recovery production as the Oil Corey exponent decreases. Furthermore, an increase on the Oil Corey exponent, decreases the oil recovery and the breakthrough takes more time to occur. As a consequence, the imbibition rate is slower than for strongly water-wet system; before breakthrough takes place, the oil production decreases as imbibition progresses which means the drop on oil production rate might be influenced by the oil relative permeability. After the breakthrough, the co-current production reduces as the Oil Corey exponent increases and the counter-current production drops as shown on the Figure 5-8 and Table 5-4. A higher oil mobility is generated when the oil Corey exponent rises as the counter-current production decreases which makes the production mostly co-current.

Table 5-4 The Change of Oil Recovery with Increasing Oil Corey Exponent

	Break-through Time [min]	**Oil Recovery at breakthrough [fraction]**			**Oil Recovery after breakthrough [fraction]**		
		Counter Current	**Co Current**	**Total**	**Counter Current**	**Co Current**	**Total**
Ref. ($n_o = 2$)	120	0.032	0.784	0.817	0.055	0.825	0.88
Case B1 ($n_o = 4$)	240	0.012	0.647	0.659	0.049	0.729	0.77
Case B2 ($n_o = 6$)	410	0.008	0.586	0.598	0.026	0.624	0.65

5.1.1.3. Case C: Change of oil recovery with increasing n_o with constant n_w for mobility ratio M = 31.02

For case B, the oil Corey exponent is adjusted from Reference Relative Permeability to investigate the Oil Recovery. Like case A above, the oil relative permeability end-point is kept constant due to the initial conditions of the model. The alteration of oil Corey exponent does not make an impact on another parameter, as it occurs when the water Corey exponent is modified. The following table contains the values of oil Corey exponent.

Table 5-5 Parameter of Relative Permeability for Case B (an increase of oil Corey exponent)

M = 31.02 (μ_o = 103.4 & μ_w = 1.00)			
	Reference	Case B1	Case B2
n_o	2	4	6
k_{reo}	1		
n_w	6		
k_{rew}	0.300		

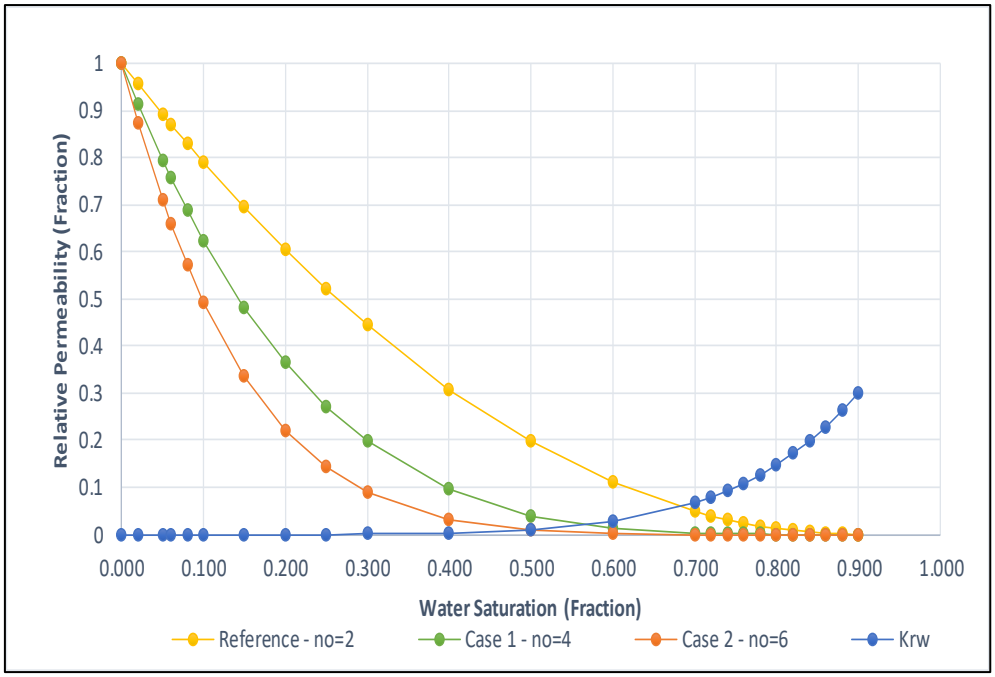

Figure 5-9 Relative Permeability Curves - Case B (an increase of oil Corey exponent)

The Figure 5-9 shows that the relative permeability curve moves to the left as the oil Corey exponent increases which causes the shape of oil relative permeability is more concave up. The end point of water and oil relative permeability remained constant; as the various relative permeability curves were generated, the parameter study is analysed by exploring the impact of the different relative permeability curves on the oil recovery. The results and analysis are explained as follows:

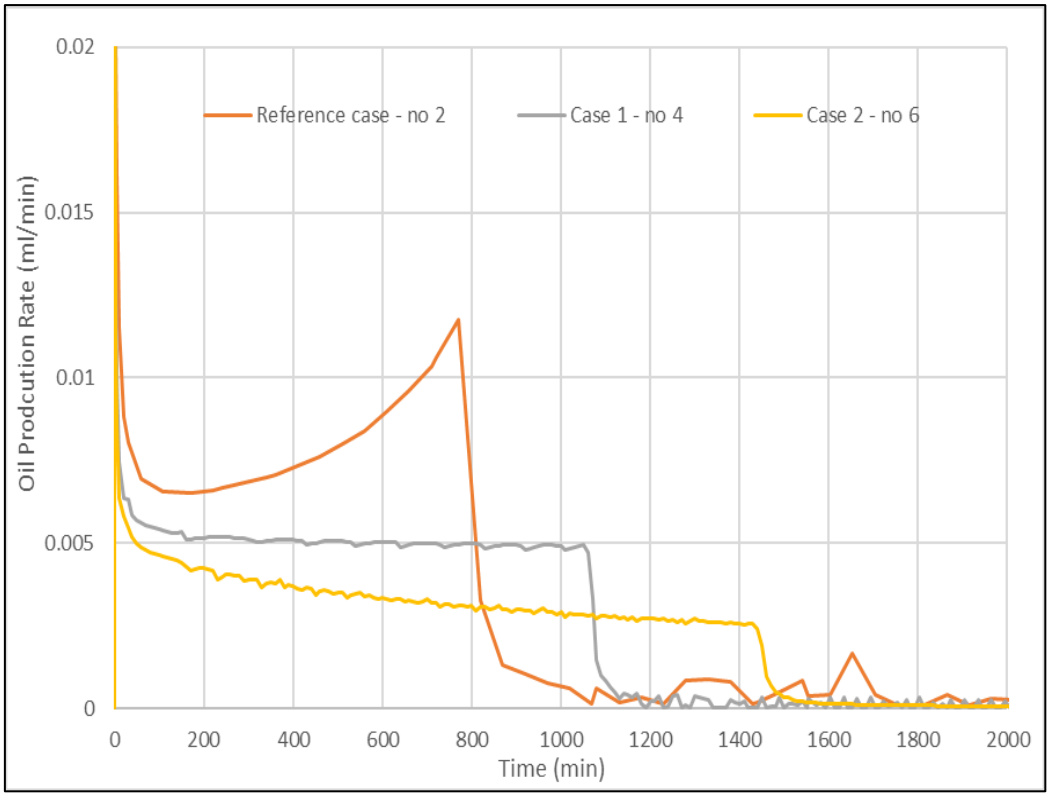

Figure 5-10 Total (Co-Current + Counter-Current) Oil Producation Rate - Case C (an increase of oil Corey exponent)

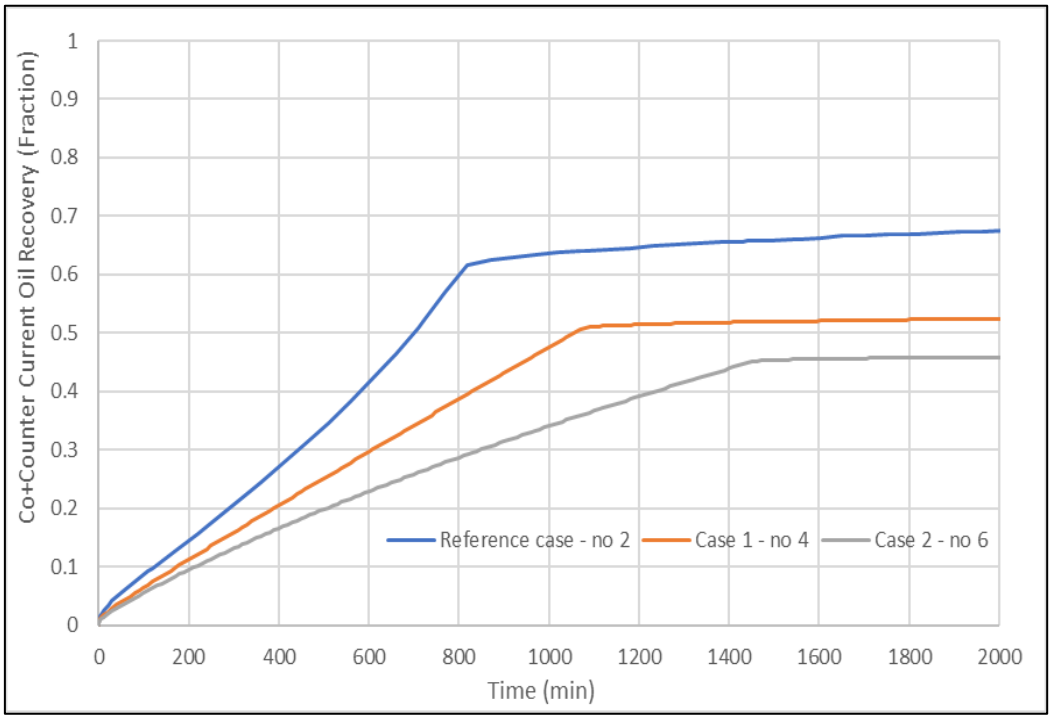

Figure 5-11 Total (Co-Current + Counter Current) Oil Production Rate - Case C (an increase of oil Corey exponent)

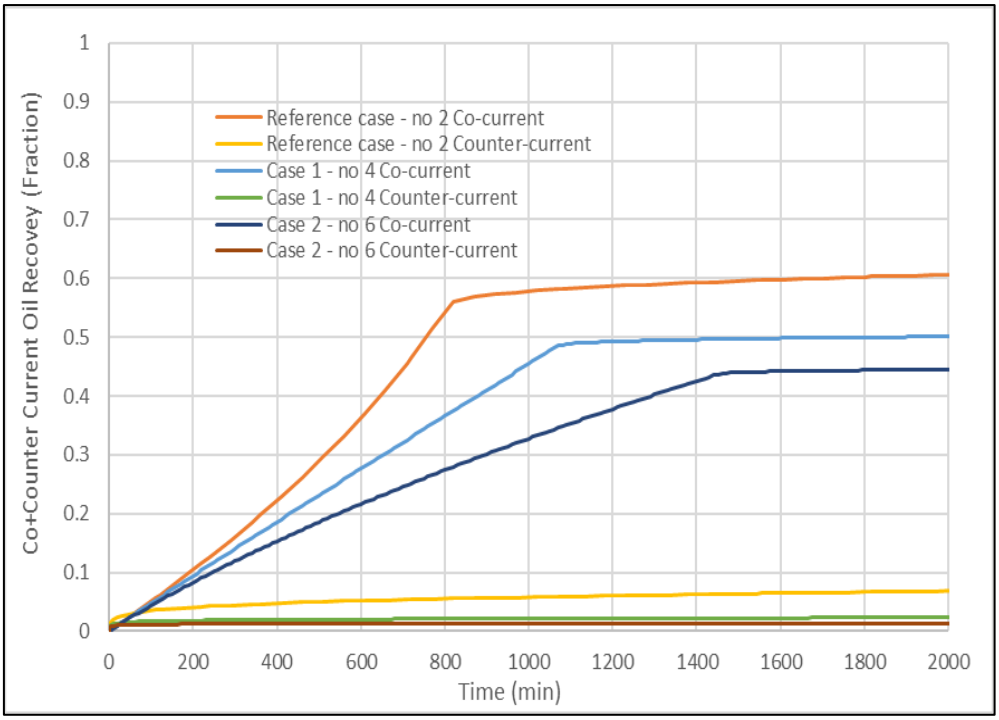

Figure 5-12 Co-Current + Counter-current Oil Recovery - Case C (an increase of oil Corey exponent)

As in the case B outlined above, in the Figure 5-10 a delay on production rate drop holds up the water to reach the outlet as the Oil Corey exponent is increased. However, in the case A, the co-current production increases as water Corey exponent increases; for the case C, the co-current production drops with increasing Oil Corey exponent, while the counter-current oil recovery rises when the Oil Corey exponent decreases. Furthermore, one particular trend can be seen in this case as for the case no = 2 the oil production showed an increasing trend compared to other two cases where there was a decreasing on production. Before breakthrough takes place, the oil production decreases as imbibition progresses which means the drop on oil production rate might be caused owing to change on the oil relative permeability curve. After the breakthrough, the co-current production reduces as the Oil Corey exponent increases as well as the counter-current production drops as the oil Corey exponent increases as seen on the Figure 5-12 and Table 5-6.

Table 5-6 The Change of Oil Recovery with Increasing Oil Corey Exponent

	Break-through Time [min]	Oil Recovery at breakthrough [fraction]			Oil Recovery after breakthrough [fraction]		
		Counter Current	Co Current	Total	Counter Current	Co Current	Total
Ref. ($n_o = 2$)	819	0.056	0.569	0.625	0.156	0.714	0.870
Case B1 ($n_o = 4$)	1090	0.022	0.488	0.510	0.061	0.559	0.620
Case B2 ($n_o = 6$)	1440	0.014	0.435	0.449	0.027	0.473	0.500

5.1.2. Parameter Study of Mobility Ratio

For parameter study of viscosity ratio, the information is taken from experimental data in the Table 4-1 (chapter 4). The mobility ratio for each case are summarized in the Table 5-7.

Table 5-7 Various of Viscosity Ratio for Increasing Oil Viscosity

	Oil viscosity (cP)	Water Viscosity (cP)	End-point water relative permeability (krew)	End-point oil relative permeability (kreo)	Mobility Ratio (λ_w/λ_o)
Case 1	0.0018	1.00	0.30	1.00	0.0005
Case 2	2.80	1.00	0.30	1.00	0.84
Case 3	25.6	1.00	0.30	1.00	7.6
Case 4	103.4	1.00	0.30	1.00	31.02

By using the reference J-Function and Relative Permeability curves into those experimental input data in the simulator, the effect of viscosity ratios on the oil recovery and oil production rate can be seen below in the following graphs.

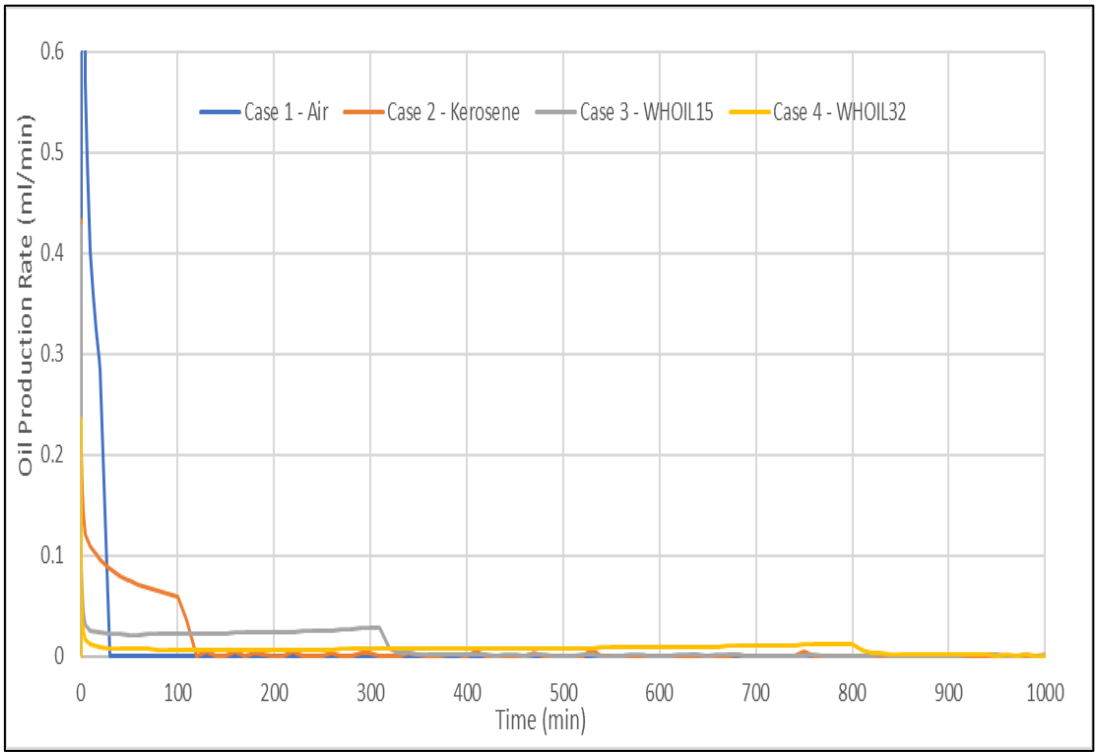

Figure 5-13 Total (Co-Current + Counter Current) Oil Production Rate for increasing Viscosity Ratio

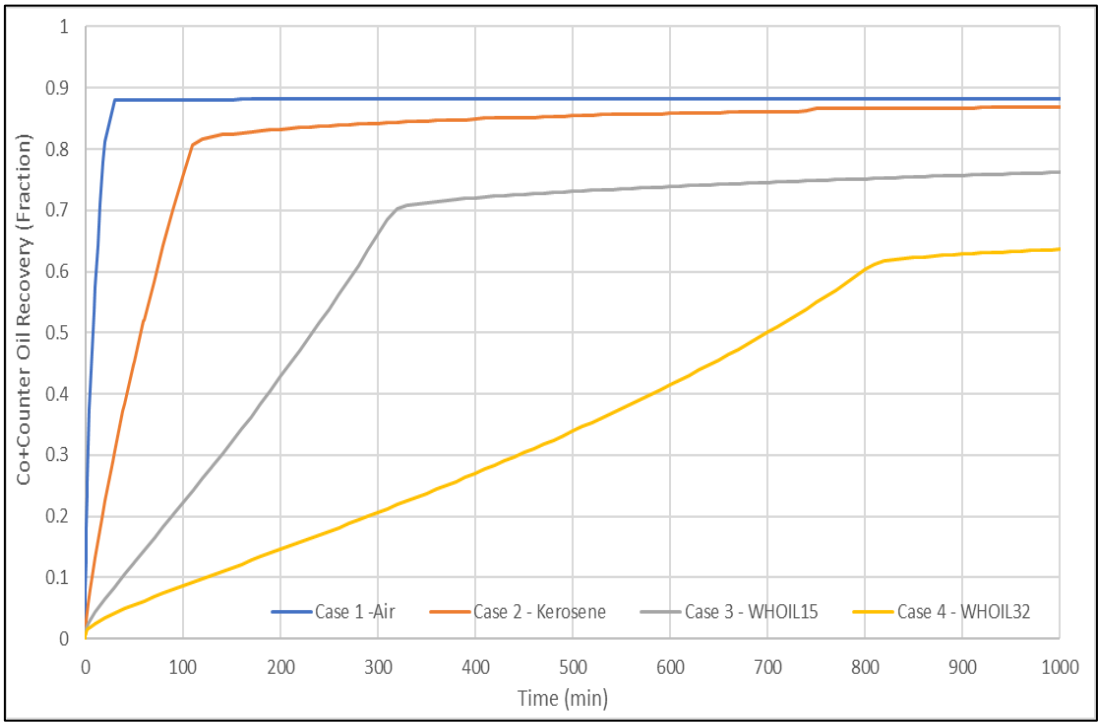

Figure 5-14 Total (Co-Current + Counter Current) Oil Recovery for increasing Viscosity Ratio

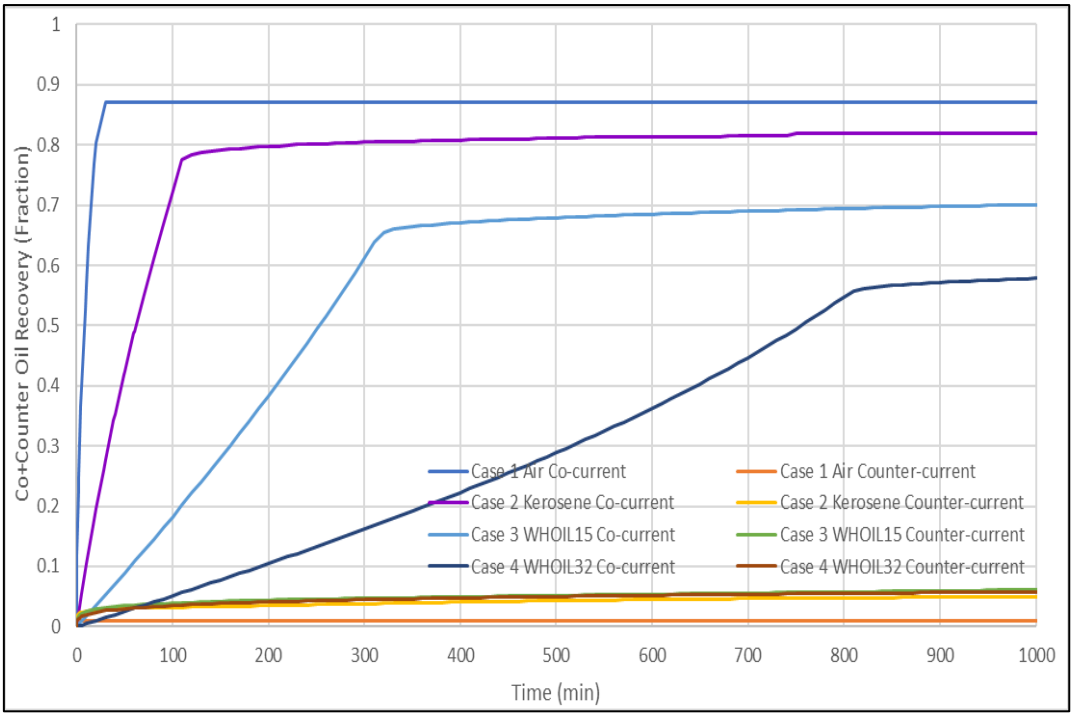

Figure 5-15 Co-Current + Counter-current Oil Recovery for increasing Viscosity Ratio

Figure 5-13 shows that Oil production rate drops first for the lowest mobility ratio and takes longer to occur for the highest mobility ratio. The longer the time of oil production rate to decline, the longer the time for water to reach the producer as seen in the Figure 5-14. Furthermore, for the case 1 and case 2 there is a decreasing trend on production compared to the case 3 and case 4 which shows an increasing trend on production. The increasing of the mobility ratio due to a more viscous oil leads to a delay on the breakthrough which is opposite from what it is expected from the theoretical knowledge as the highest the mobility ratio, the earliest the breakthrough is and the poorest the recovery process is. However, once the breakthrough is reached for every case, the final oil recovery for all the cases reaches the same value (Around 0.87).

As the oil viscosity increases, the counter current production will also rise, while the co-current production decreases at and after the breakthrough as shown in the Figure 5-15. This situation is similar with the case B for permeability ratio study already outlined above where it is shown by reducing oil mobility, the oil tends to produce more counter-currently. The reason is because a high oil pressure is needed for water to imbibe the viscous-oil-saturated porous medium, the counter-current production might take place in the inlet. The Table 5-8 shows an increase on counter-current production over the co-current oil recovery.

Comparing the simulation results obtained against the experimental by (Meng et al., 2015) the trends are the same as the first two cases (Air and kerosene) showed a decreasing oil production compared to the other cases (White Oil No. 15 and White Oil No. 32) where the oil production showed an increasing trend. However, for the last two cases (White Oil No. 15 and White Oil No. 32) the breakthrough times obtained from the simulations are quite differents from the ones obtained experimentally. The last section of this project consist of History Matching of the simulation results to the experimental ones.

Table 5-8 Result of increasing Viscosity Ratio Effect on Oil Recovery

	Break-through Time [min]	**Oil Recovery at Breakthrough [fraction]**			**Oil Recovery after Breakthrough [fraction]**		
		Counter-Current	**Co-Current**	**Total**	**Counter-Current**	**Co-Current**	**Total**
Air - μ_o/μ_w = 0.0018	20	0.009	0.823	0.812	0.009	0.871	0.881
Kerosene - μ_o/μ_w = 2.8	105	0.032	0.750	0.782	0.055	0.825	0.880
Wh Oil 15 μ_o/μ_w = 25.6	360	0.048	0.666	0.714	0.110	0.760	0.870
Wh Oil 32 μ_o/μ_w = 103.4	920	0.057	0.573	0.630	0.156	0.714	0.870

The fractional flow equations were plotted assuming the classical theory of Bucley-Leverett. A higher NW phase viscosity leads to a lower f_w where the tangent line to the f_w curve, drawn from S_w=0, indicates the front saturation S_f in the B-L theory also leads to a lower average saturation at breakthough. Lower saturations are expected at higher viscosities ratios which matched to the simulation results where the experiments with the highest NW phase viscosities had lower saturations fronts as shown in the Figure 5-16 and their displacements will be affected by a larger saturations interval which means a higher uncertainty. According to the Buckley-Leverett theory, variations in imbibition rate depend more on saturation distribution, according to the total mobility and the capillary pressure curve (Andersen et al., 2018).

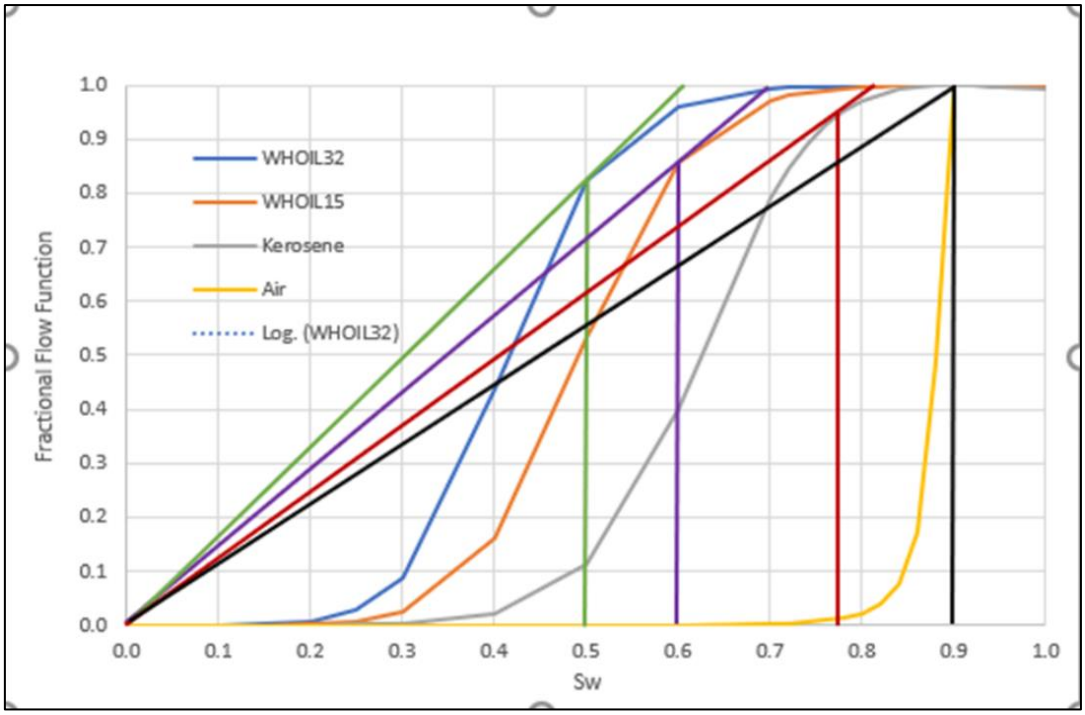

Figure 5-16 Fractional Flow Functions for the (Meng et al., 2015) glass-beads experiments. The intersection with the tangent line indicates the Buckley-Leverett front saturation.

Furthermore, the saturation profiles against position from inlet calculated by the numerical simulator were plotted along with the Buckley-Leverett profiles where it can be seen the saturation profiles roughly correspond to the B-L profiles before the water reaches the outlet of the glass column. Also, the numerical saturation profiles are smoother compared to the B-L profiles possibly due to the capillary diffusion phenomenon which happens during the imbibition process. A trend observed on the cases analysed are as the NW phase viscosity increases, the front saturation decreases which also leads to a lower saturation at breakthrough which matches with the results obtained from the experiments. For the Air-Brine experiment saturation profiles, no B-L profiles were plotted as the S_f is 0.9 which is above the charts obtained. Below the saturation profiles are shown in the Figure 5-17.

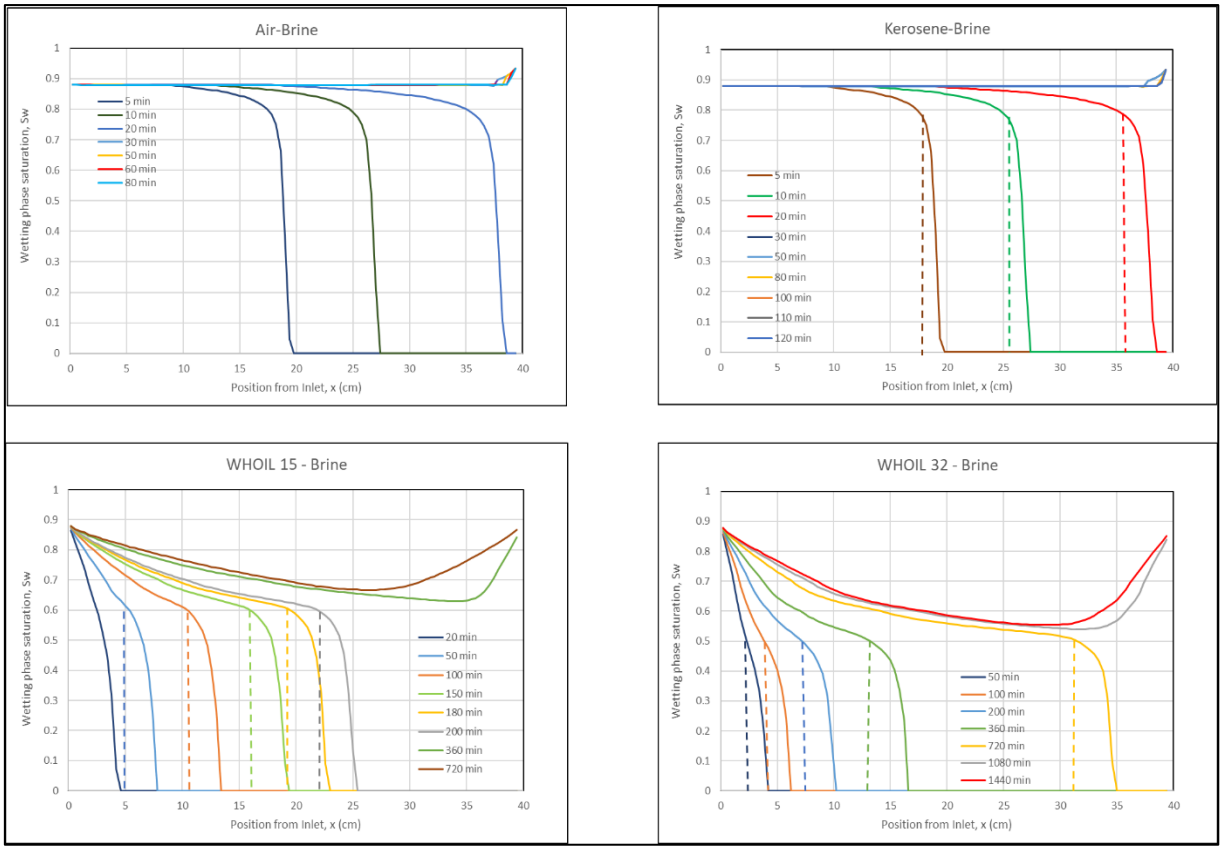

Figure 5-17 Simulated wetting phase saturation profiles compared to Buckley-Leverett saturation profiles for the four experiments by (Meng et al., 2015).

5.1.3. Parameter study of glass column length

An increase of glass column length is investigated to examine its impact on the oil recovery and oil production rate. In this case, the input reference data for simulation is used where three cases with different mobility ratios will be analysed. All the glass column properties keep constant except the glass column length; the glass column length is enlarged by two and three times the reference length shown as case 1 and case 2. These number are summarized in the Table 5-9 followed by the simulation result.

5.1.3.1. Case 1 M = 0.84

The first case is related to the experiment with kerosene whose mobility ratio is 0.84. Below is outlined the chart with the different lengths and the graphs with several parameters analysed.

Table 5-9 The Result of different lengths effect on Oil Recovery

Remark	Reference	Case 1	Case 2
Glass column Length [cm]	40	80	120

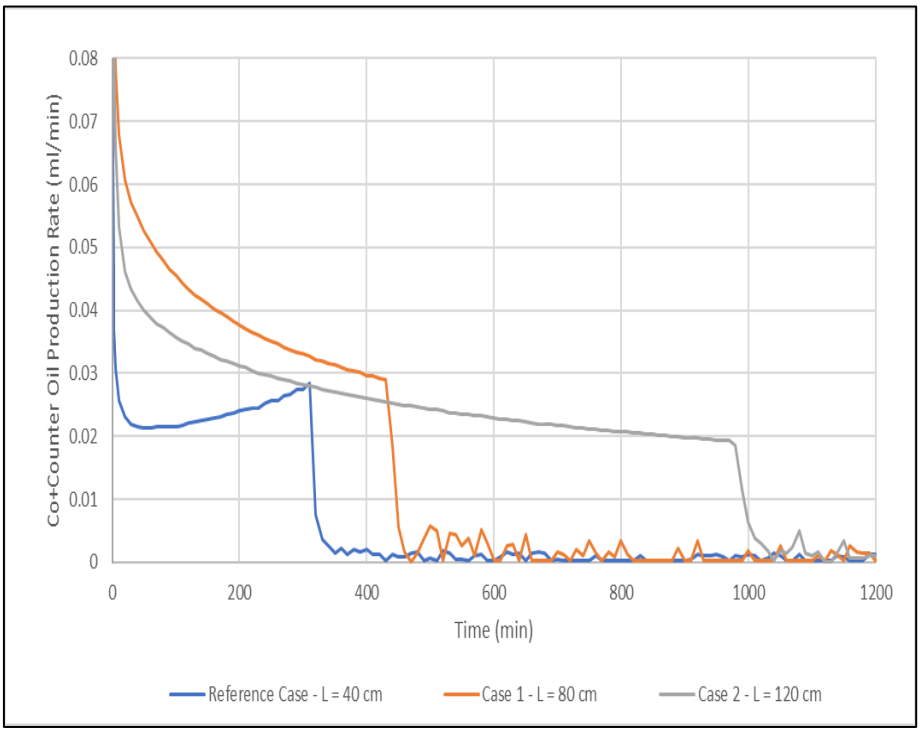

Figure 5-18 Total (Co + Counter Current) Oil Production Rate for different glass column lengths for M=0.84

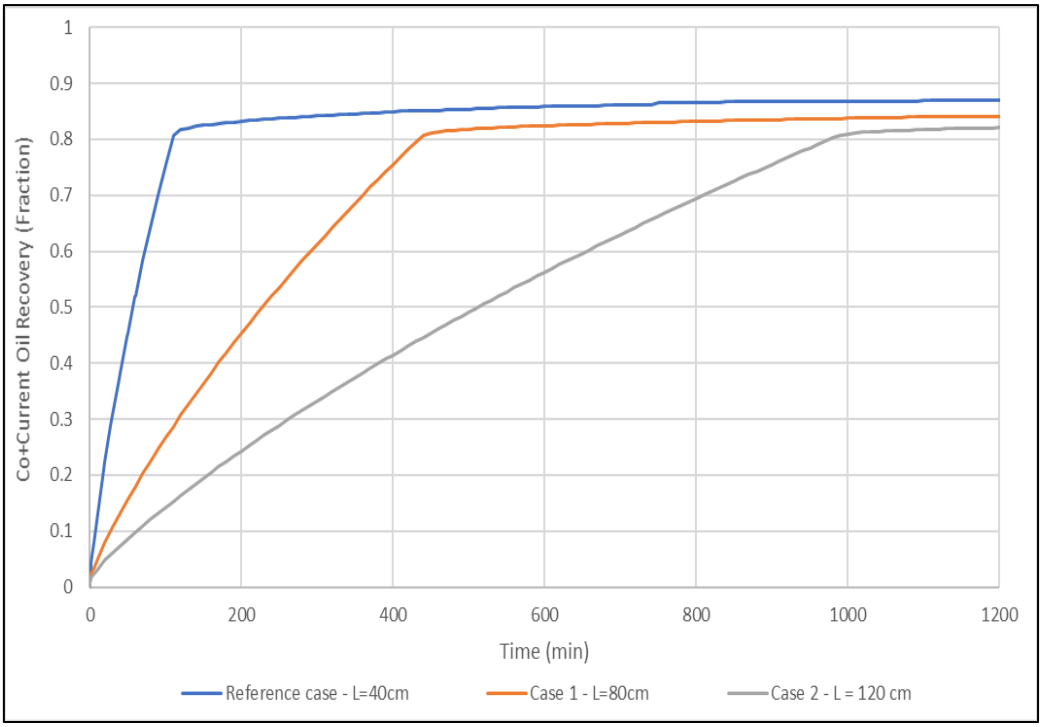

Figure 5-19 Total Co- & Counter Current Oil Recovery for different glass column lengths for M = 0.84

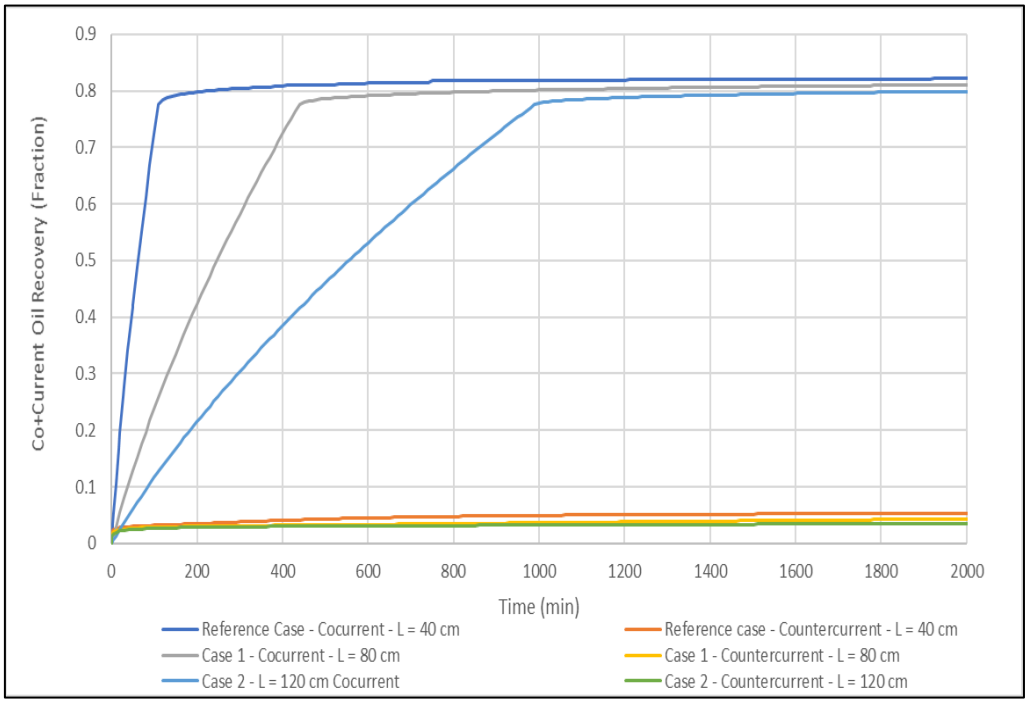

Figure 5-20 Co-Current and Counter-current Oil Recovery for different glass column length for M = 0.84

An increase of glass column length makes the production rate drop as well as the breakthrough takes place at a later time (see Figure 5-18 and Figure 5-19). After breakthrough, the oil production still increases gradually until it reaches the maximum oil recovery (RF = 0.87).

On the other hand, as the glass column length is increased, the production takes longer time to reach the maximum oil recovery.

Figure 5-20 shows the co-current and counter-current production decreases as the length is increased. Co-current production shows a decrease at the breakthrough, somehow it rose afterwards and reached the plateau around the oil recovery factor of 0.82. The co-current oil production is below the maximum production due to some oil has been produced counter-currently as the system might has been invaded by water; counter-current oil production yields in significant rise on oil recovery for all cases after the breakthrough. The amount of oil recovery at the breakthrough is summarized in the Table 5-10.

A particular trend observed for this case was for the reference length case, the oil production rate showed an increasing trend whereas the oil production showed a decreasing trend. It seems there was a problem on the simulator and/or code used to run as both curves should show the same trend.

Table 5-10 The Result of Different Tube Length on The Oil Recovery for M=0.84

Remark	**Breakthrough Time [minute]**	**Oil Recovery at Breakthrough [fraction]**			
		Counter Current	**Co Current**	**Total**	**Ratio Counter / Co-Current**
Reference Case (L = 40 cm)	120	0.032	0.784	0.817	0.04130
Case 1 (L = 80 cm)	460	0.032	0.781	0.814	0.04127
Case 2 (L = 120 cm)	1020	0.032	0.780	0.813	0.04127

5.1.3.2. Case 1 M = 7.6

The second case is related to the experiment with White Oil No. 15 whose mobility ratio is 7.6. Below is outlined the chart with the different lengths as well as the graphs with the parameters analysed.

Table 5-11 The Result of different lengths effect on Oil Recovery

Remark	Reference	Case 1	Case 2
Glass column Length [cm]	40	80	120

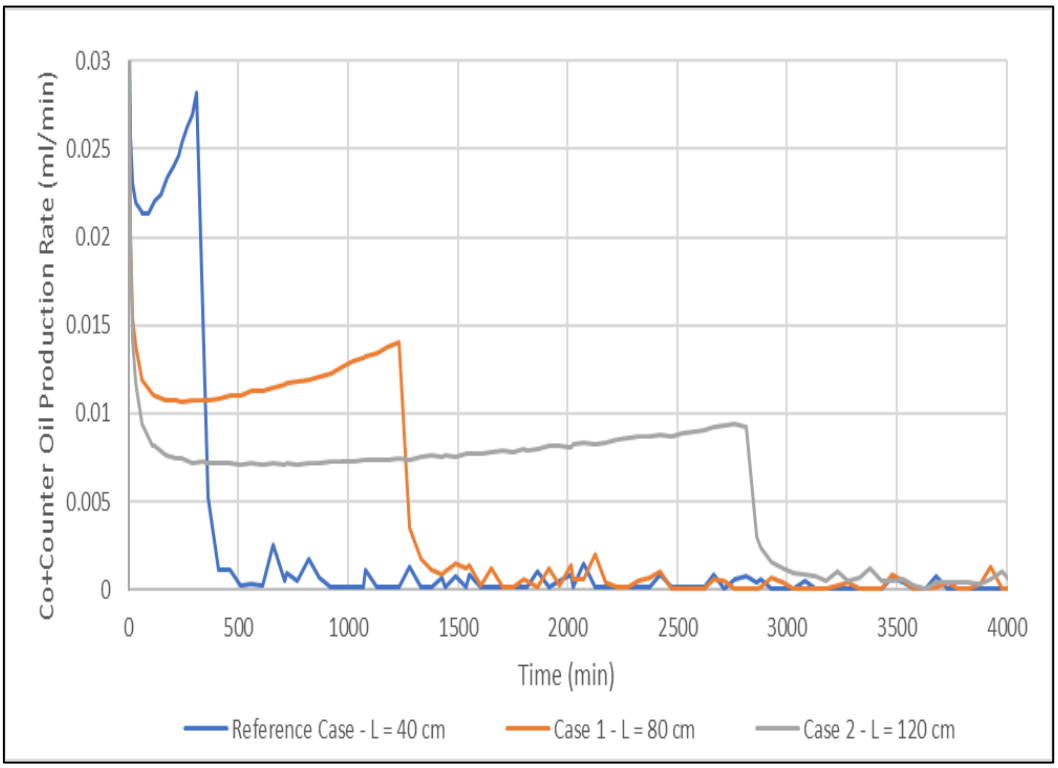

Figure 5-21 Total (Co + Counter Current) Oil Production Rate for different glass column length for M = 7.6

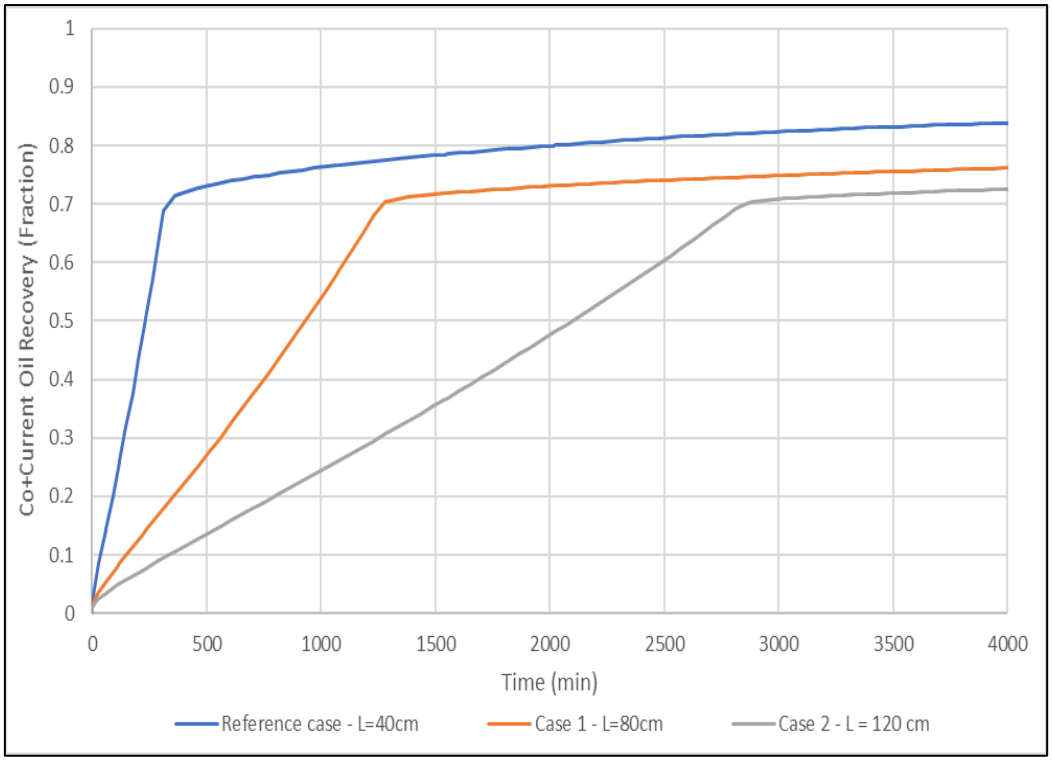

Figure 5-22 Total Co- & Counter Current Oil Recovery for different glass column length for M = 7.6

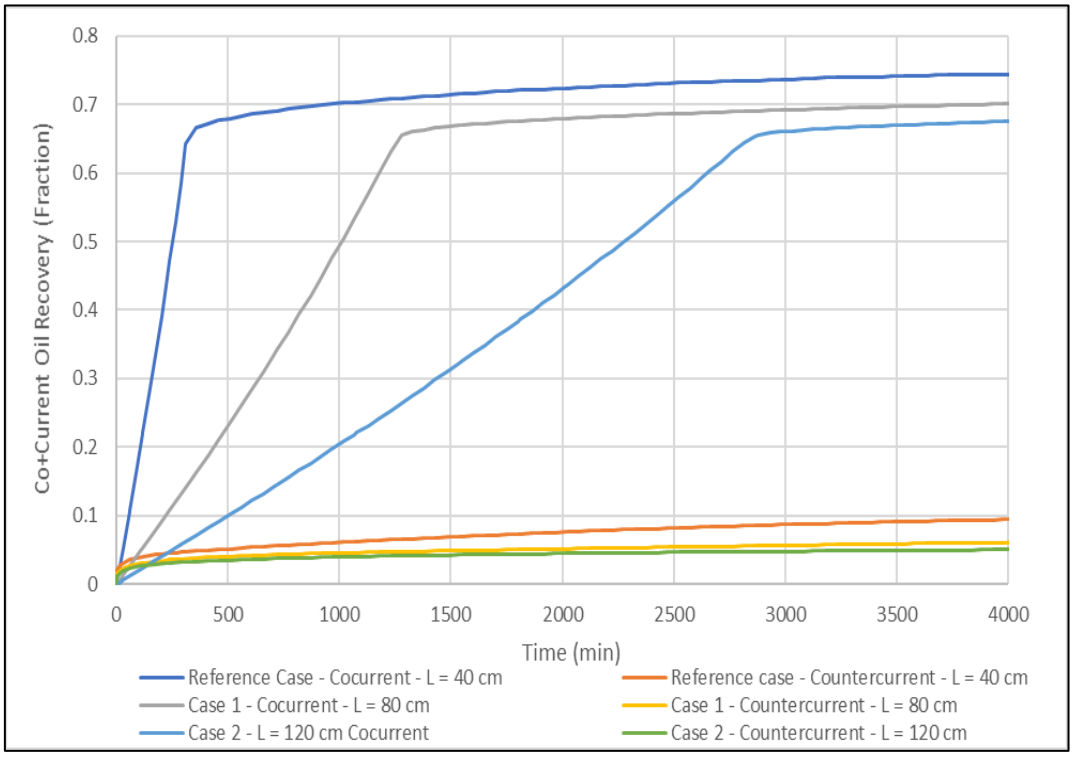

Figure 5-23 Co-Current and Counter-current Oil Recovery for different glass column length for M = 7.6

An increase of glass column length makes the oil production rate to drop and the breakthrough to occur at a late time compared to the reference length case (see Figure 5-21 and Figure 5-22); also, the oil recovery start increasing once the imbibition begins up to the breakthrough having the sharpest increase on the shorter length case and a steady growth on the longest length case. After breakthrough, the oil production continue increasing progressively until it achieves the maximum oil recovery (RF = 0.87 for 40 cm, RF=0.86 for 80 cm and RF=0.82 for 120 cm). Furthermore, the longer the glass column length is, the longer time it takes the maximum oil recovery to occur.

On Figure 5-23 shows the co-current and counter-current production decreases as the length is increased; co-current production shows an increasing trend up to the breakthrough, later it continued rising where it reached the plateau below the oil recovery factor of 0.8. The amount of oil recovery at the breakthrough is summarized in the Table 5-12.

Table 5-12 The Result of Different Tube Length on The Oil Recovery for M = 7.6

Remark	**Breakthrough Time [minute]**	**Oil Recovery at Breakthrough [fraction]**			
		Counter Current	**Co Current**	**Total**	**Ratio Counter / Co-Current**
Reference Case (L = 40 cm)	340	0.048	0.662	0.710	0.07248
Case 1 (L = 80 cm)	1280	0.048	0.659	0.706	0.07240
Case 2 (L = 120 cm)	2854	0.047	0.653	0.700	0.07265

5.1.3.3. Case 1 M = 31.02

The third case is related to the experiment with White Oil No. 32 whose mobility ratio is 31.02. Below is outlined the chart with the different lengths and the graphs with the parameters analysed.

Table 5-13 The Result of different lengths effect on Oil Recovery

Remark	Reference	Case 1	Case 2
Glass column Length [cm]	40	80	120

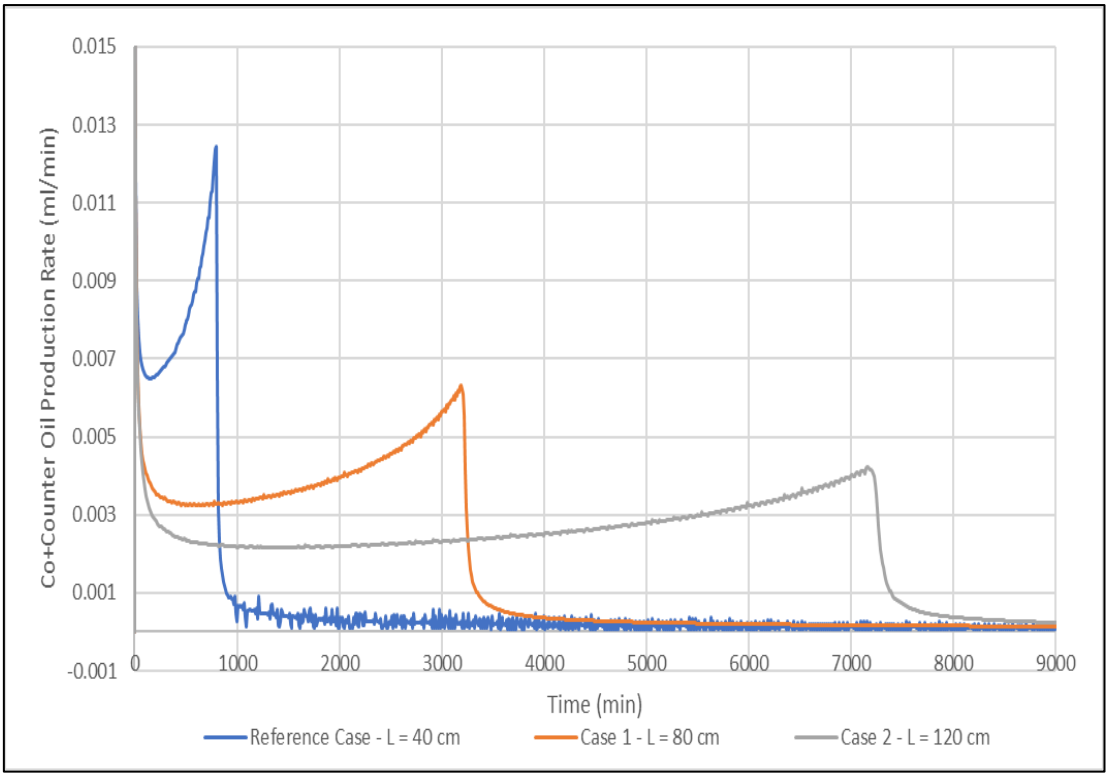

Figure 5-24 Total (Co + Counter Current) Oil Production Rate for different glass column length for M = 31.02

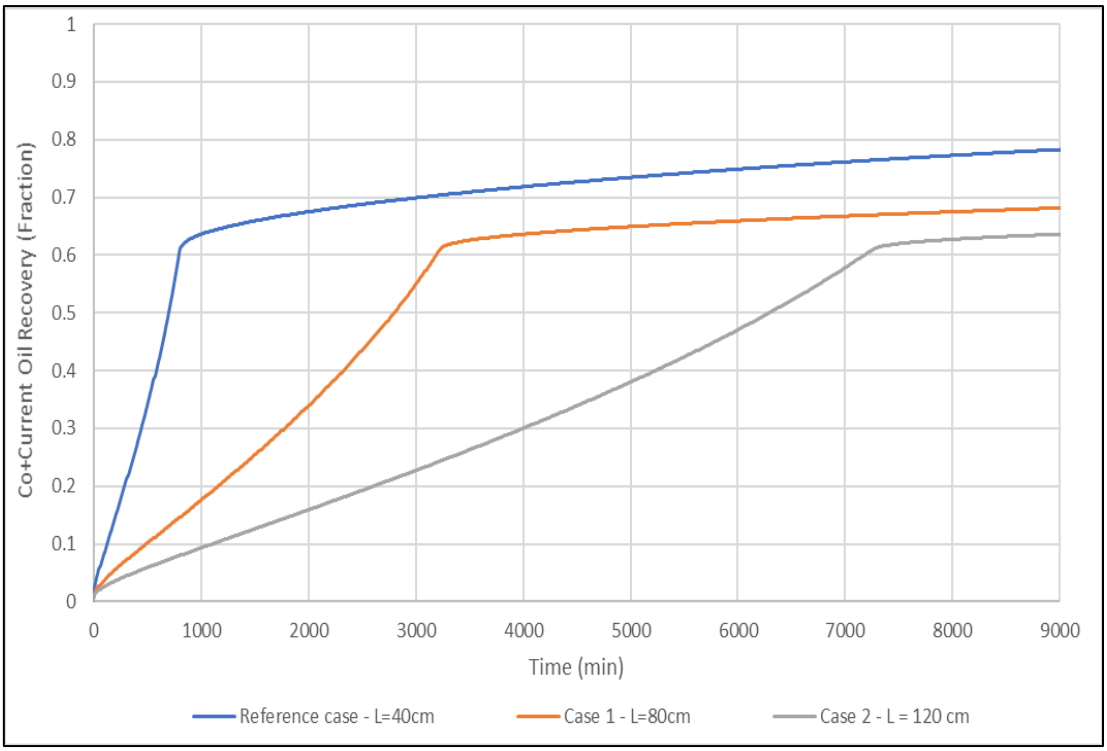

Figure 5-25 Total Co- & Counter Current Oil Recovery for different glass column length for M = 31.02

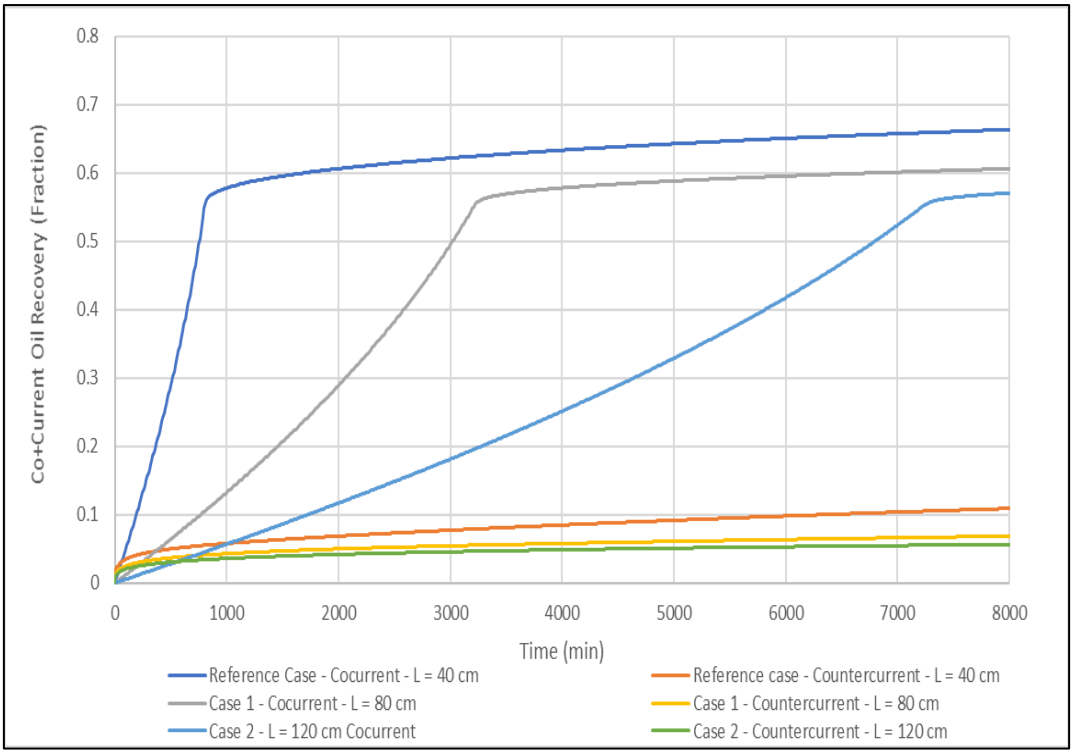

Figure 5-26 Co-Current and Counter-current Oil Recovery for different glass column length for M = 31.02

An increase of glass column length makes the production rate to drop and the breakthrough to happen at a later time compared to the glass column reference length (see Figure 5-24 and Figure 5-25); also, the oil recovery increases once the imbibition starts up to the breakthrough having the sharpest rise on the shorter distance case and a flat rise on the longest distance case. Once the breakthrough occurs, the oil production continue increasing steadily until it reaches the maximum oil recovery (RF = 0.87 for 40 cm, RF=0.81 for 80 cm and RF=0.74 for 120 cm).

On Figure 5-26 shows the co-current and counter-current production decreases at the breakthrough as the length is increased; co-current production shows an increase on oil production up to the breakthrough, later it continued rising where it reached the plateau below the oil recovery factor of 0.9. The amount of oil recovery at the breakthrough is summarized in the Table 5-14.

Table 5-14 The Result of Different glass column Length on The Oil Recovery for M = 31.02

Remark	**Breakthrough Time [minute]**	**Oil Recovery at Breakthrough [fraction]**			
		Counter Current	**Co Current**	**Total**	**Ratio Counter / Co-Current**
Reference Case (L = 40 cm)	800	0.055	0.548	0.603	0.10073
Case 1 (L = 80 cm)	3190	0.055	0.545	0.600	0.10118
Case 2 (L = 120 cm)	7180	0.055	0.545	0.601	0.10113

In summary, as the mobility ratio rises owing to the increase of the oil viscosity and when the length is increased twice and three times the reference length, the production rate decreases and the breakthrough takes more time to occur. Once the imbibition starts, the oil recovery showed an increasing trend up to the breakthrough where the sharpest increase takes place at the reference length case and the flattest occurs on the longest distance case; the higher the mobility ratio, the lowest the oil recovery at the breakthrough owing to the increasing viscosity of the oil which makes it more difficult to be swept by the displacing fluid (water) and lower the performance of the recovery process. After the breakthrough, the oil recovery continue increasing until it reaches the maximum oil recovery which is around 0.9.

Another trend observed is the total production, both co-current and counter-current oil production were the same for the three mobility ratios at breakthrough. However, for the M=0.84 case, the total production, co-current and counter-current production were the same for the three lengths. For the M=7.6 case, the total and co-current production decreases as the length increases; for the counter-current production, the highest value was obtained when the length was 80 cm. Finally, for the M=31.02 case, the total production as well as the co-current and counter-current oil productions decreases as the length increases. As a conclusion, as the oil viscosity and length increase in the system, the oil recovery decreases which matches the theoretical behaviour already explained above in previous cases.

5.1.4. Parameter Study of Capillary Pressure

To analyse the capillary pressure, the parameters of J-function formula are adjusted to change the shape of capillary pressure curve. The objective in this parameter study is to investigate the effect of altered capillary pressure curve shape on the production profile and the oil recovery.

There are 2 cases which will be established in this parameter study, such as decreasing slope (case 1) and increasing slope (case 2) compared to the reference capillary pressure (reference case) for different mobility ratios. To form the capillary pressure curve, either concave up – slope increasing curve or concave down – slope decreasing curve, E_{R1}, E_{L1} and S_{R1} are adjusted from Table 4-6 (reference case). The result of those capillary pressure is illustrated in the following figure.

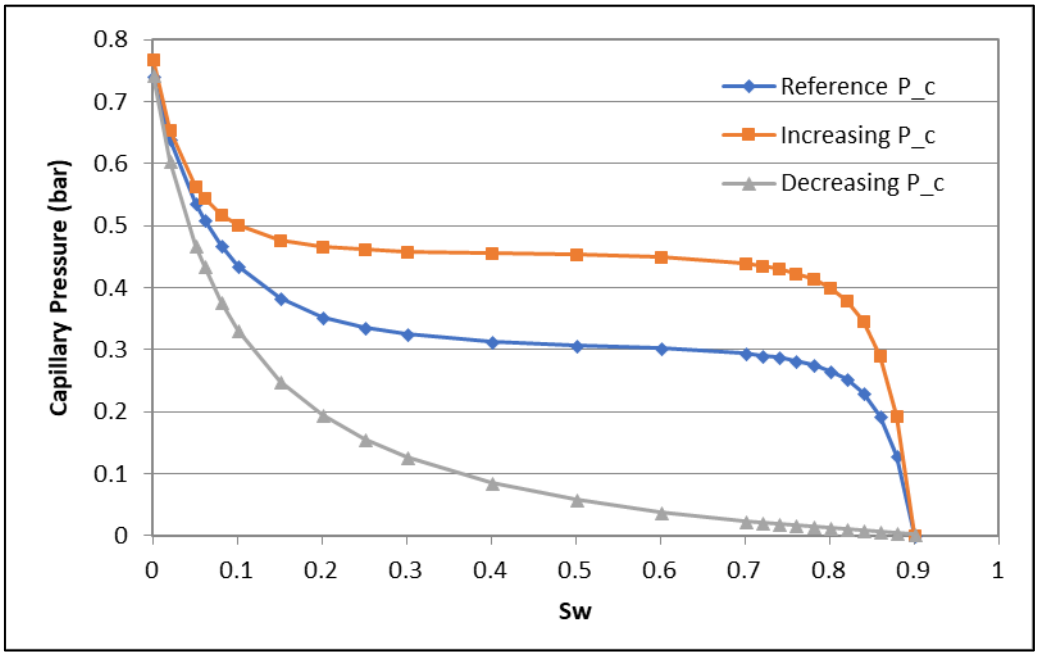

Figure 5-27 Capillary Pressure Curve of Case A (Change Pc Shape)

As the capillary curves are formed Figure 5-27, capillary pressure at initial water saturation and at residual oil saturation remains constant, the only modification is the shape of the curve. The reference relative permeability curve is used as the input of relative permeability – capillary pressure table into the model.

5.1.4.1. Case1: Alteration of Capillary Pressure Curve Shape for a mobility ratio M = 0.84

The first case analysed is where the mobility ratio is below 1. For this case, the second experiment (keresone) whose mobility ratio is 0.84 was chosen; the results obtained are explained below:

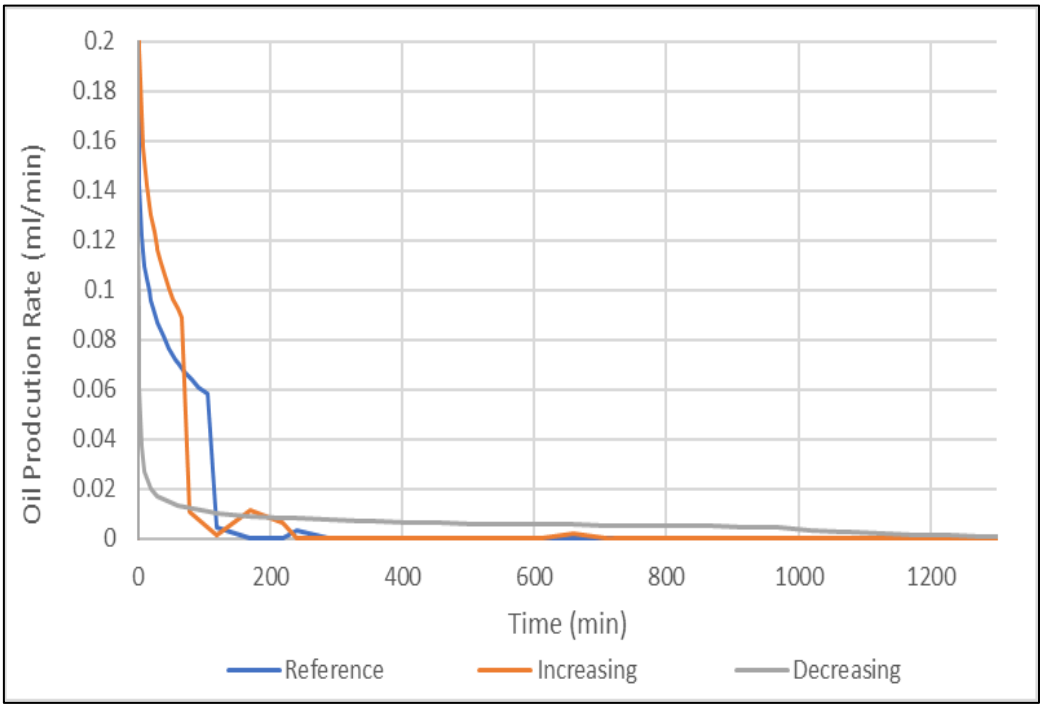

Figure 5-28 Total (Co + Counter Current) Oil Production Rate for Case A (Change of Pc Shape)

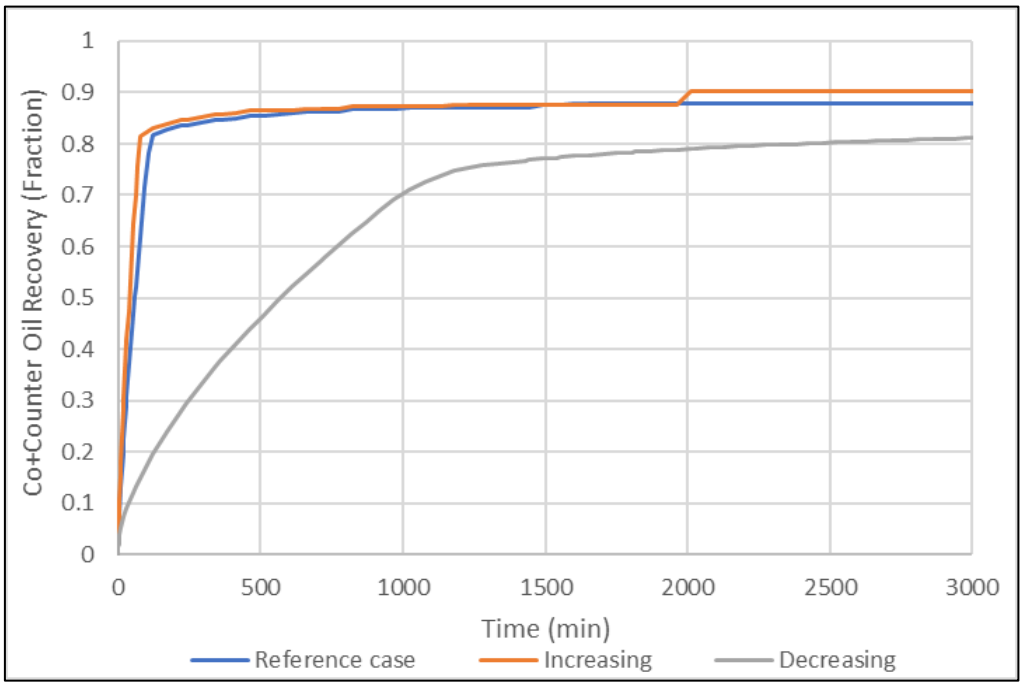

Figure 5-29 Total Oil Recovery Case A (Change of Pc Shape)

Figure 5-28 shows for the decreasing slope case, the oil production rate drop as well as the water breakthrough takes more time to occur. The oil production rate drop (decreasing slope) occurs around 1080 min after the drop of the reference production rate case. The oil production rate for the case 1 (decreasing slope) takes more time to drop compared to the other cases owing for the increasing slope case the production drop and the breakthrough happens first as the oil recovery showed a decreasing trend once the imbibition started up to the breakthrough. As a consequence, the oil production at the case 1 is lower than the reference case; also, the breakthrough (see Table 5-15) occurs at a later time and it also takes longer time to reach the maximum of oil recovery at residual oil saturation as shown in Figure 5-29.

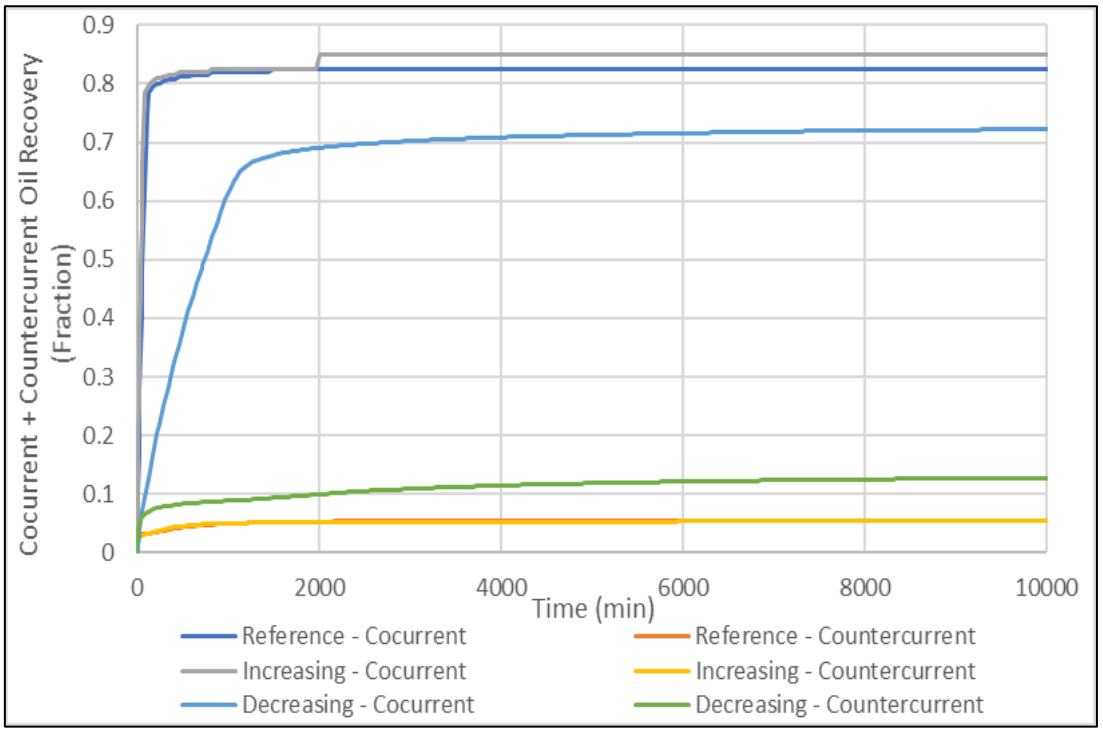

Figure 5-30 Co-Current + Counter-current Oil Recovery (Change of Pc Shape)

Figure 5-30 shows there is a reduction on co-current oil production, whereas there is an increase on counter-current oil production as the shape of capillary pressure curve is decreased which affects the oil mobility, so the water as displacing fluid needs more power to moves out the oil.

On the other side, for the increasing Capillary Pressure curve case makes the oil more mobile, so the water needs less power to sweep the oil; just little oil is produced counter-currently. The breakthrough happens at an early time as the production showed a decreasing trend.

In summary, for a mobility ratio below 1 the breakthrough happens first for the increasing slope case, followed by the reference slope case and finally by the decreasing slope case. For the increasing and reference slope cases the breakthrough times are close to each other and the counter-current imbibition of both cases are similar and low compared to the decreasing slope case where the breakthrough time happens at a later time and the counter-current production is higher owing mostly to the oil mobility.

Table 5-15 Simulation Results of Capillary Pressure – Case A (Change Pc Shape)

Remark	**Breakthrough Time [minute]**	**Oil Recovery at the breakthrough [fraction]**			**Oil Recovery after the breakthrough [fraction]**		
		Counter Current	**Co Current**	**Total**	**Counter Current**	**Co Current**	**Total**
Case 1 (Decreasing slope)	1180	0.090	0.657	0.750	0.138	0.732	0.870
Reference Case	105	0.032	0.750	0.782	0.055	0.825	0.880
Case 2 (Increasing slope)	78	0.031	0.785	0.815	0.052	0.849	0.901

5.1.4.2. Case 2: Alteration of Capillary Pressure Curve Shape for a mobility ratio M = 31.02

The first case analysed is where the mobility ratio is above 1. For this case, the fourth experiment whose fluid is white oil No. 32 and its mobility ratio is 31.02 was chosen to run the simulations. The results obtained are explained below:

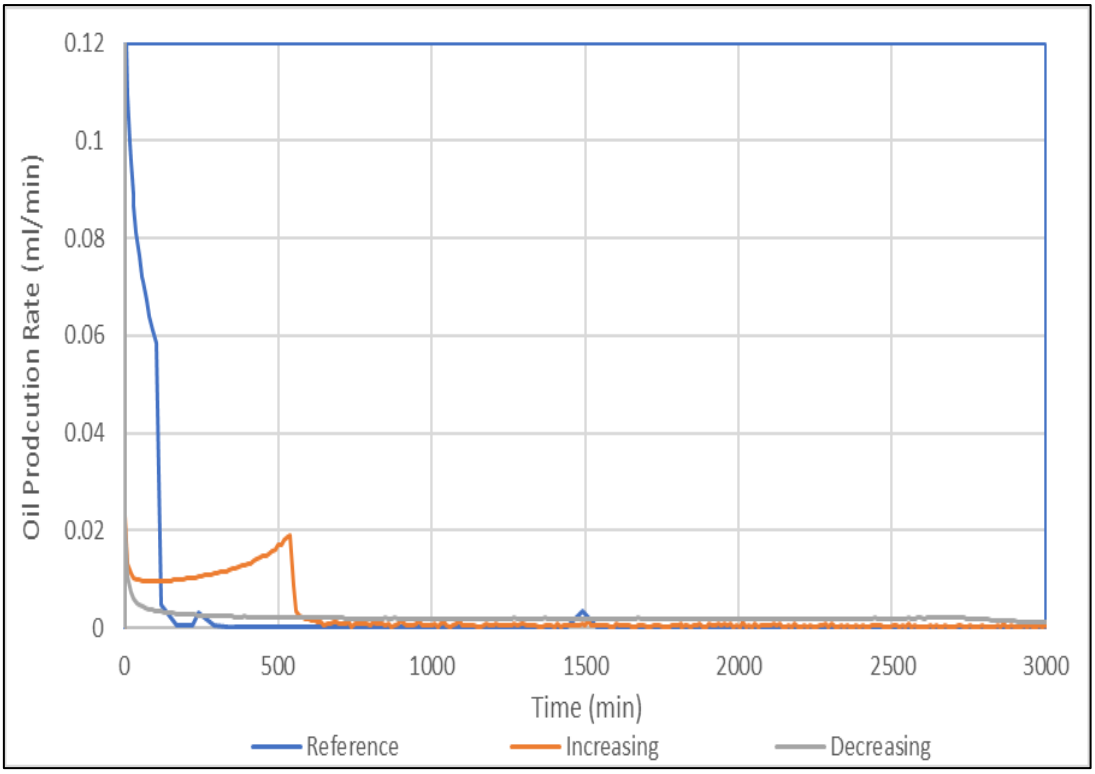

Figure 5-31 Total (Co + Counter Current) Oil Production Rate of Case B (Change Pc Shape)

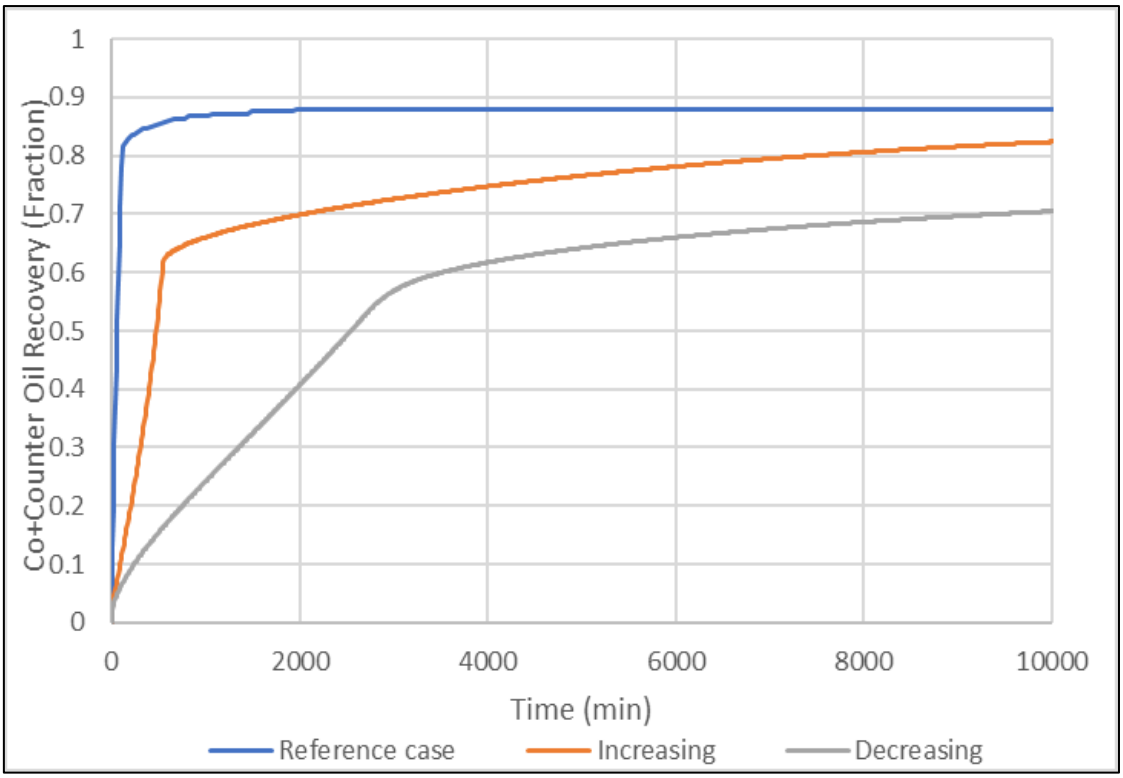

Figure 5-32 Total Oil Recovery for Case B (Change Pc Shape)

Figure 5-31 shows for the decreasing slope case, the oil production rate drop and the water breakthrough takes more time to occur. The oil production rate drop (decreasing slope) occurs around 2710 min after the drop of the reference production rate case. The oil production rate of the case 1 (decreasing slope) takes more time to drop compared to the other cases; the production drop and the breakthrough happens first for the reference case as the oil recovery showed a decreasing trend on production once the imbibition began up to the breakthrough and the mobility of the oil is less compared to the other two cases. Furthermore, the breakthrough for the decreasing slope case (see Table 5-16) occurs at a later time and it also takes longer time to reach the maximum of oil recovery at residual oil saturation as shown in Figure 5-32.

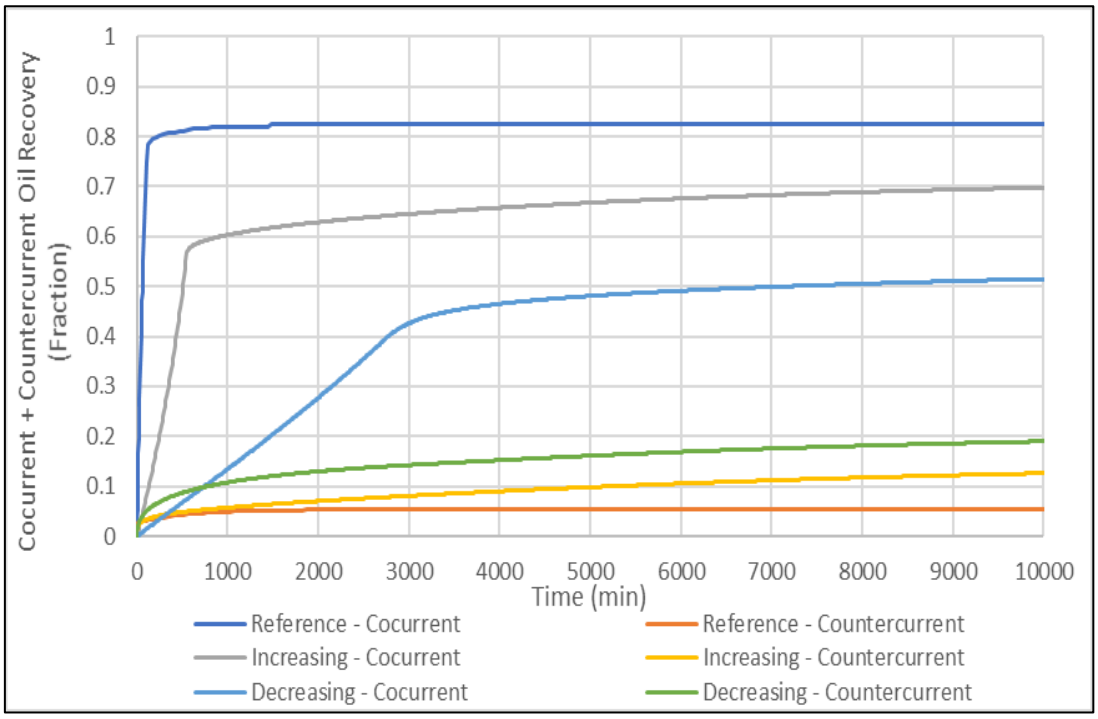

Figure 5-33 Co-Current and Counter-current Oil Recovery for case B (Change of Pc Shape)

Figure 5-33 shows there is a reduction on co-current oil production, whereas there is an increase on counter-current oil production as the shape of capillary pressure curve is decreased. On the other side, for the reference Capillary Pressure curve case, the oil can flow easily along the system and just little oil is produced counter-currently as no invasion of water into the system happened.

In summary, compared to the previous case for a mobility ratio above 1, the breakthrough happens first for the reference slope case, followed by the increasing slope case and finally by the decreasing slope case. For this case, the breakthrogh times and the oil production of the three cases are neither similar nor close to one another as it happened in the previous case. The main reason of this behaviour might be the fluid mobility of the non-wetting phase which is highly influenced by the viscosity which it is higher compared to the previous situation and the decreasing of the capillary pressure curve. For both cases, some instabilities in the simulation results are obtained probably related to the instability of the numerical solution (simulator precision and stability issues).

Table 5-16 Simulation Results of Capillary Pressure – Case A (Change Pc Shape)

Remark	Breakthrough Time [minute]	Oil Recovery at the breakthrough [fraction]			Oil Recovery after the breakthrough [fraction]		
		Counter Current	Co Current	Total	Counter Current	Co Current	Total
Case 1 (Decreasing slope)	105	0.032	0.750	0.782	0.055	0.825	0.880
Reference Case	740	0.053	0.591	0.644	0.149	0.721	0.870
Case 2 (Increasing slope)	2844	0.141	0.410	0.551	0.237	0.563	0.800

5.1.5. Parameter Study of Mobility Ratio

For this analysis, some input parameters like viscosities and end-point relative permeabilities were modified to obtain three different mobilities ratios based on its definition outlined in the section 2.4. Three cases were analysed, the first when the mobility ratio is below 1, the second when the mobility ratio is equal 1 and the last when the mobility ratio is above 1. The main goal is to analyse the Oil Recovery based on the Mobility Ratio, the input parameters are summarized in the Table 5-17.

Table 5-17 Three types of mobility ratios obtained to analyze the Oil Recovery.

	Oil viscosity (cP)	**Water Viscosity (cP)**	**End-point water relative permeability (krew)**	**End-point oil relative permeability (kreo)**	**Mobility Ratio (λ_w/λ_o)**
Case 1	2.80	1.00	0.30	1.00	0.84
Case 2	2.80	2.80	1.00	1.00	1
Case 3	5.60	1.00	0.30	1.00	1.68

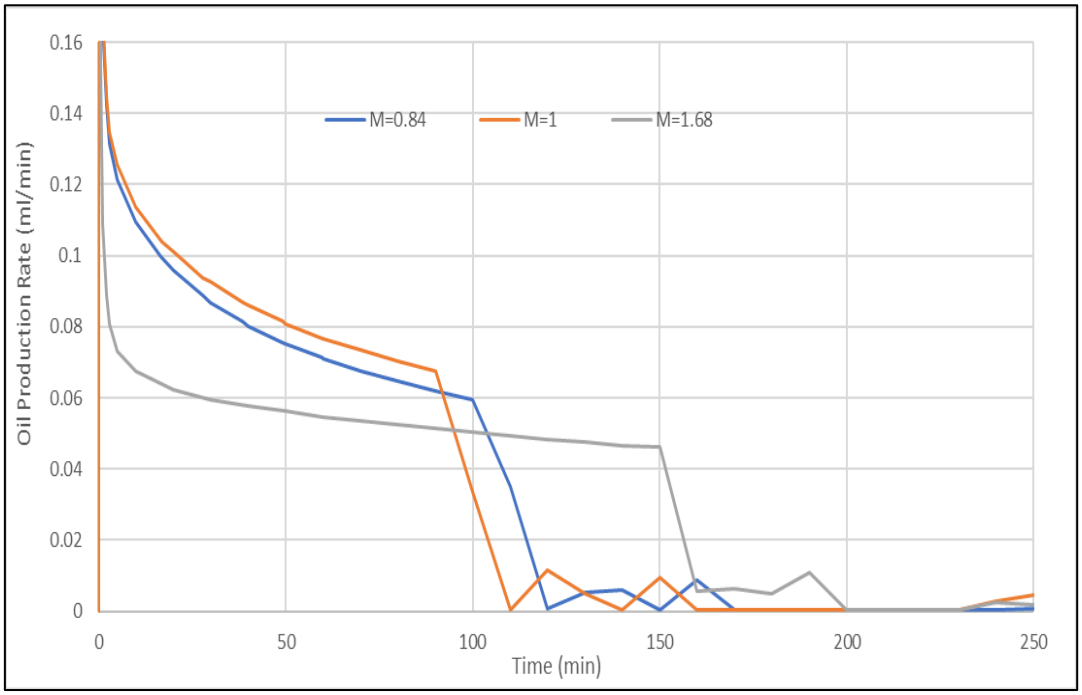

Figure 5-34 Total (Co-Current + Counter Current) Oil Production Rate for different mobility ratios

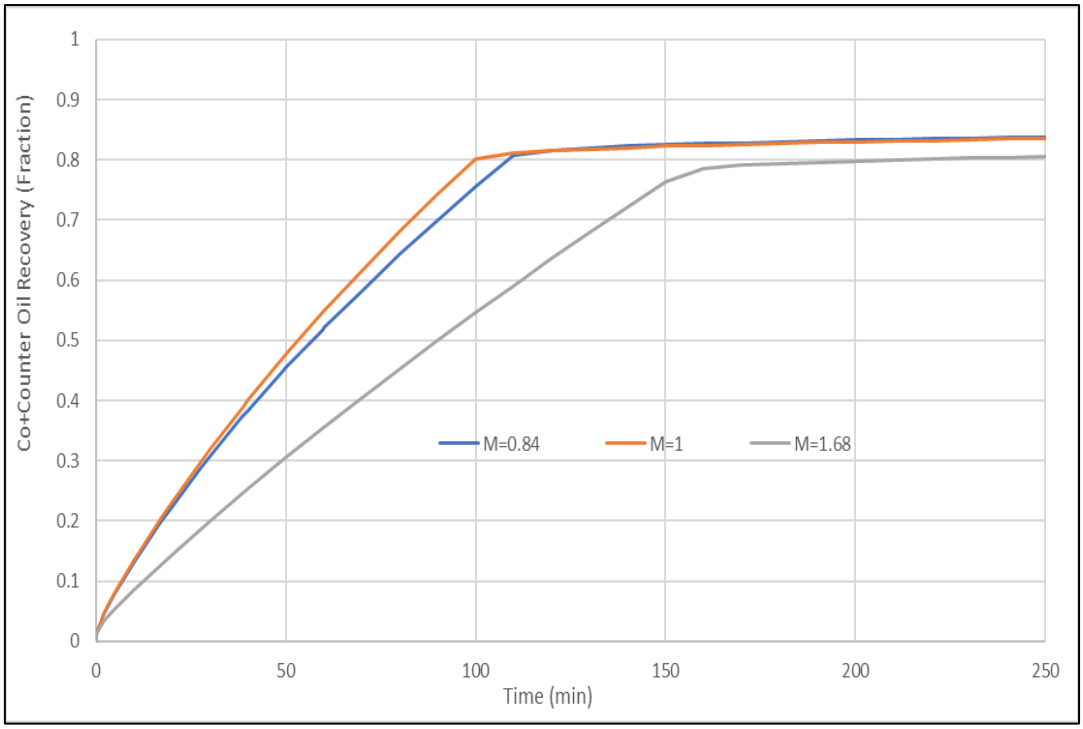

Figure 5-35 Total (Co-Current + Counter Current) Oil Recovery for different mobility ratios

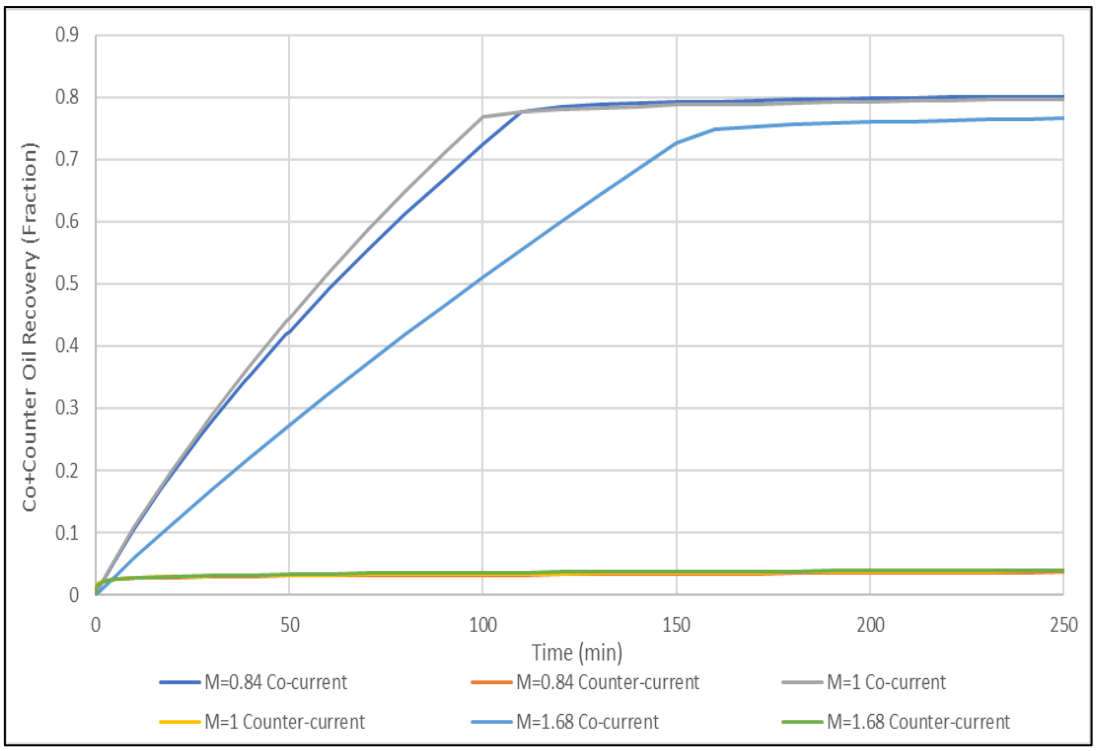

Figure 5-36 Co-Current + Counter-current Oil Recovery for different mobility ratios.

Figure 5-34 shows that Oil production rate drops first when the mobility ratio is equal 1 and takes longer to occur when the mobility ratio is above 1. According to the theory of inmsicible fluids displacement, a mobility ratio above 1 results in an early breakthrough of the

displacing fluid owing to water can travel with a velocity higher than the displaced fluid and the oil will be by-passed. However, the simulation results showed a different trend as when the mobility is above 1 it is expected the breakthrough to occur earlier than the other two cases analyzed (M=1 and M<1) and in the Figure 5-35 the opposite situation is shown as the breakthrough took place at a later time. The reason for this to happen might be the mobility ratios used are closed to one another and for the case M=1 the krew were changed from 0.3 to 1 which changed the water relative permeability curve compared to the other two cases where the krew remained constant.

Another trend observed in this analysis were for the mobility ratios M=0.84 and M=1 the values are similar for total, co-current and counter-current production at and after breakthrough. However, for the mobility ratio M>1 the results obtained are different as the breakthrough takes place at a later time compared to the other two cases and the counter-current production is less as the oil might be more mobile.

Table 5-18 Result of Decrease Viscosity Ratio Effect on Oil Recovery

	Break-through Time [min]	**Oil Recovery at Breakthrough [fraction]**			**Oil Recovery after Breakthrough [fraction]**			
		Counter-Current	**Co-Current**	**Total**	**Counter-Current**	**Co-Current**	**Total**	**Ratio Counter / Co-current**
Case 1 M = 0.84	130	0.035	0.765	0.795	0.059	0.812	0.870	0.07238
Case 2 M = 1	100	0.033	0.769	0.802	0.054	0.816	0.870	0.06618
Case 3 M = 1.67	1170	0.014	0.852	0.866	0.014	0.856	0.870	0.01636

5.1.6. Parameter Study of imbibition rate with different mobility ratios

The second experiment from Meng et al. whose non-wetting phase is kerosene was selected to analyse the behaviour of the imbibition rate with different mobility ratios where the viscosities of the involved phases as well as the end-point relative permeabilities were modified to analyse the behaviour of the oil recovery by using the analytical solution already outlined above in the section 2.8

5.1.6.1. Mobility Ratio below 1 (M=0.84)

As mentioned in the section 2.4, having a M ≤1 is considered a favorable mobility ratio; on the Figure 5-37 the imbibition rate starts at a low value and as the imbibition front travels through the glass column, the imbibition rate increases exponentially until it reaches the total length as well as the highest value. The main reasons of this behavior might be because the non-wetting phase (Oil) travels with a velocity equal or greater than the wetting phase (Water) where there is no chance for the oil to be by-passed which leads to a sharp interface between the fluids and usually the breakthrough takes place longer which makes the recovery process efficient.

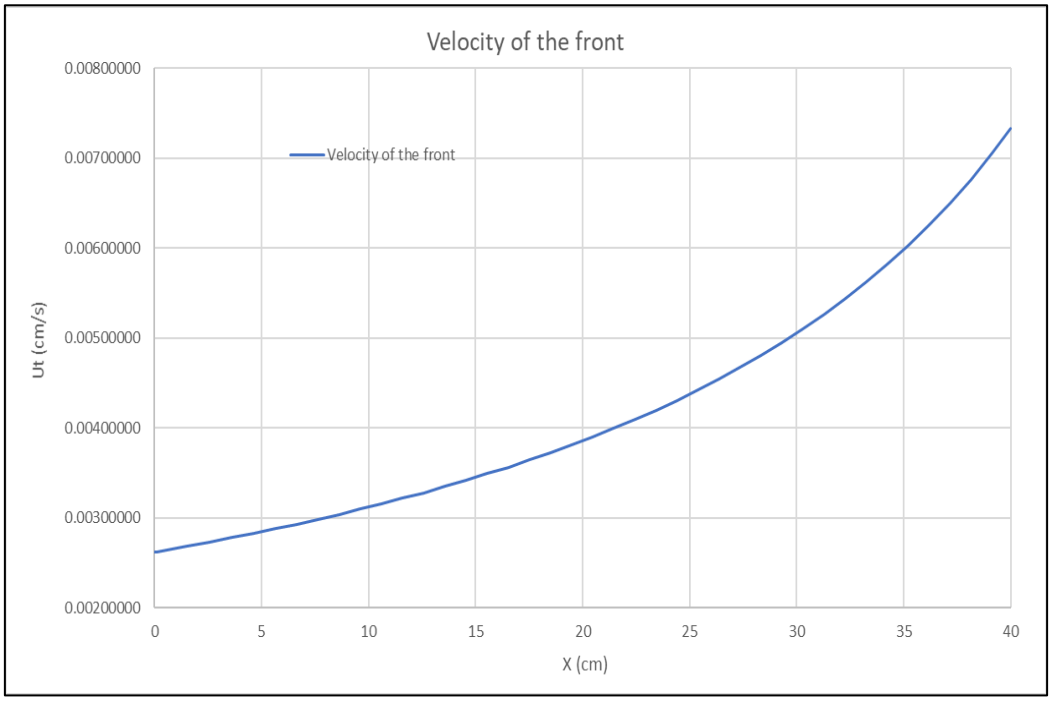

Figure 5-37 Imbibition rate versus distance for M below

5.1.6.2. Mobility Ratio equals 1 (M=1)

When the mobility ratio is equal 1, the imbibition rate is constant along the glass column as shown on the Figure 5-38 owing to both viscosities and end-point relative permeabilities are equal which makes the displacement process takes place steadily constant as none of the involved phases pushes each other owing they both have the same velocity and properties.

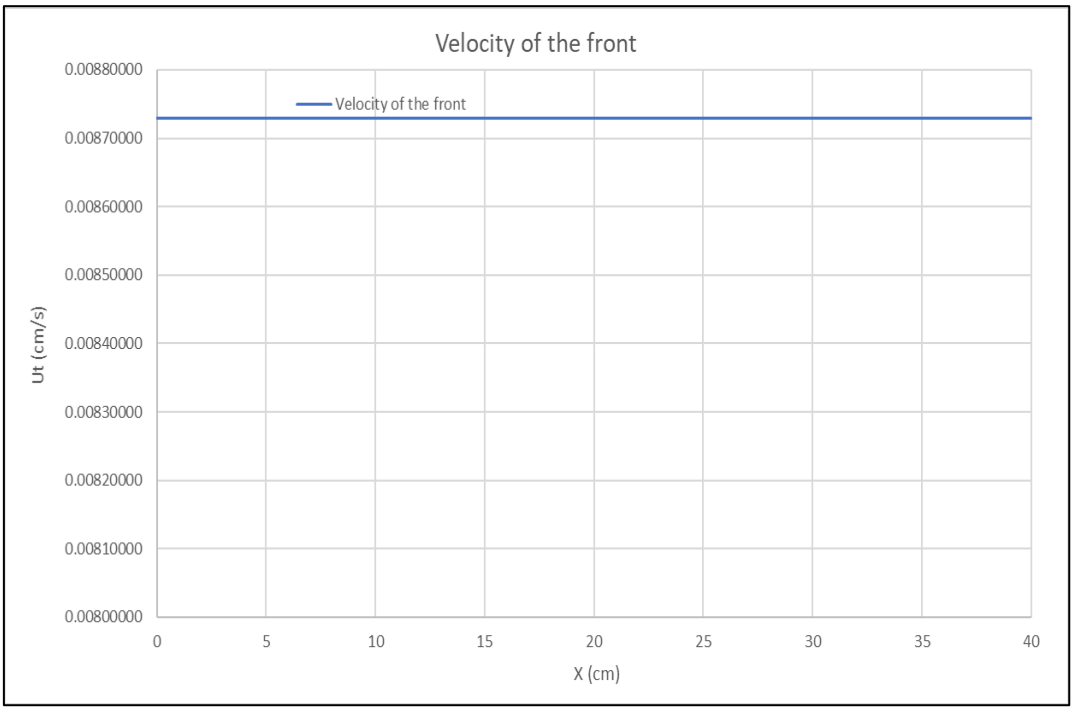

Figure 5-38 Imbibition rate versus distance for M equal 1

5.1.6.3. Mobility Ratio above 1 (M=1.68)

When the mobility ratio is above 1, it is considered unfavourable as the sweep decreases for a given volume of fluid injected. However, the results obtained from the analytical solution showed the same trend as when M<1 whose main explanation might be the ratio values analysed are close to one another and it did not allow to fully explain the trend . According to the theory when the mobility ratio is above 1, the imbibition rate drops exponentially through the system until it reaches the lowest value at the outlet, the reasons of this trend are the wetting phase (water) can travel with a velocity higher than the non-wetting phase (oil) which makes the flow become unstable (non-uniform displacement front), also the stability of the displacement process

is affected and creates viscous fingering which develops unfavorable water saturation profile (Kantzas, Apostolos et al., 2016). Also, a high mobility ratio causes an early breakthrough which make the recovery inefficient.

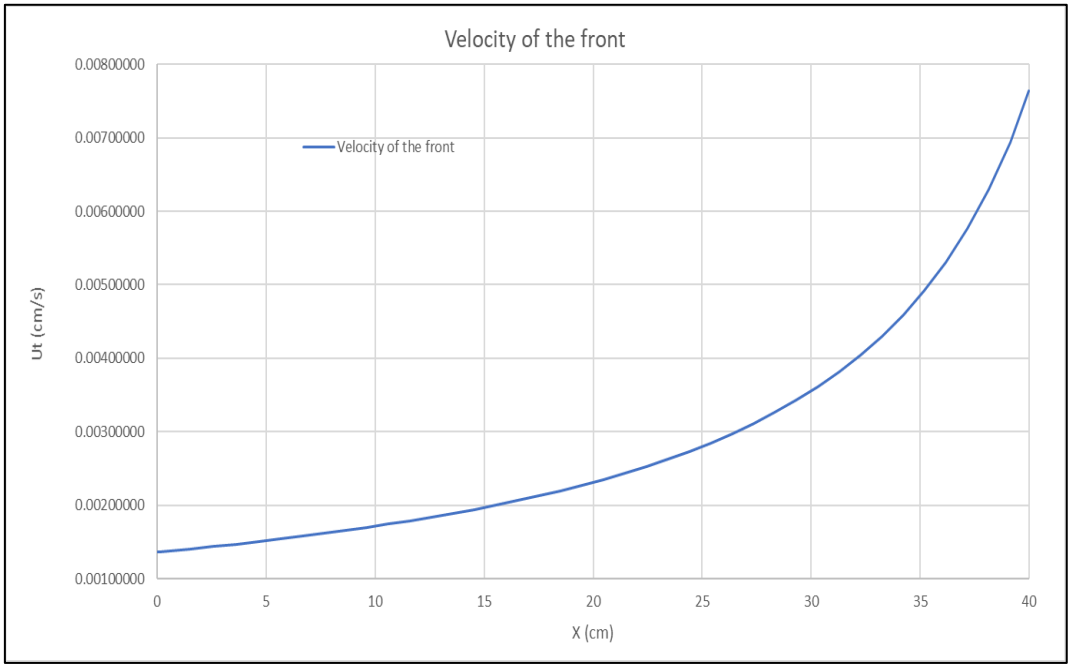

Figure 5-39 Imbibition rate versus distance for M above 1

The fractional flow function of the three cases were plotted against the water saturation using the principles of Bucley-Leverett theory. The higher the NW phase viscosity is, the lower f_w where the tangent line to the f_w curve, drawn from S_w=0, indicates the front saturation S_f in the B-L theory. Lower saturations are expected at higher viscosities ratios which matched to the simulation results as shown in the Figure 5-40.

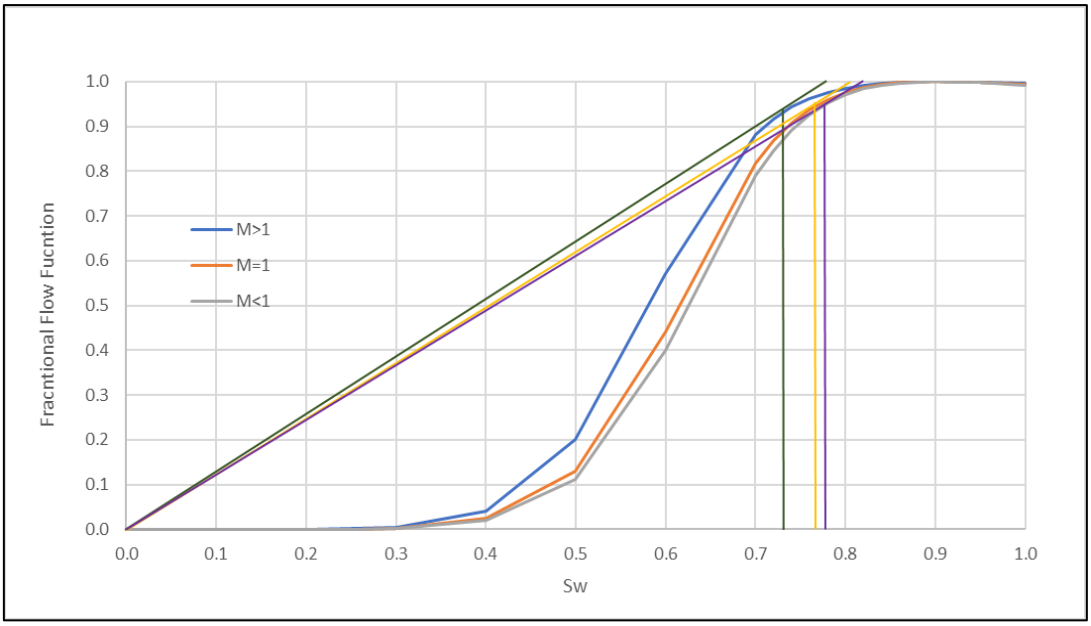

Figure 5-40 Fractional Flow Functions for the Kerosene experiment setup by (Meng et al., 2015) glass-beads experiment. The intersection with the tangent line indicates the Buckley-Leverett front saturation.

Additionally, the saturation profiles against position from inlet obtained from numerical simulator were plotted along with the Buckley-Leverett profiles like in the case outlined above for the four experiments. As the NW phase viscosity increases, the front saturation decreases which also leads to a lower saturation at breakthrough which in this situation did not match with the results obtained from the experiments probably owing to the mobility ratios used as shown in Figure 5-41.

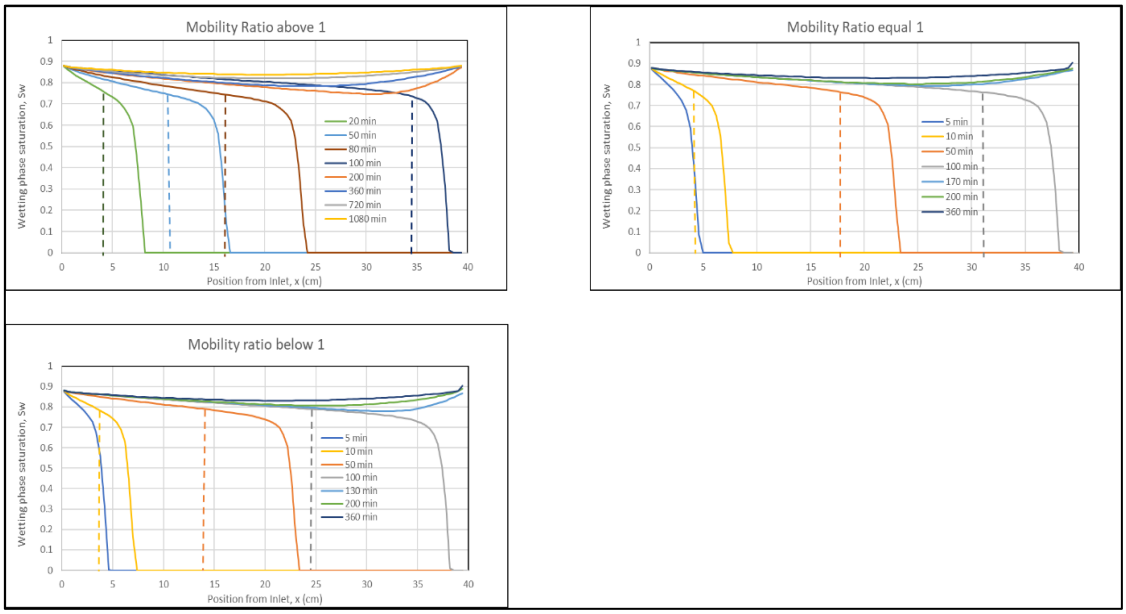

Figure 5-41 Simulated wetting phase saturation profiles compared to Buckley-Leverett saturation profiles for the Kerosene-Brine experiment with different mobility ratio by Meng et al. (Meng et al., 2015)

5.2. History Matching (HM)

To obtain acceptable understanding between simulation results and experimental data which in this thesis are obtained from the experiments by (Meng et al., 2015), History Matching is required. The manual tasks for such History Matching are achieved by adjusting the input data, run the simulations and plot against the experimental data to improve match. The input data is adjusted based on knowledge and experience from previous cases. There are 4 experiment results that are going to be matched against the simulation results (Air-Brine, Kerosene-Brine, White Oil No. 15 – Brine, White Oil No. 32).

At first, the reference HM were done with a Sor of 0.1 and later this parameter was switched to 0.08 for running the HM to have a better match for the oil recoveries and breakthrough times according to the values used in the experiments.

For all the experiments, the reference J-Function curve and the Relative Permeability curves used are outlined above in the section 4.5 which were also used for the sensitivities analysis. To have a good match between the experimental results and the simulated data some modifications were made to the input data. The end-point for the water relative permeability curve was increased from 0.3 to 0.4, the water Corey exponent was lowered from 6 to 5, the oil Corey exponent was also lowered from 2 to 1, the J-function interval was decreased from 2.43 to 0.4 and its value at 1-Sor was slightly modified. The main goals was to increase somehow the water mobility to reduce the time scale and also decreasing the driving force which is represented by the J-Function. Furthermore, by tuning the Corey exponents you can adjust the end recoveries; for instance, by reducing the Eo exponent it is possible to get a higher saturation front according to BL theory and also improve the recovery at breakthrough.

5.2.1. Curve Match of Air-Brine Experiment with Viscosity Ratio (μ_o/μ_w) = 0.0018

For the Air-Brine experiment, the reference case is shown below and later the respective History Matching process will be outlined.

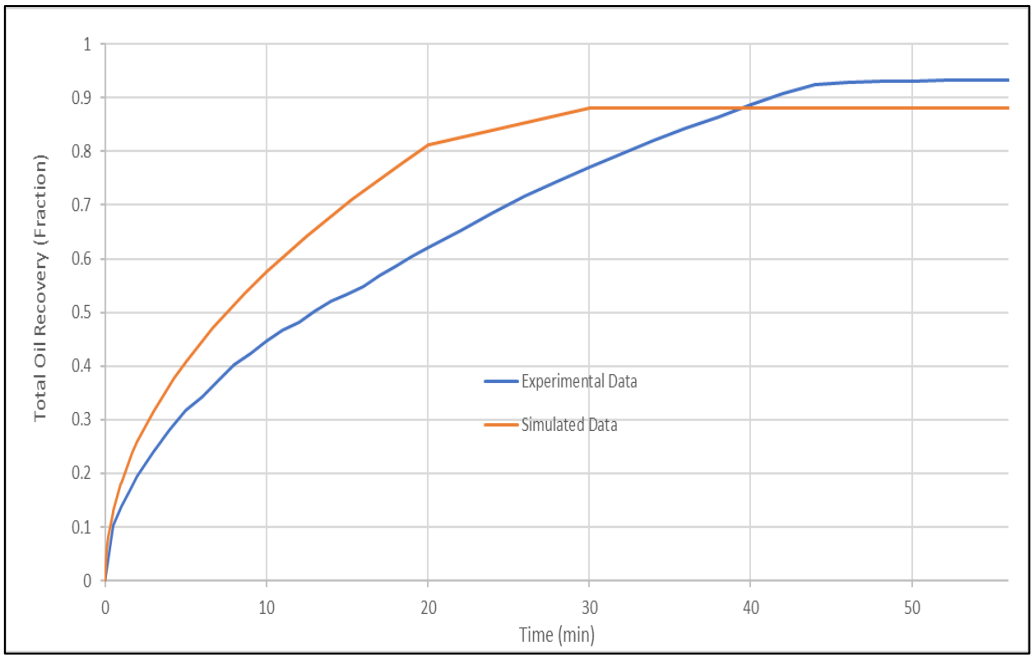

Figure 5-42 Total oil recovery for the Air-Brine experiment reference case

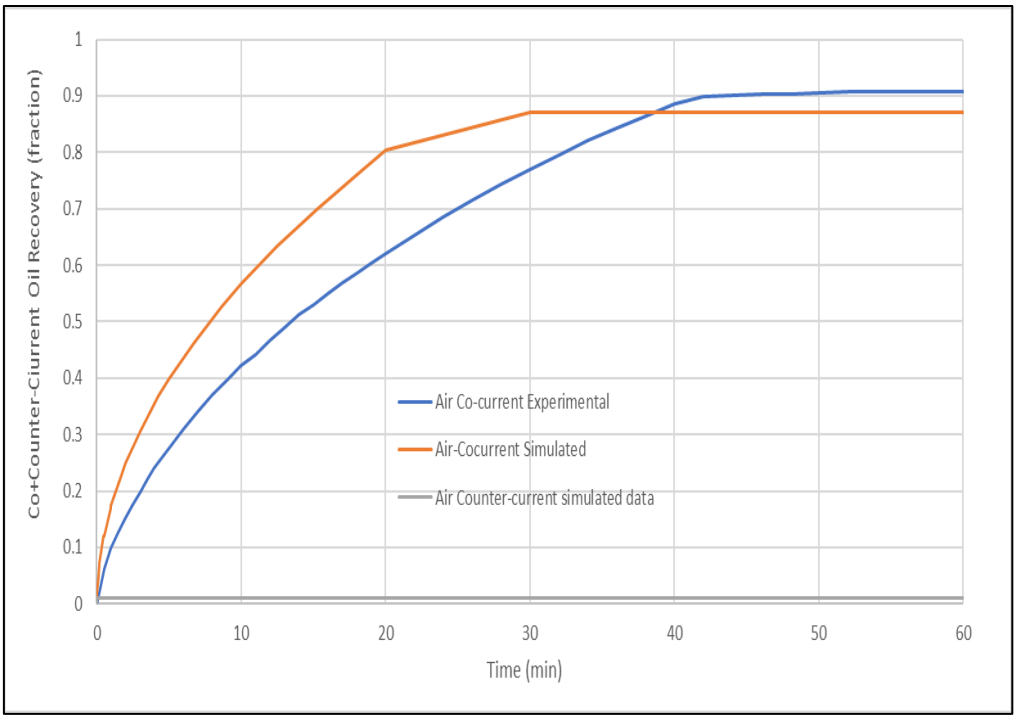

Figure 5-43 Co-current and counter-current Oil Production for the Air-Brine experiment reference case

For the reference case shown above, the comparison between the experimental and simulated values are listed below in the Table 5-19.

Table 5-19 Comparison of Simulation and Experiment Result for the reference case Air-Brine Experiment.

Remark	Breakthrough Time [minute]	Oil Recovery at the breakthrough [fraction]			Oil Recovery after the breakthrough [fraction]		
		Counter Current	Co Current	Total	Counter Current	Co Current	Total
Simulation	20		0.81	0.81		0.88	0.88
Experiment	44		0.92	0.92		0.92	0.92

For match the experimental result of Air-Brine with the simulation result, the following input data is used.

Table 5-20 HM Reference Kr - Pc Table for Curve Matching Experiment Air-Brine

Remark	Sw	Krw	Kro	Jow
Siw	0.000	0.000	1.000	0.40494
	0.020	0.000	0.989	0.39228
	0.050	0.000	0.972	0.37850
	0.060	0.000	0.967	0.37494
	0.080	0.000	0.956	0.36896
	0.100	0.000	0.944	0.36421
	0.150	0.000	0.915	0.35602
	0.200	0.000	0.885	0.35108
	0.250	0.001	0.853	0.34797
	0.300	0.001	0.821	0.34592
	0.400	0.006	0.752	0.34347
	0.500	0.019	0.676	0.34192
	0.600	0.047	0.590	0.34027
	0.700	0.102	0.489	0.33686
	0.720	0.117	0.466	0.33557
	0.740	0.135	0.442	0.33385
	0.760	0.154	0.417	0.33152
	0.780	0.175	0.390	0.32824
	0.800	0.199	0.361	0.32349
	0.820	0.225	0.330	0.31629
	0.840	0.254	0.295	0.30484
	0.860	0.286	0.255	0.28548
	0.880	0.320	0.209	0.24993
	0.890	0.339	0.181	0.22049
	0.900	0.358	0.147	0.17703
	0.91	0.379	0.104	0.11007
1-Sor	0.92	0.40	0.00	0.00134

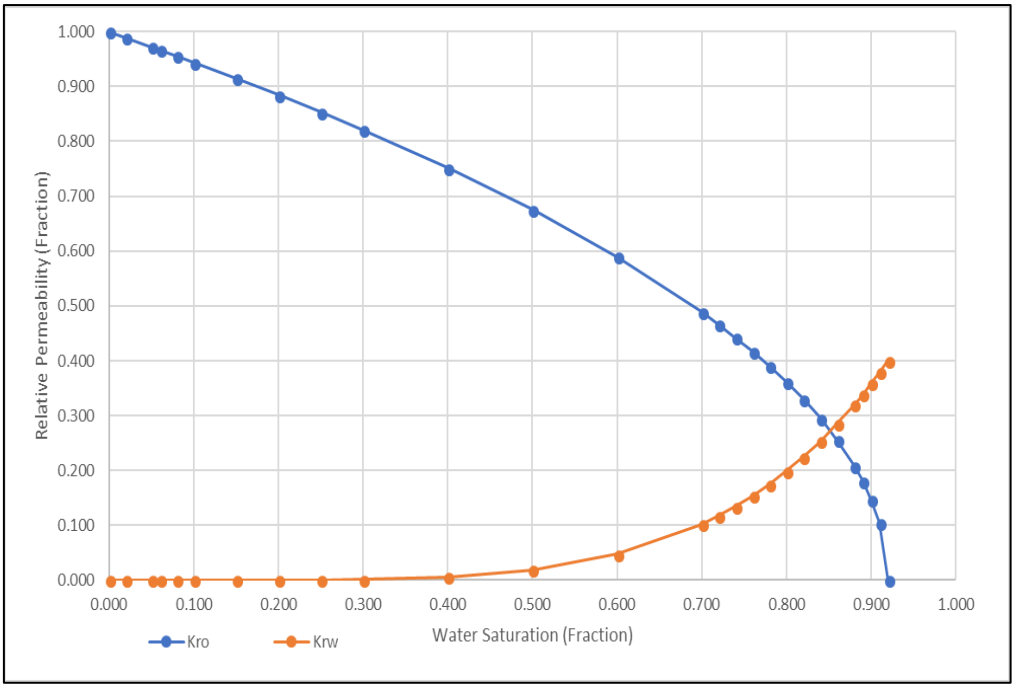

Figure 5-44 HM Reference Relative Permeability For Curve Match Experiment (Air-Brine)

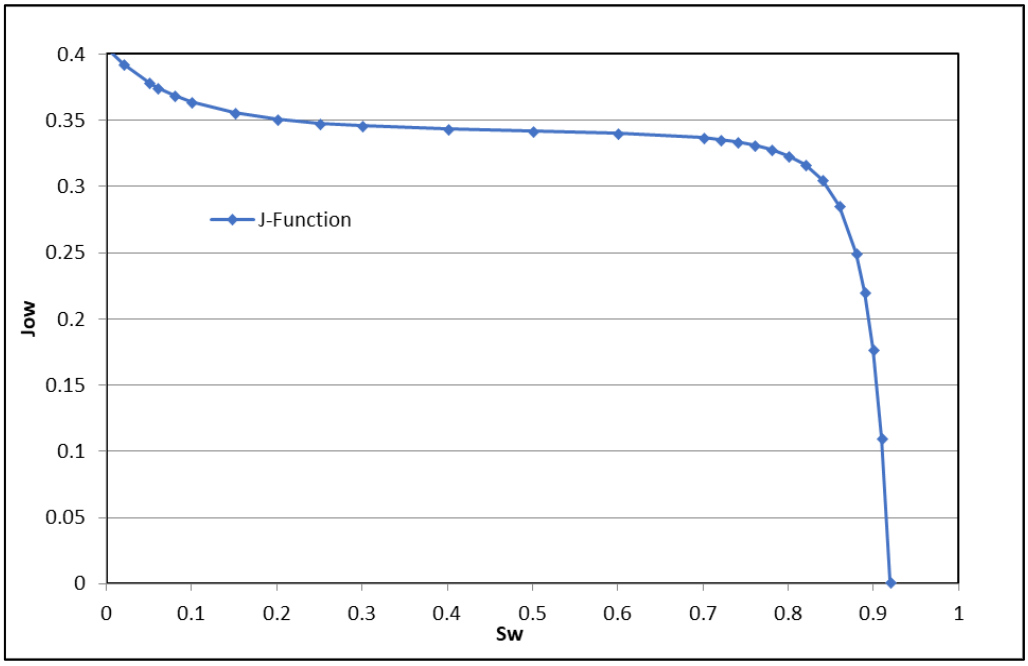

Figure 5-45 HM Refernce Capillary Pressure For Curve Match Experiment (Air-Brine)

5.2.1.1. History Matching for the Air-Brine experiment

Note that in the Air-Brine experiment, the oil is produced co-currently as there was no counter-current production reported. By running the simulations with the input data of the model, the results obtained almost match the experimental data in the recovery profile. The matched curves of total oil recovery for the experimental and simulated results are seen in the Figure 5-46 showed a decreasing trend. There are similar trends for the total oil recovery between the simulated and the experimental results, similar breakthrough times; however, the values of total oil recovery are slightly divergent along the time where the simulated values were under the experimental results at and after the breakthrough.

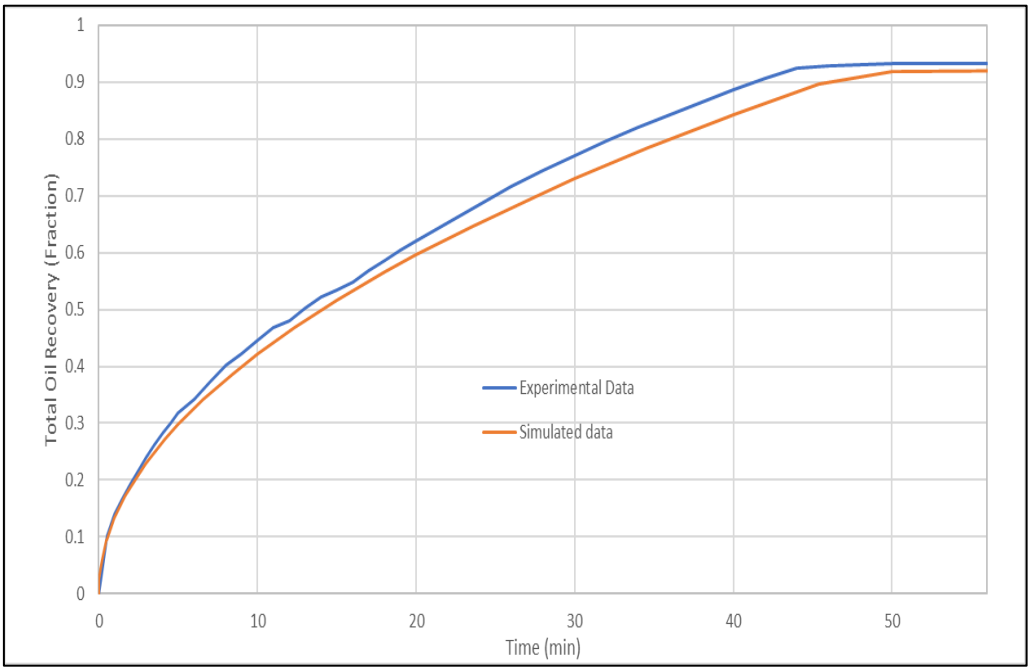

Figure 5-46 Total Oil Recovery Air-Brine Experiment– History Matching

There are similar trends for the co-current production curves between the simulation and the experimental results as shown in the Figure 5-47, similar breakthrough time; however, the values observed between the experimental and simulated results of co-current production had a gap along the time as the simulated data showed counter-current production. Furthermore, the simulated data were always under the experimental results at and after the breakthrough as listed in the Table 5-21.

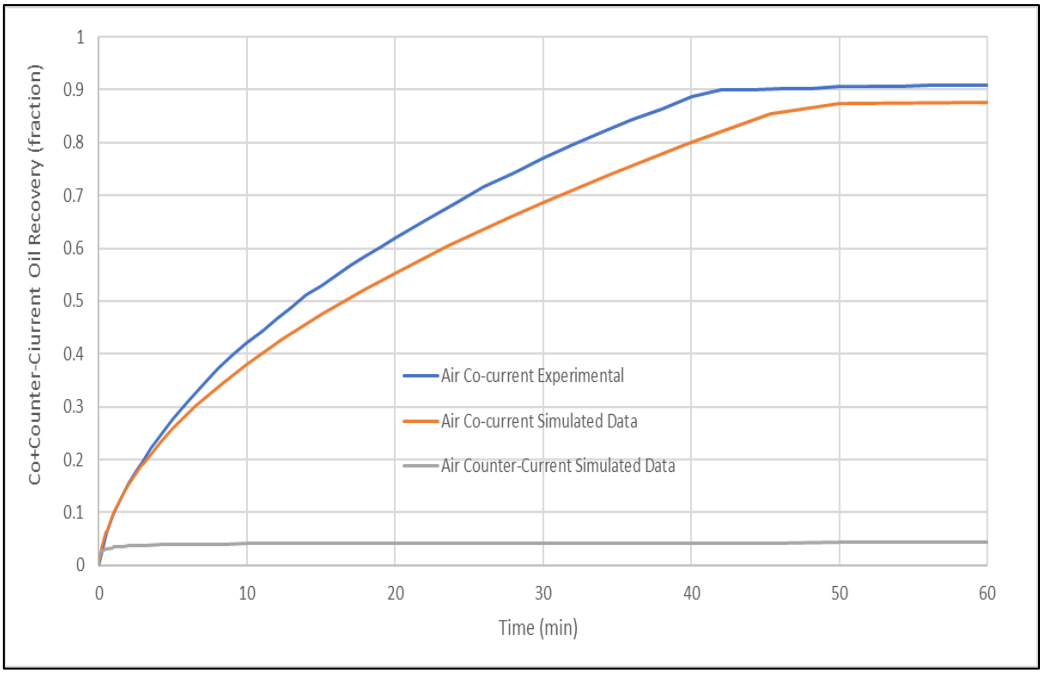

Figure 5-47 Co-current and counter-current oil production of Air-Brine Experiment– History Matching

Regarding the counter-current oil production, the maximum value registetred was 0.044 with no reference data from the experiment; the reason of this value might be the J-Function used in the model which is more concave down and flat which makes the oil less mobile. Nonetheless, the co-current production is still dominating for all the time.

Table 5-21 Comparison of Simulation and Experiment Result of Curve Match Air-Brine Experiment.

Remark	**Breakthrough Time [minute]**	**Oil Recovery at the breakthrough [fraction]**			**Oil Recovery after the breakthrough [fraction]**		
		Counter Current	**Co Current**	**Total**	**Counter Current**	**Co Current**	**Total**
Simulation	45	0.12	0.78	0.9	0.12	0.79	0.91
Experiment	44		0.92	0.92		0.92	0.92

5.2.2. Curve Match for Ker-Brine Experiment with Viscosity Ratio (μ_o/μ_w) = 2.80

For the Kerosene-Brine experiment, the reference case is shown below and later the respective History Matching process will be explained.

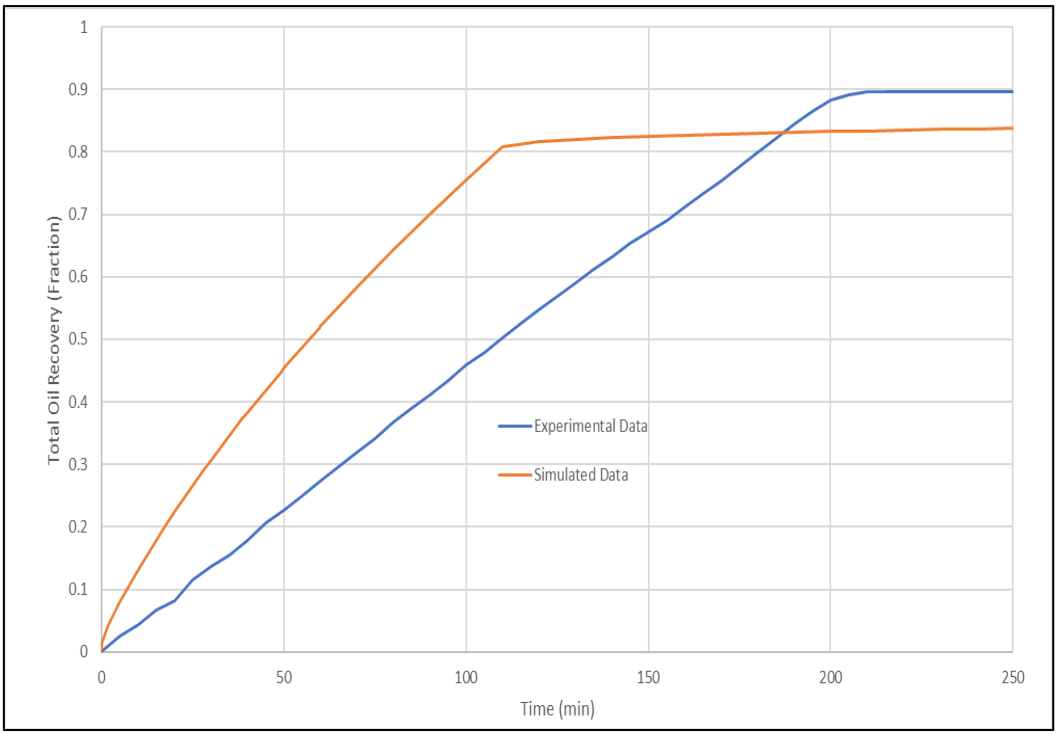

Figure 5-48 Total oil recovery for the Kerosene-Brine experiment reference case

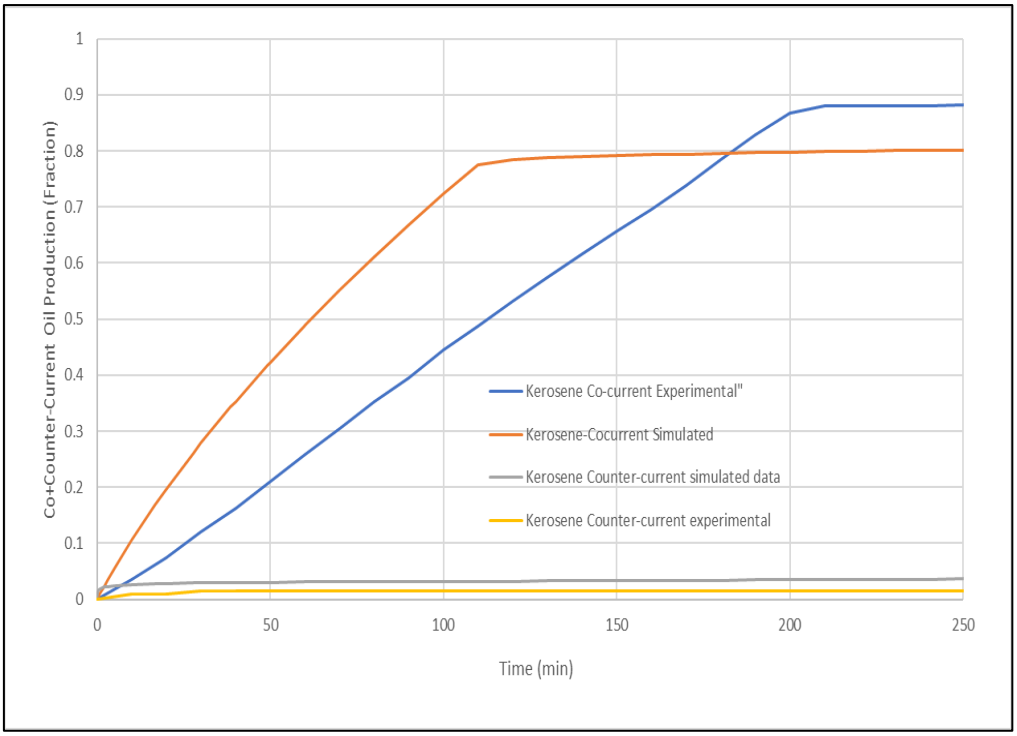

Figure 5-49 Co-current and counter-current Oil Production for the Kerosene-Brine experiment reference case

5.2.2.1. History Matching for the Kerosene-Brine experiment

For the reference case shown above, the comparison values between the experimental and simulated values are listed below in the Table 5-22.

Table 5-22 Comparison of Simulation and Experiment Results for the reference case Kerosene-Brine Experiment

Remark	Breakthrough Time [minute]	Oil Recovery at the breakthrough [fraction]			Oil Recovery after the breakthrough [fraction]		
		Counter Current	Co Current	Total	Counter Current	Co Current	Total
Simulation	110	0.03	0.77	0.80	0.03	0.80	0.83
Experiment	200	0.01	0.87	0.88	0.01	0.88	0.89

For matching the curves for the kerosene-brine experiment with the simulation results, the reference capillary pressure and relative permeability curves used to run the simulations are listed above in the section 4.5 and for this case the Oil Corey Exponent (Eo) used was 1.0. As shown in the Figure 5-50 the simulation curve attempted to match the experimental results curve where the first one had higher values over the latter up to 130 min and later they overlapped one another until the breakthough point as at first the experimental curve had a faster rate compared

to the simulated curve and later the opposite effect occurs. From that point on, the simulated results remained slightly above the experimental data.

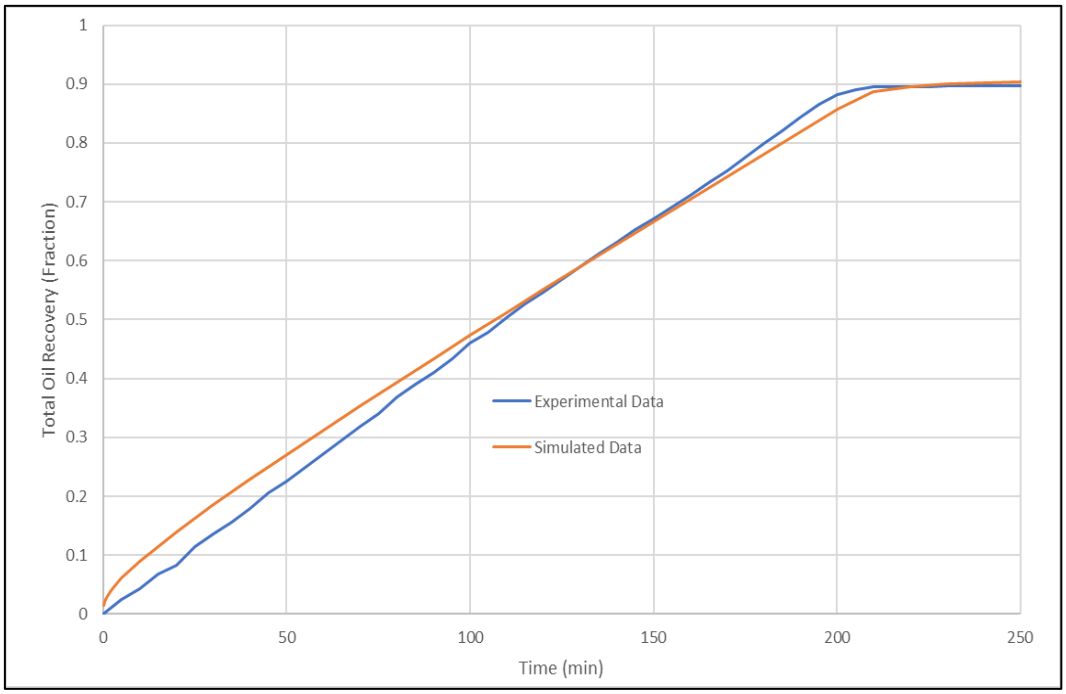

Figure 5-50 Total Oil Recovery for Kerosene-Brine Experiment– History Matching Results

Regarding the results obtained for the co-current and counter-current production as seen in the Figure 5-51 showed the co-current production curve for the simulated data is below the experimental curve as the latter had a faster imbibition rate compared to the former and for the counter-current production the opposite phenomenon takes place owing to the J-Function used might not be higher enough to force more water imbibes the model which causes a reduction of imbibition rate and lower the co-current oil production. The oil recovery at the breakthrough and after did not register the same value neither for the co-current production nor for the counter-current production. Moreover, the production curves for the simulated results showed a constant decreasing trendline along with the experimental results. Regarding the counter-current oil production, the maximum value registetred was 0.09 for the simulated results and 0.015 for the experimental data. Finally, as listed in the Table 5-23 the breakthrough time obtained from the simulation data was above the experimental results as well as the total oil production at and after the breakthrough owing to the Oil Corey Exponent used in the History Matching.

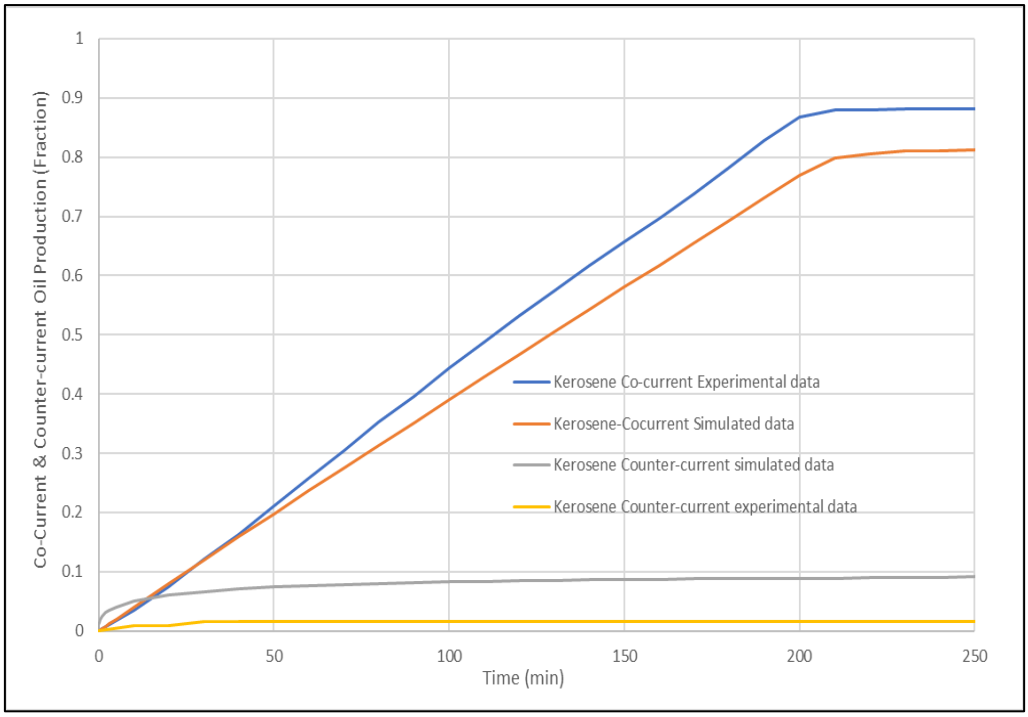

Figure 5-51 Co-current and counter-current Oil Production for the Kerosene-Brine experiment – History Matching

Table 5-23 Comparison of Simulation and Experiment Results of Curve Match Kerosene-Brine Experiment

Remark	**Breakthrough Time [minute]**	**Oil Recovery at the breakthrough [fraction]**			**Oil Recovery after the breakthrough [fraction]**		
		Counter Current	**Co Current**	**Total**	**Counter Current**	**Co Current**	**Total**
Simulation	210	0.09	0.80	0.89	0.09	0.81	0.90
Experiment	200	0.01	0.87	0.88	0.01	0.88	0.89

5.2.3. Curve Match of Experiment WHOIL 15 with Viscosity Ratio (μ_o/μ_w) = 25.6

For the WHOIL15-Brine experiment, the reference case is shown below and later the respective History Matching process will be explained.

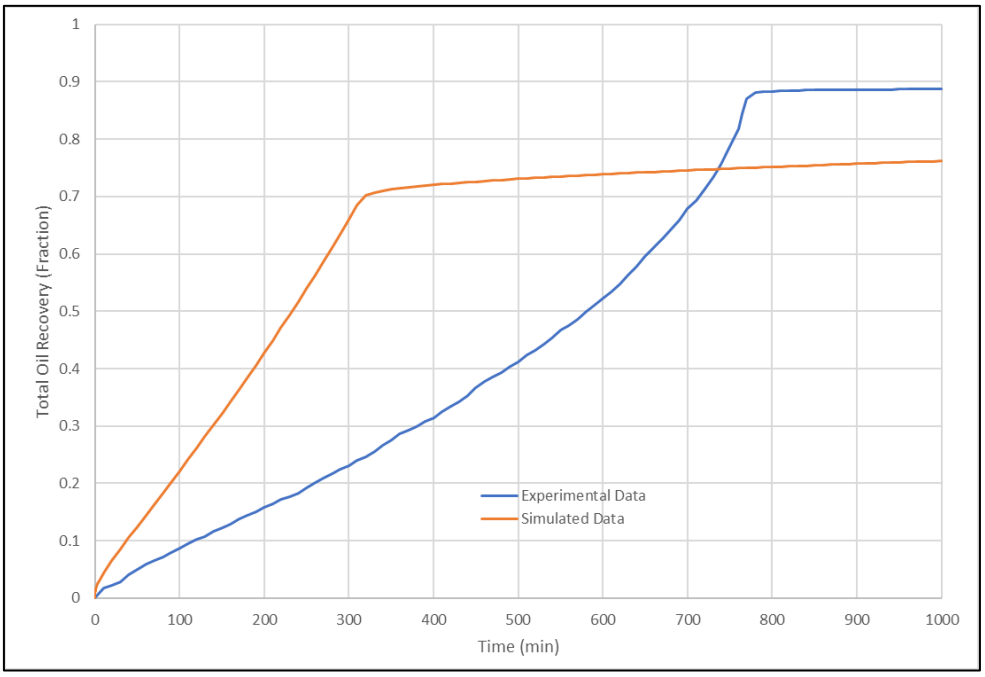

Figure 5-52 Total oil recovery for the WHOIL15-Brine experiment reference case

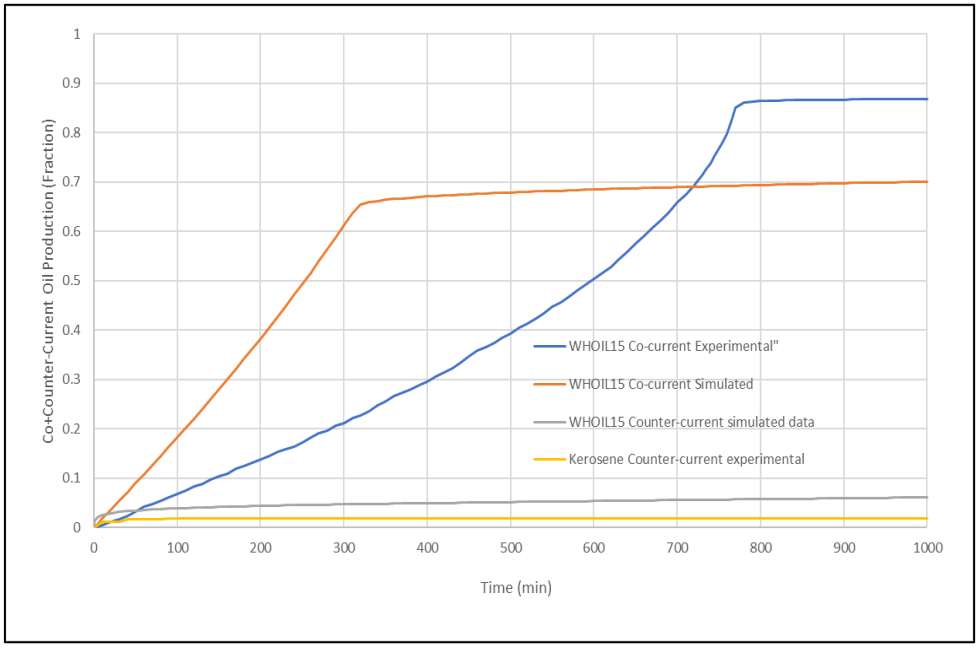

Figure 5-53 Co-current and counter-current Oil Production for the WHOIL15-Brine experiment reference case

5.2.3.1. History Matching for the WHOIL15-Brine experiment

For the reference case shown above, the comparison values between the experimental and simulated values are listed below in the Table 5-24.

Table 5-24 Comparison of Simulation and Experiment Results for the reference case WHOIL15-Brine Experiment

Remark	Breakthrough Time [minute]	Oil Recovery at the breakthrough [fraction]			Oil Recovery after the breakthrough [fraction]		
		Counter Current	Co Current	Total	Counter Current	Co Current	Total
Simulation	320	0.05	0.65	0.70	0.06	0.7	0.76
Experiment	770	0.05	0.85	0.90	0.02	0.87	0.89

For matching the curves for the WHOIL15-brine experiment against the simulation results, the reference J-Function and relative permeability curves used to run the simulations are listed above in the section 4.5 and for this case the Eo used was 1.0. As seen in the Figure 5-54, the simulation curve was above the experimental curve since the beginning of the imbibition process up to 760 min where the experimental curve started having values above the simulated data until the end of the imbibition; the imbibition rate showed an increasing trend up to the breakthrough and from this point on, the rate continued increasing at a faster rate for the simulation results although it remained under the experimental curve. Regarding the experimental curve, it started the process with an increasing rate up to the breakthrough where it flattened until the end of the displacement.

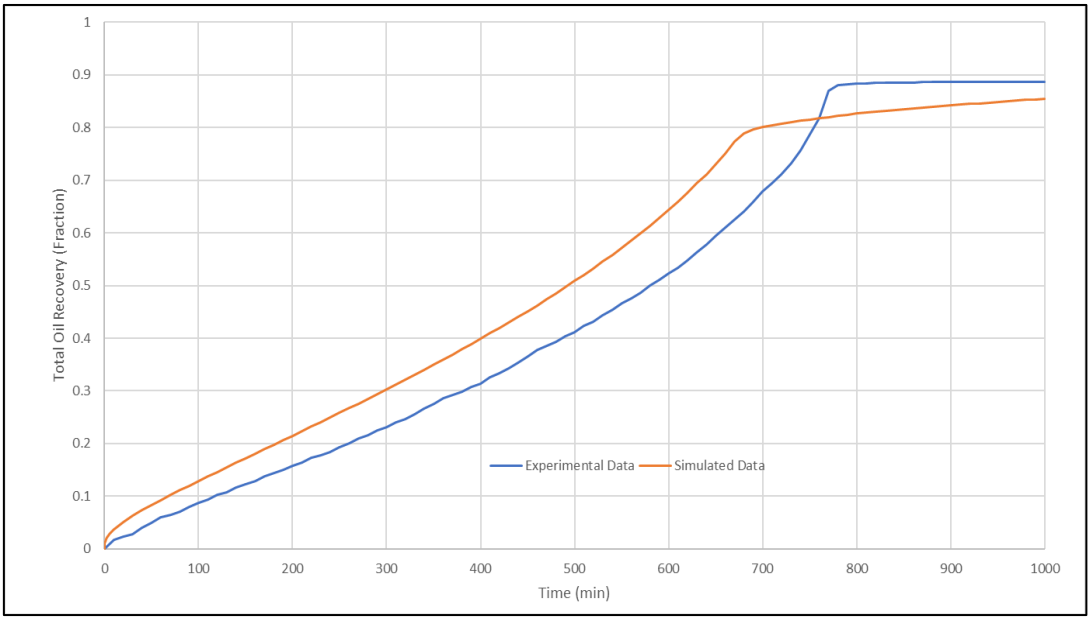

Figure 5-54 Total Oil Recovery for WHOIL15-Brine Experiment– History Matching Results with an Eo of 1

Regarding the results obtained for the co-current and counter-current production as seen in the Figure 5-55 showed the co-current production curve for the simulated data as well as the experimental curve matched well up to 470 min where the simulated curve started having higher values compared to the experimental curve up to the breakthrough around 690 min where the former continued with an increasing rate but with a faster pace. Regarding the experimental curve, it became flat from the breaktrough until the displacement is finished. About the counter-current oil production, the maximum value registered for the simulated result was 0.12 and it had an increasing rate along the whole displacement and 0.02 for the experimental data whose rate was constant along the time.

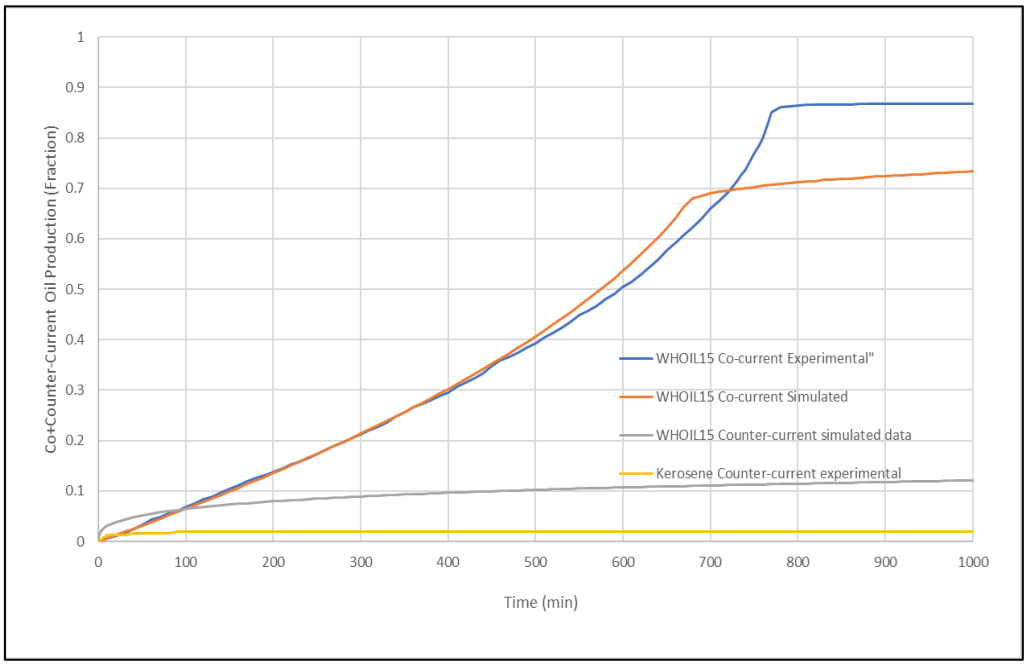

Figure 5-55 Co-current and counter-current Oil Production for the WHOIL15-Brine experiment – History Matching

Table 5-25 Comparison of Simulation and Experiment Results for HM WHOIL15-Brine Experiment

Remark	**Breakthrough Time [minute]**	**Oil Recovery at the breakthrough [fraction]**			**Oil Recovery after the breakthrough [fraction]**		
		Counter Current	**Co Current**	**Total**	**Counter Current**	**Co Current**	**Total**
Simulation	680	0.11	0.68	0.79	0.12	0.74	0.86
Experiment	770	0.05	0.85	0.90	0.02	0.87	0.89

5.2.4. Curve Match of Experiment WHOIL 32 with Viscosity Ratio (μ_o/μ_w) = 103.4

For the WHOIL32-Brine experiment, the reference case is shown below and later the respective History Matching process will be explained.

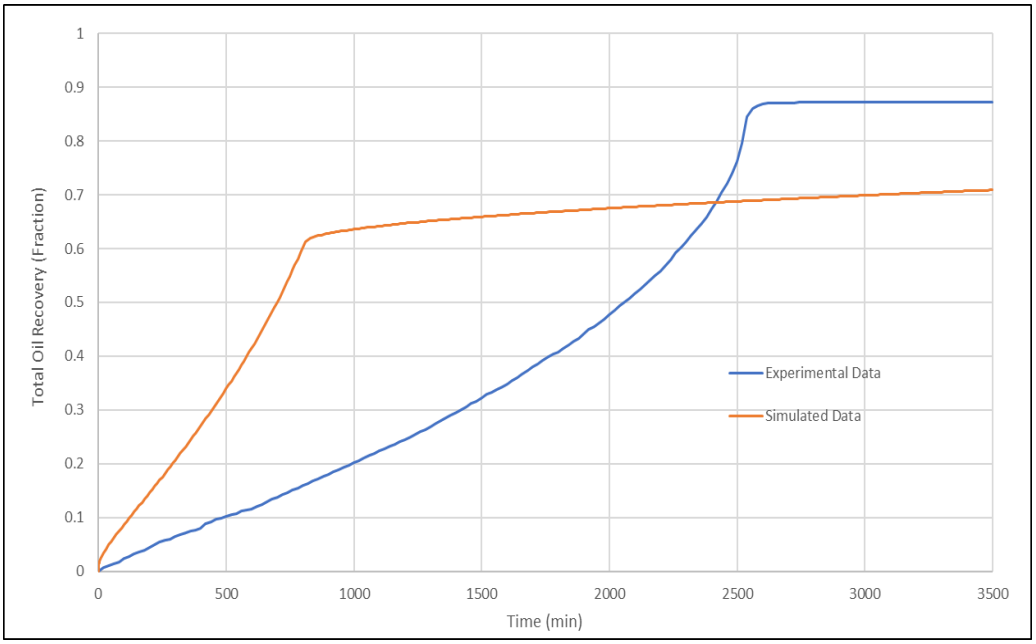

Figure 5-56 Total oil recovery for the WHOIL32-Brine experiment reference case

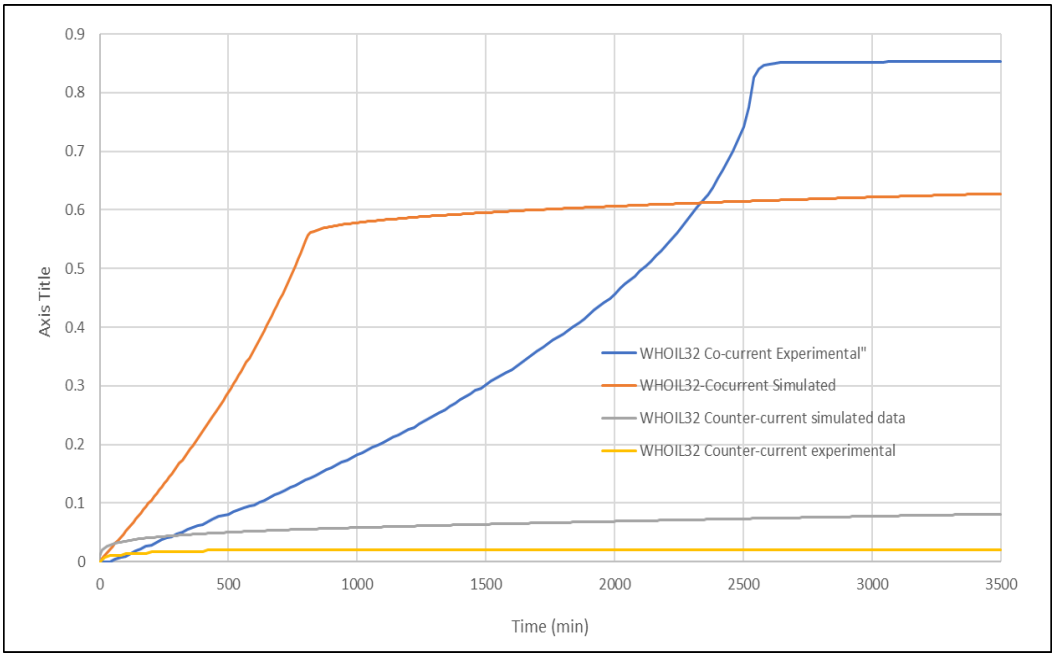

Figure 5-57 Co-current and counter-current Oil Production for the WHOIL32-Brine experiment reference case

For the reference case shown above, the comparison values between the experimental and simulated values are listed below in the Table 5-26.

Table 5-26 Comparison of Simulation and Experiment Result for the reference case WHOIL32-Brine Experiment

Remark	Breakthrough Time [minute]	Oil Recovery at the breakthrough [fraction]			Oil Recovery after the breakthrough [fraction]		
		Counter Current	Co Current	Total	Counter Current	Co Current	Total
Simulation	800	0.05	0.55	0.6	0.08	0.63	0.71
Experiment	2540	0.02	0.82	0.84	0.02	0.85	0.87

5.2.4.1. History Matching for the WHOIL32-Brine experiment

For matching the curves for the WHOIL32-brine experiment against the simulation results, the reference J-Function and relative permeability curves used to run the simulations are listed above in the section 4.5 and for this case the Oil Corey Exponent used was 1.0. As seen in the Figure 5-58, the simulation curve was above the experimental curve since the beginning of the imbibition process up to 2504 min where experimental curve started having values above the simulated data until the end of the displacement; the imbibition rate showed an increasing trend up to the breakthrough and from this point on, the rate continued increasing at a faster rate for the simulated data curve. Regarding the experimental curve, it started the process with an increasing rate up to the breakthrough where it flattened until the end of the displacement.

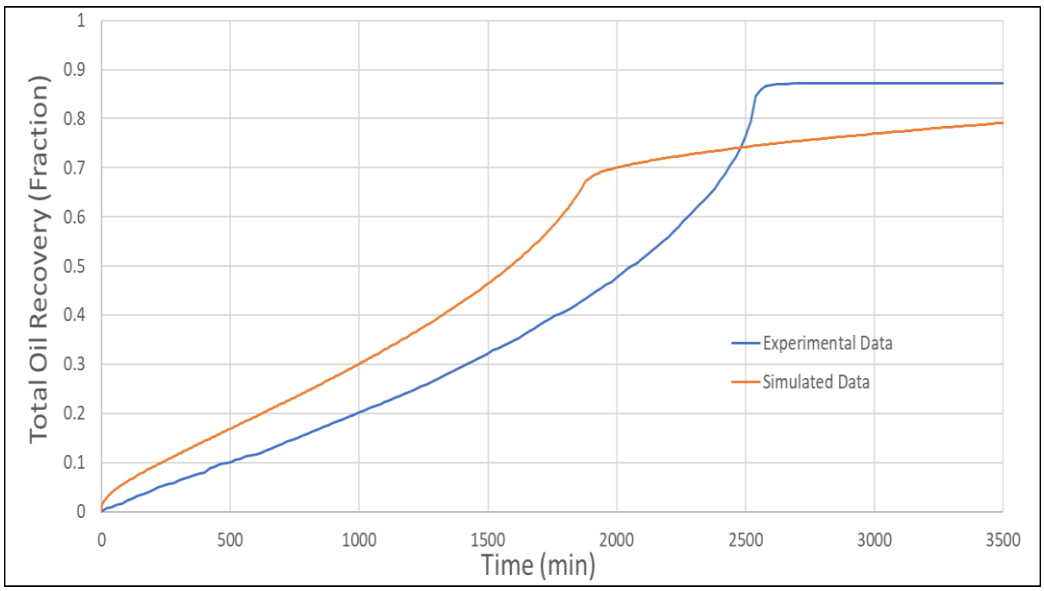

Figure 5-58 Total Oil Recovery for WHOIL32-Brine Experiment– History Matching Results with an Eo of 1

Regarding the results obtained for the co-current and counter-current production as seen in the Figure 5-59 showed the co-current production curve for the simulated data and the experimental curve where the former always showed higher values compared to the latter up to the breakthrough around 1894 min where the simulated data curve showed a fast increasing rate until the end of the displacement; regarding the experimental curve, it became flat from the breaktrough until the end of the imbibition. Respect the counter-current oil production, the maximum value registered for the simulated results was 0.14 and it had an increasing rate along the whole imbibition and 0.02 for the experimental data whose rate was constant along the time.

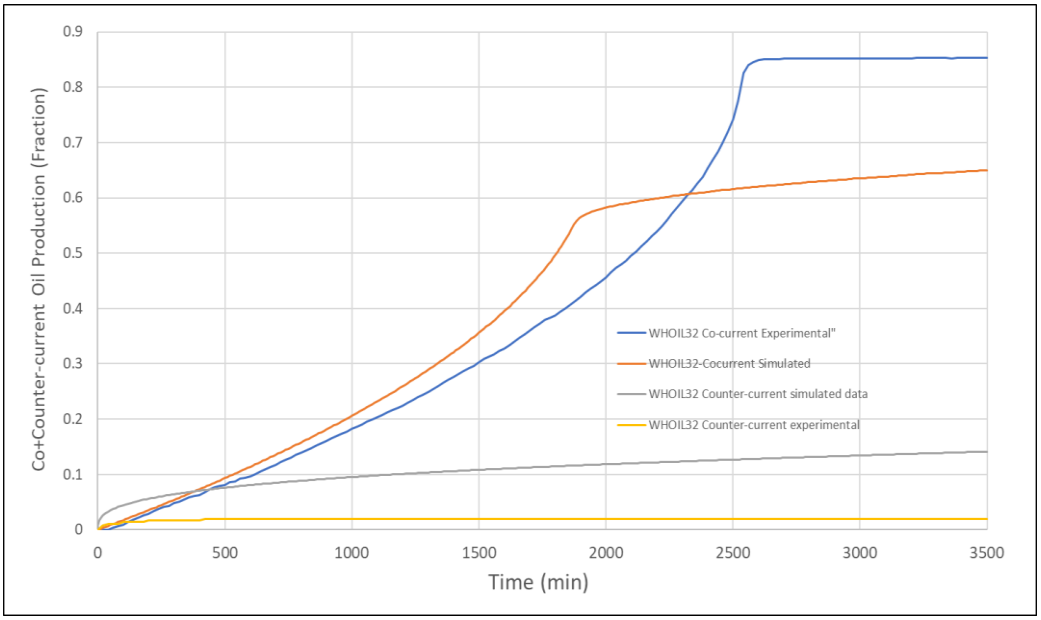

Figure 5-59 Co-current and counter-current Oil Production for the WHOIL32-Brine experiment – History Matching Results for an Eo of 1.0

Table 5-27 Comparison of Simulation and Experiment Results for HM WHOIL32-Brine Exp for an Eo of 1.0

Remark	**Breakthrough Time [minute]**	**Oil Recovery at the breakthrough [fraction]**			**Oil Recovery after the breakthrough [fraction]**		
		Counter Current	**Co Current**	**Total**	**Counter Current**	**Co Current**	**Total**
Simulation	1864	0.12	0.54	0.66	0.14	0.66	0.80
Experiment	2540	0.02	0.82	0.84	0.02	0.85	0.87

6. Conclusion

1D rectangular model (100x1x1) with 40 cm x 0.8720 cm x 0.8720 cm has been built with TEOFSI boundary condition where the inlet of the glass column is in contact with water and the opposite side is in contact with oil. With an initial water saturation at zero and an average oil residual saturation around 90%, the correlation for relative permeability and capillary pressure is generated. Parameter studies of relative permeability, mobility ratio, glass column length, imbibition rate , capillary pressure and viscosity ratio have been investigated by model simulation based on the reference case of relative permeability and capillary pressure. The manual history matching has been done as well by matching the simulation result with the 4 experiments (Air, Kerosene, White Oil No. 15 and White Oil No. 32). All the results from the Sensitivity Analysis and History Matching from the Chapter 5 are summarized as follows:

1. A high imbibition rate and a decreasing trend on oil production occurred when the oil was more mobile than water. On the other hand, when the water was more mobile than the oil the imbibition rate decreased and the oil production showed an increasing trend.
2. An increase on the Oil Corey Exponent decreased the mobility of the oil and makes the imbibition rate slower compared to a strongly water-wet system.
3. For the most part, the co-current production was always more dominating than counter-current production during the imbibition for the four experiments along the time.
4. An increase on imbibition rate implied a significant increase on co-current oil production and much less counter-current oil production. On the contrary, as the counter-current production increased, the co-current oil recovery decreased which leaded a lower imbibition rate. The maximum oil recovery reached by counter-current production was about 15%, while the co-current oil recovery is about 71%.
5. As the oil viscosity increased, the front saturation decreased which also leaded to a lower saturation at breakthrough which matched the Bucley-Leverett theory.
6. The imbibition rate is highly influenced by the glass column length. From the simulation result, by increasing the glass column length twice and three times the reference length, the total oil production rate decreased and the breakthrough took more time to occur. Also, as the mobility ratio increased, the total production decreased and the breakthrough time happened at a later time.

7. The oil production is also affected by the shape of the capillary pressure curve. A concave up-slope J-Function curve caused a delay on water breakthrough and a lower oil production recovery. This type of shape produced a lower co-current oil recovery and a higher counter-current oil recovery owing to the high oil pressure generated.
8. For a mobility ratio below 1, the breakthrough happens first for the increasing slope case followed by the reference and finally for the decreasing slope case. Also, for the increasing and reference slope cases, the breakthrough times and the counter-current production were similar and low compared to the decreasing slope case owing mostly to the oil mobility. Whereas for the mobility ratio above 1, the breakthrough times and the oil production of the three cases are neither similar nor close whose main reason might be the fluid mobility of oil which it is low compared to the mobility of water.
9. For the analysis of different mobility ratios, the simulation results showed a different behaviour as it is expected when M>1 the breakthrough to takes place at an earlier time, the results showed the breakthrough time happened at a later time. Probably, the reason of this finding might be the mobility ratios used are close and for the case M=1 the krew was modified.
10. The numerical saturation profiles were plotted against position from inlet and were compared to the B-L profiles where the saturation profiles matched roughly and were smoother to the B-L profiles possibly due to the capillary diffusion phenomenon which happened during the imbibition process.
11. Some features like jumps and instabilities on the curves obtained from the simulations were observed probably due to some issues related to the numerical solution and/or softwate simulator which should be addressed to the author of IORcoresim (Arild Lohne) to continue improving the performance, stability and accuracy of the software.

All the results and discussions from the History Matching process outlined in the chapter 5 are summarized as follows:

1. The reference cases for the four experiments were run with a S_{or} of 0.1 and for the History Matching, the S_{or} was decreased to 0.08 to have a better match with the oil recoveries and breakthrough times according to the values reported in the experiments.
2. The main objectives to run a History Matching was to increase the water mobility to diminish the time scale and to reduce the driving force of the imbibition represented by the J-Function. Furthermore, by tuning the Corey exponents the end recoveries were adjusted.
3. For the Air and Kerosene experiments as the viscosity ratio was low, the imbibition rates showed a decreasing trend and the HM reference input data leaded to a minor mismatch between the curves on the production profile. For an Eo of 1, the simulated data curve at breakthrough was under the experimental data curve and after the opposite effect occurred.
4. For the WHOIL15 and WHOIL32 experiments as the viscosity ratio was high, the imbibition rates had an increasing trend where the experimental results showed a delay compared to the experimental data. For the case where the Eo was 1, the simulated data curve at breakthrough was above the experimental data curve and after this point the opposite effect occurred in despite the simulation curve had a faster increasing rate than the experimental curve.
5. For the four experiments, the counter-current production obtained was always higher compared to the experimental results mostly caused by the J-Function used which was not high enough to force more water imbibes the model and it caused a reduction on the imbibition rate and lowered the co-current oil production.
6. To obtain a better match for the four experiments it is recommended to make some adjustments on the J-Fucntion curve like making the top flatter and also adjust the last part to make it steeper around 1-$S_{or.}$ and do more sensitivities to get a better match between the experimental and simulated curves.

7. References

Abdallah et al. (2007). Fundamentals of Wettability. *Oilfied Review, 19*(2), 44-61. Retrieved from https://www.slb.com/~/media/Files/resources/oilfield_review/ors07/sum07/p44_61.pdf

Alyafei, Nayef et al. (2014). Investigation of co-current and counter-current spontaneous imbibition using micro-computerized tomography. *International Symposium of the Society of Core Analysis* (pp. 1-6). Avignon, France: SCA.

Andersen et al. (2017, October). Modelling of Spontaneous Imbibition Experiments with Porous Dic - On the Validity of Exponential Prediction. *SPE Journal, 22*(05), 1-20. doi:https://doi.org/10.2118/186094-PA

Andersen et al. (2017). Numerical Interpretation of laboratory spotaneous imbibition - Incorporation of the Capillary Back Pressure and how it affects SCAL. *Abu Dhabi International Petroleum Exhibition & Conference* (pp. 1-20). Abu Dhabi: SPE. doi:https://doi.org/10.2118/188625-MS

Andersen et al. (2018, April 1). Darcy Scale Simulation of Boundary Condition Effects during Capillary Dominated Flow in High Permeability Systems. *SPE R&E*, 1-27.

Andersen et al. (2018). Darcy scale simulation on bounday condition effects during capillary dominated flow in high permeability systems. *SPE JPT*, 1-27.

Behbahani et al. (2005, October 14). Simulation of counter-current imbibition in water-wet fractured reservoirs. (D. o. Engineering, Ed.) *Journal of Petroleum Science and Engineering, 50*(1), 21-39. doi:https://doi.org/10.1016/j.petrol.2005.08.001

Bratton et al. (2006). The Nature of Naturally Fractured Reservoirs. *Oilfield Review, 18*(2), 4-23.

Corey, A. (1954, November). The interrelation between gas and oil relative permeabilities. *Producers Monthy, 19*(1), 38-41.

El-Amin, M.F.; Sun, Shuyu. (2011, January 8). Effects of gravity and inlet/outlet location on a two-phase cocurrent imbibition in porous media. (Z. Chen, Ed.) *Journal of Applied Mathematics, 2011*, 1-18. doi:doi:10.1155/2011/673523

Fernø et al. (2015). Spontaneous imbibition revisited - A new method to determine Kr and Pc by inclusion of the Capillary Backpressure. *European Symposium on Improved Oil Recovery. We B04*, pp. 1-18. Dresden: IOR 2015. doi:10.3997/2214-4609.201412131

Fernø, M.A. et al. (2015). Quick and affordable SCAL: Spontaneous core analysis. In S. o. Analysis (Ed.), *Society of Core Analysis. 55*, pp. 1-12. St. John: SCA2015-A055.

Fernø, Martin A. (2012). *Enhanced Oil Recovery in Fractured Reservoirs, Introduction to Enhanced Oil Recovery (EOR) Processes and Bioremediation of Oil-Contaminated Sites.* (D. o. Techology, Ed.) Bergen, Hordaland, Norway: Intech. Retrieved from Intechopen: : http://www.intechopen.com/books/introduction-toenhanced-oil-recovery-eor-processes-and-bioremediation-of-oil-contaminated-sites/enhanced-oil-recovery-infractured-reservoirs

Foley et al. (2017, April 21). The impact of capillary backpressure on spontaneous counter-current imbibition in porous media. (D. o. Engineering, Ed.) *Advances in water resources, 107,* 405-420. doi:https://doi.org/10.1016/j.advwatres.2017.04.012

Glover, P. (2010). *Petrophysics MSc Course Notes.* Aberdeen: University of Aberdeen.

Haugen et al. (2014, March 1). Capillary Pressure and relative permeability estimated from a single spontaneous imbibition test. *Journal of Petroleum Science and Engineering, 115*(25), 66-77. Retrieved from http://dx.doi.org/10.1016/j.petrol.2014.02.001

Haugen et al. (2014). Measurement of core properties using a new technique - two ends open spontaneous imbibition. In D. o. Technology (Ed.), *International Symposium of the Society of Core Analysis* (pp. 1-12). Avignon: SCA 2014-006.

Hongjung et al. (2013, Ocotober 30). Fractal analysis of dimensionless capillary pressure function. *International Journal of heat and mass transfer, 69*, 26-33. Retrieved from https://doi.org/10.1016/j.ijheatmasstransfer.2013.10.006

Kantzas, Apostolos et al. (2016). *Fundamentals of fluid flow in porous media.* Calgary, Alberta: University of Calgary.

Langtangen, H. (1991, April 18). Sensitivity analysis of an enhanced oil recovery process. (D. o. Mathematics, Ed.) *Applied mathematical Modelling*, *15*(9), 467-474. doi:https://doi.org/10.1016/0307-904X(91)90036-O

Leverett, M.C. (1940, June 14). Capillary behaviour in porous solids. *Transactions of the AIME*(1223), 1-18.

Lomeland et al. (2005). A new versatile relative permeability correlation. *International symposium of the society of core analysis. 112,* pp. 1-12. Toronto: SCA 2005.

MA, S., Zhang, X., & Morrow, N. (1999, July). Influence of fluid viscosity on mass transfer between rock matrix and fractures. *Journal of Canadian Petroleum Technology, 38*(07), 25-30. doi:https://doi.org/10.2118/99-07-02

Mason, G., & Morrow, N. (2013, August 24). Developments in spontaneous imbibition and possibilities for future work. *Petroleum science and engineering, 110,* 268-293. doi:https://doi.org/10.1016/j.petrol.2013.08.018

Meher, R. (2011). Solution of nonlinear equations of single and double phase flow phenomena arising in oil recovery process. *PhD. Thesis*.

Meng et al. (2015, February 2). Entrapment of the non-wetting phase during co-current spontaneous imbibition. (E. a. Fuels, Ed.) *ACS Publication, 29*(2), 686-694. doi:10.1021/ef5025164

Meng, Q et al. (2016, January 19). Effect of Wetting-Phase viscosity on Co-current Spontaneous imbibition. (A. C. Society, Ed.) *ACS Publications, 30*(2), 835-842. doi:10.1021/acs.energyfuels.5b02321

Meng, Q. et al. (2017, April 17). A critical review on fundamental mechanisms of spontaneous imbibition and the impact of boundary condition, fluid viscosity and wettability. *Advances in Geo-Energy Research, 1*(1), 1-17. doi:10.26804/ager.2017.01.01

Mirzaei-Paiaman et al. (2014, February 10). Scaling of Recovery by cocurrent spontaneous imbibition in fractured petroleum reservoirs. *Enegy Technology, 2*(2), 166-175. doi:10.1002/ente.201300155

Mirzaei-Paiaman et al. (2017, February 14). Scaling one- and multi-dimensional co-current spontaneous imbibition processes in fractured reservoir. (FUEL, Ed.) *Elsevier, 196*, 458-472. doi:https://doi.org/10.1016/j.fuel.2017.01.120

Morrow, N. R., & Mason, G. (2001, August). Recovery of oil by spontaneous imbibition. *Colloid and interface science, 6*(4), 321-337. doi:https://doi.org/10.1016/S1359-0294(01)00100-5

Nolen-Hoeksema, Richard. (2016). Wettability. *Oilfield Review*, 1-2.

Standnes, D. C. (2004, January 1). Experimental study of the impact of boundary conditions conditions on Oil Recovery by Co-current and counter-current Spontaneous Imbibition. *Energy & Fuels, 18*(1), 271-282. doi:10.1021/ef030142p

Torabi et al. (2015, September 25). Predicting heavy oil/water relative permeability using modified Corey-based correlations. (F. o. Science, Ed.) *FUEL, 163*, 196-204. doi:https://doi.org/10.1016/j.fuel.2015.09.035

Unsal et al. (2009, February 12). Bubble snap-off and capillary back pressure during counter-current spontaneous imbibition into model pores. *American Chemical Society, 25*(6), 3387-3395. doi:10.1021/la803568a

Yadav, Saroj R.; Mehta, Manoj N. (2014, January 29). Analytical approximate expression for cocurrent imbibition during immiscible two-phase flow through porous media. (C. M. Khalique, Ed.) *Mathematical problems in Engineering, 2014*, 1-6. doi:http://dx.doi.org/10.1155/2014/638409

Zhang, X.; Morrow, N.; MA, S. (1996, November). Experimental verification of a modified scaling group for spontaneous imbibition. *SPE Reservoir Engineering, 11*(04), 280-285. doi:https://doi.org/10.2118/30762-PA

Zolotukhin, A., & Ursin, J. (2000). *Introduction to Petroleum Reservoir Engineering.* Oslo: Norwegian Academic Press.